PB-228 046

FACTORS INFLUENCING STREAM TEMPERATURES. PART I. THE EFFECT OF SURFACE CONFIGURATION ON EVAPORATION FROM A POROUS STREAM MODEL

Bruce Alan Tichenor

Oregon State University
Corvallis, Oregon

June 1966

DISTRIBUTED BY:

NTIS
National Technical Information Service
U. S. DEPARTMENT OF COMMERCE
5285 Port Royal Road, Springfield Va. 22151

PB 228 046

THE EFFECT OF SURFACE CONFIGURATION ON EVAPORATION FROM A POROUS STREAM MODEL

by

BRUCE ALAN TICHENOR

A THESIS

submitted to

OREGON STATE UNIVERSITY

in partial fulfillment of
the requirements for the
degree of

DOCTOR OF PHILOSOPHY

June 1966

176

Reproduced by
NATIONAL TECHNICAL
INFORMATION SERVICE
U S Department of Commerce
Springfield VA 22151

The work on Aim 1 of the research project "Factors Influencing Stream Temperatures" was done by Bruce Alan Tichenor, Ph. D. student in the Department of Civil Engineering who graduated with a Ph. D. Degree in 1966.

This thesis is submitted as the results obtained under this grant in pursuance of Aim 1, "The Effect of Surface Configuration on Evaporation from a Porous Stream Model."

The Principal Investigator on this project was John Seaders, Associate Professor of Civil Engineering at Oregon State University.

AN ABSTRACT OF THE THESIS OF

Bruce Alan Tichenor for the **Ph. D** in **Civil Engineering**
(name) (Degree) (Major)

Date thesis is presented March 31, 1966

Title THE EFFECT OF SURFACE CONFIGURATION ON EVAPORATION FROM A POROUS STREAM MODEL

Abstract approved ____________________________
(Major Professor)

A stream's temperature is a major factor in its ability to support fish life and to be utilized for other beneficial purposes. The approach most generally used for stream temperature prediction is the Energy-Budget method, which involves the inventory of all the energy entering and leaving the stream. A temperature prediction study on the coast fork of the Willamette River was conducted in 1963 using this method. Subsequent analysis of the data revealed a poor correlation between predicted and measured stream temperatures at night. Due to the relative magnitudes of the terms in the Energy-Budget, it became evident that the term for evaporative heat loss was in error. Since the evaporative heat loss can be computed directly from a value of evaporation rate, one can state that an accurate determination of evaporation rate is essential to the successful analysis of any Energy-Budget Equation applied to streams.

B 11 7

Several types of mass transfer equations, both theoretical and experimental, have been developed for predicting evaporation from lakes and reservoirs. There has not yet been developed, however, a method which relates specific stream parameters, such as surface configuration and stream turbulence, to evaporation. Therefore, as an initial step in the search for needed knowledge, this thesis undertook as its purpose the evaluation of the effect of surface configuration on the magnitude of evaporation from a modeled stream surface.

There are three types of mass transfer equations which are commonly used for the prediction of evaporation. The most common type is a general equation which employs Dalton's relationship between evaporation and vapor pressure differences together with a correction for wind velocity. The other two types (the discontinuous and continuous mixing approaches) are based upon the structure of the turbulent boundary layer above the evaporation surface. The equations of Norris and of Thornthwaite and Holzman, based on the discontinuous mixing approach, and the equations of Sutton, based on the continuous mixing approach, were evaluated using experimental data to establish their utility as tools for predicting stream evaporation.

The research involved the measuring of evaporation rates from porous stream models of five surface configurations placed in a low velocity wind tunnel and the measurement of physical parameters which are included in various evaporation equations. Several test conditions were used for each surface configuration.

The analysis of the data had two parts. First, the evaporation rates computed from several existing equations were compared to measured evaporation, and second, an effort was made to establish a relationship between surface configuration and evaporation. Several statistical tests were used in these analyses, and the following conclusions were reached:

1. Equations based on the structure of the overlying air may be used to predict evaporation rates, without any specific knowledge concerning the stream surface configuration.

2. Of the three theoretical methods tested, Sutton's method gave the best correlation between computed and measured evaporation rates. The method of Norris was next, followed by the equation of Thornthwaite and Holzman.

3. The mass transfer coefficient, B', in an experimentally developed equation of the form $E = B' u(e_s - e_a)$ is related to model surface configuration. Using wave steepness, H/L, as a characteristic of model surface configuration, B' increases as H/L increases. Therefore, when an equation of this form is used, evaporation rate increases as wave steepness increases.

4. The failure during the 1963 study made on the coast fork of the Willamette River to compute accurate stream temperatures

during nighttime periods can be attributed, at least in part, to errors in underestimating the evaporation rates.

5. Surface configuration does affect evaporation rates from streams, but its full quantitative evaluation awaits further research.

APPROVED:

Professor of Civil Engineering

In Charge of Major

Acting Head of Department of Civil Engineering

Dean of Graduate School

Date thesis is presented March 31, 1966

Typed by Gail Dailey

ACKNOWLEDGEMENTS

The author herewith acknowledges the support received from the following individuals and organizations.

The National Defense Education Act, Title IV, for financial assistance during the first three years of graduate training.

The United States Public Health Service, Division of Water Supply and Pollution Control, for financial aid during the last year of graduate training in the form of a traineeship under Grant No. WP-25-04 and for financial support of Research Grant No. 00684-01 (Factors Influencing Stream Temperatures) under which this thesis research was carried out.

The Department of Mechanical Engineering for the use of their wind tunnel facilities in the Aero Laboratory.

Mr. Fred J. Burgess, Professor of Civil Engineering, for his help and guidance as the author's major professor.

Dr. Edwin J. Hughes, Assistant Professor of Statistics, for his assistance in checking the author's assumptions and methods with regard to the statistical analyses used.

The Department of Civil Engineering staff and fellow graduate students for their guidance and companionship.

Finally, special thanks are given to the author's wife, Jayne, for her typing of draft copies and for her unending confidence, and to

the author's two daughters, Karen and Kristin, for their affection and for the lighter moments which they continually provided.

TABLE OF CONTENTS

Page

INTRODUCTION 1

PURPOSE AND SCOPE 17

MASS TRANSFER THEORY AS APPLIED TO WATER SURFACES 18

- General 18
- Atmospheric Structure 20
- Discontinuous Mixing 23
- Continuous Mixing 27
- Surface Roughness of Lakes and Streams 31
- Computation of Stream Evaporation 34

SELECTION OF RESEARCH MODE 39

- Previous Use of Saturated Surfaces 39
- Preliminary Investigations 43

DESCRIPTION OF EXPERIMENTAL FACILITIES 54

- Porous Stream Model 54
- Wind Tunnel 56
- Velocity Instrumentation 58
- Temperature Instrumentation 58
- Relative Humidity Instrumentation 59
- Water Supply 61
- Evaporation Measurement 61
- Other Instruments 63

EXPERIMENTAL PROCEDURES 66

COMPUTATIONS AND RESULTS 75

- Data Reduction 75
- Preliminary Calculations 77
- Computations Using Existing Equations 80
- Development of Experimental Equations 85

ANALYSIS AND DISCUSSION OF RESULTS 100

- Comparison of Existing Equations 100

Page

Analysis of Experimentally Developed Equations 105
Application of Results to Real Streams 121

CONCLUSIONS 124

RECOMMENDATIONS FOR FUTURE RESEARCH 126

BIBLIOGRAPHY 127

APPENDICES

A Thermistor Placement 132
B Example of Computational Methods 132
C Data Summary 147
D Evaporation Equations Not Given in the Text 153
E Instrument Specifications 156
F Photographs of Four Sine Wave Surfaces 159

LIST OF FIGURES

Figure		Page
1	Installed Model Surfaces	57
2	Wind Tunnel Test Section	57
3	Hot-wire and Relative Humidity Probe	60
4	Water Distribution and Evaporation Measuring System	62
5	Arrangement of Tubing for Water Supply and Evaporation Measurement	64
6	Holder for Linear Motion Potentiometer	64
7	Overall View of Test Facilities	65
8	Evaporation Computed Using the Equations of Norris vs. Measured Evaporation	85
9	Evaporation Computed Using the Equation of Thornthwaite and Holzman vs. Measured Evaporation	86
10	Evaporation Computed Using the Equations of Sutton vs. Measured Evaporation	87
11	Evaporation Computed Using the Equation of Delay and Seaders vs. Measured Evaporation	88
12	Evaporation Computed Using the Equation of Cermak and Koloseus vs. Measured Evaporation	89
13	Evaporation Computed Using Equation 4 vs. Measured Evaporation	96
14	Evaporation Computed Using Equation 21 vs. Measured Evaporation	97
15	Evaporation Computed Using Equation 5 vs. Measured Evaporation	98

Figure **Page**

16 Evaporation Computed Using Equation 22 vs. Measured Evaporation 99

17 Curves of $E = (A + Bu)(\Delta e)$ for the Five Model Surfaces 106

18 Curves of $E = B'u(\Delta e)$ for the Five Model Surfaces 107

19 Curves of $E = a\,(u)^{b}(\Delta e)$ for the Five Model Surfaces 108

20 Curves of $N = \alpha R_{*}^{\beta}$ for the Five Model Surfaces 109

21 The Sheltering Effect 119

LIST OF TABLES

Table		Page
1	Energy Budget Terms for Tiller Reservoir from July 1 to July 10	11
2	Previous Use of Saturated Surfaces	40
3	Surface Configurations	47
4	Number of Profile Sets	66
5	Empirical Coefficients and Correlation Indexes	94
6	Res. SS/n for Figures 8 - 16	101
7	Test of Homogeneity of Regression Coefficients	111
8	Test of Homogeneity of Adjusted Means	112
9	t-Tests for A Values Equal to Zero	114
10	Tests of Individual Degrees of Freedom of B'	116

THE EFFECT OF SURFACE CONFIGURATION ON EVAPORATION FROM A POROUS STREAM MODEL

INTRODUCTION

During recent years there has been a growing concern among fisheries biologists and water resource planners in the Pacific Northwest about the temperatures in many of the streams in the region. Water temperature is an important water quality parameter when considering agricultural and industrial water use, pollution abatement, water supply treatment, and stream biota.

In the Pacific Northwest the most important aspect of the water temperature problem is its influence on the stream biota, and especially upon salmon, and other species of fish life present. The concern of the water resource planner is directed at the maximum temperatures which many of the streams in the region attain during the summer months of July and August. In Oregon, thermograph stations located on the Rogue and Umpqua Rivers have shown that excessively high water temperatures in the range of 76°F to 81°F do exist at times during these months.

Biologists indicate that there is a temperature zone of about 15°F within which each species of fish may live in relative comfort. Even though this range does exist, a sudden temperature change of a small magnitude may prove lethal (25). In the case of some species of trout this change is only four to six degrees Fahrenheit. There is also a maximum temperature at which fish can live. For trout, various researchers have set the maximum temperature limit in the range of from 75 °F to 85 °F. Any time the maximum temperature limit is exceeded, death is imminent. Even in the temperature is too high for only a short period of time, the results could be serious in terms of lost fish life.

Certain species of fish can survive changes in their thermal environment by acclimatization, but these are usually the coarse fish whose commercial and recreational value is negligible by Pacific Northwest standards.

One of the reasons that temperature is such a vital factor in the fish life of a stream involves the dissolved oxygen content of the water. It is a well known fact that as the temperature of a body of water increases, the ability of that water to hold oxygen decreases. For example, at 20°C water becomes saturated with oxygen at a concentration of 9.17 mg/l, while at 30° C this saturation value is only 7.63 mg/l.

As water temperature increases, the metabolic rate and corresponding oxygen requirements of fish and other aquatic organisms also increase. This increased metabolic rate follows vant' Hoffs Law which implies that the rate at which respiration and other oxidation processes proceed is approximately doubled or even tripled for every 10° C rise in water temperature.

These two factors of decrease in available oxygen and increase in metabolic reaction rate at increased temperatures combine to render a stream less compatible to fish life at high stream temperatures. At low water temperatures in the range of zero to four degrees Centigrade, a dissolved oxygen level of one to two mg/l is sufficient for many species of fresh water fish. When the temperature reaches 15-20° C, three mg/l of dissolved oxygen is often not enough to sustain fish life. At such high temperatures, oxygen levels as high as five mg/l are sometimes required to support minimum activity. Laberge (25, p. 537) states that The Aquatic Life Advisory Committee of the Ohio River Valley Water Sanitation Commission suggests stringent dissolved oxygen criteria. This committee states that for warm water fish not less than five mg/l of dissolved oxygen should be maintained during at least 16 hours of any 24 hour period. The dissolved oxygen content may be less than five mg/l for a period not to exceed three hours within any 24 hour period, but at no time should be less than three mg/l. For coarse fish they recommend five mg/l, but for eight hours out of a 24 hour period it may go down to two mg/l.

Another effect of stream temperature on the stream biota, other than dissolved oxygen, is that of synergistic action. Synergism can be defined as the simultaneous action of separate agents which, together, have a greater total effect than the sum of their individual effects. In reference to the problem of stream temperatures, synergistic action refers to the fact that as the water temperature increases the toxicity of poisonous materials in the stream is increased, and the susceptibility of the fish to many diseases is also increased. For example, a ten degree Centigrade rise in water temperature doubles the toxicity to fish of potassium cyanide, and an eight degree Centigrade rise triples the toxicity of o-xylene (25). Laberge (25, p. 537) also states that,

> Since the temperature effect on toxicity varies with each substance and with concentrations of any specific material, no formulation of a hard and quick rule may be made in determining this temperature effect.

Since domestic and industrial waste discharges are becoming more and more numerous on our nation's streams, the synergistic action between water temperature and toxicity is a relatively common occurrence. Laberge also points out that in polluted waters, fish kills have accompanied a small rise in stream temperature which may have been relatively harmless in an unpolluted stream where toxic substances were absent. The reverse of this is also true. That is, toxic substances may be of such a concentration as to be unable to cause fish kills without a corresponding higher temperature.

Even though the thermal environment of a stream is an important factor in the dynamics of fish growth and behavior, diseases play an even greater role. Some types of myxobacteria are pathogenic to fish. For example, the species Chondrococcus columnaris is one of the most destructive of all fish pathogens (43). The virulence of this organism increases rapidly at higher temperatures, and this microbe has often been responsible for extensive and destructive epidemics in both trout hatcheries and natural fish populations.

While a stream's ability to maintain a healthy biota is a most important consideration, it is by no means the only factor which the water resources manager should consider with respect to a stream's thermal environment. One must also be concerned with the effect of water temperature on:

1. the cost of treating domestic water supplies,
2. the planning and justification of industries requiring large quantities of water for cooling and other purposes, and
3. the ability of a stream to assimilate both domestic and industrial wastes.

Jaske (16) also points out that with the advent of nuclear power production, the spent cooling water from such facilities will make higher river temperatures an increasingly important problem. Therefore, more attention will have to be given to the legal aspects of thermal pollution.

Finally, since its effect is so important, temperature must be included as a parameter in all research involving water. A knowledge of the effect of temperature on the physical, chemical, and biological processes which occur in water will permit the water resources manager to effectively plan for the full beneficial use of this valuable natural resource.

The preceding discussion has given evidence that a stream's thermal environment is a major factor in the ability of any stream to support fish life and to be utilized for other beneficial purposes.

In many of the streams in the Pacific Northwest maximum stream temperatures are becoming alarmingly high, and remedial steps should be taken. An obvious method of lowering the high summer stream temperatures would be the release, from upstream reservoirs, of cold water at such a temperature and rate that downstream temperatures would be lowered to a desired predetermined level. The use of multiple level outlets for deep storage reservoirs would permit the discharge of water from different depths, and thus, due to the thermal stratification of reservoirs, make possible the selection of water at different temperatures.

This use of stored water for improvement of downstream temperatures will require that reservoir management agencies can determine:

a) the quantity of water required,

b) the temperature at which this water should be released, and

c) the time at which the release should occur.

A complete understanding of these three factors is necessary for successful operation of reservoirs for the improvement of the downstream thermal environment.

Development of a method for predicting stream temperatures in terms of river flow, travel time, and meteorological factors would make it possible to compute the parameters a, b, and c above. The Energy-Budget Method, now under intensive investigation by Oregon State University, the U. S. Corps of Engineers, the Oregon State Water Resources Board, and others, offers a solution to the problem of stream temperature prediction. The Energy-Budget Method, sometimes referred to as the Heat-Budget, involves the inventory of all the energy entering and leaving the stream. This energy sum can then be converted into a temperature change. The Energy-Budget takes the form of the following equation:

$$Q_T = Q_S - Q_B \pm Q_H \pm Q_A - Q_E \qquad (1)$$

where,

Q_T = net gain or loss of energy;

Q_S = net incoming solar radiation;

Q_B = net effective back radiation from the water surface;

Q_H = energy exchange by conduction from water to air, or from air to water;

Q_A = energy advected into the water by tributary streams, precipitation, ground water inflow, etc.;

Q_E = energy loss due to evaporation, or gain due to condensation.

The computation of a Heat-Budget for a stream involves many and varied meteorological parameters. These include solar radiation, back radiation, reflection, cloud cover, wind, relative humidity, air temperature, and water temperature. Since the solution of the Energy-Budget Equation requires a value for water temperature, its use for predicting water temperature necessitates a trial and error solution. Once Q_T is determined, it may be converted into an actual temperature change by considering the river discharge, surface area, and latent heat of vaporization of water.

Several good references are available on the Energy-Budget Method, its assumptions and applications. These include Anderson (6), Raphael (39), Oregon State Water Resources Board (33), and Velz and Gannon (50), and no attempt will be made to describe in detail its various theoretical and empirical formulas and its computational procedures. It should be mentioned, however, that in the summer of 1963 a computer program was developed at Oregon State University for the Energy-Budget Method (5). Written in IBM Fortran I symbolic language, this program proved most effective in supplanting the tedious manual computations that were formerly required.

The Energy-Budget has been used extensively for predicting lake and reservoir evaporation (6, 39, 20). Its application for prediction of stream temperature has been somewhat more limited. Burt (10, 11), developed Heat-Budget terms for selected sites on the Snake River. McAlister (30) conducted a study on the Rogue below the proposed Lost Creek Dam using the Heat-Budget Method. The studies of Raphael (39), Velz and Gannon (50), and the Oregon State Water Resources Board (33), which have already received mention, also dealt with the use of the Energy-Budget on streams. The Twelfth Pacific Northwest Symposium on Water Pollution Research dealt with the problems of water temperature, and its proceedings include several pertinent studies (17, 40, 8, 51). These few examples are presented to show that the Heat-Budget Method is an increasingly important tool for predicting stream temperatures, reservior evaporation, and for determining the thermal structure of water bodies.

An examination of the basic Energy-Budget Equation (equation 1) shows that five terms must be accurately evaluated if one is to determine a "balanced" Heat-Budget. To review, Q_S and Q_B take into account the effect of both incoming short wave and outgoing long wave radiation. Q_A accounts for the energy brought in by tributary inflows, and Q_H and Q_E account for the energy exchange between the water and the air through the mechanisms of conduction, evaporation, and condensation. In evaluating these five quantities, one must rely on measured data, theoretical equations, and empirical formulas. With proper instrumentation for evaluating the various meteorological parameters, one should theoretically be able to conduct a Heat-Budget study on any body of water.

The terms of the Heat-Budget are evaluated by different physical means. Q_S, the net incoming solar radiation, can be obtained from direct measurement by a pyrheliometer or computed from empirically derived formulas. The term for back radiation, Q_B, is based upon the well known Stefan-Boltzmann relationship and can be accurately evaluated. The advected energy term, Q_A, is evaluated for influent streams, and is therefore included only when the main stem of a river is intersected by a tributary. It should also be noted that the term for advected energy is based upon hydrological rather than meteorological considerations. The other terms, Q_H and Q_E, which evaluate the energy exchange due to conduction and evaporation, depend upon the characteristics of the water surface and of the ambient atmosphere. Of these two terms, the value of Q_E is usually many times the absolute magnitude of Q_H.

An example of the magnitude of the terms in the Heat-Budget is given by Delay and Seaders (17). Computations for the Tiller Reservoir site on the Umpqua River during the period from July 1 to July 10 yielded the following values for Q_S, Q_B, Q_E, and Q_H (Table 1). The values of Q_A are not given since they are based on non-meteorological considerations, and are not of importance here since the object of these numbers is to gain an insight about their relative magnitudes.

Table 1. Energy-Budget Terms for Tiller Reservoir from July 1 to July 10

Time	Q_S	Q_B	Q_E	Q_H
0000-0700	0	2,770	1,015	290
0700-1200	1,170	1,105	1,865	0
1200-1700	1,170	745	3,905	-745
1700-2400	0	2,065	3,710	465

Values are in BTU/ft^2-day.

It is seen from these values that during the two periods when the value of Q_S is zero, the value of Q_E has a considerable magnitude. It is also evident that the magnitude of Q_E is many times greater than the magnitude of Q_H. Even during periods of sunlight when Q_S values are not zero, values of Q_E can reach high magnitudes. It must be emphasized again that the values in Table 1 are given only to show the relative magnitudes of the terms in the Heat-Budget, and they should not be considered here in any other light.

In the summer of 1963, an investigation was conducted on the coast fork of the Willamette River in western Oregon by several cooperating agencies, including the Oregon State Water Resources

Board, U.S. Corps of Engineers, and Oregon State University. This study was conducted over a three day period and included measurement of stream travel time, meteorological parameters, and stream temperature. The stream flow was controlled by regulating the releases from Dorena Dam. The travel time and meteorological information which was gathered was utilized in a Heat-Budget analysis to calculate river temperatures. These calculated temperatures were then compared with the actual temperature readings in order to judge the accuracy of the Heat-Budget analysis. Such a comparison showed good correlation during the day and poor correlation at night.

This deviation of the computed stream temperature from the actual stream temperature during periods of no solar radiation must be considered in the light of the relative magnitudes of the terms in the Heat-Budget. Table 1 shows that during periods of sunlight the relative magnitudes of Q_S, Q_B, and Q_E are similar. However, during periods of darkness, when Q_S is zero, the relative magnitudes of Q_B and Q_E are similar, and Q_H also has a greater effect on the total heat budget. Since the value for back radiation, Q_B, can be calculated with good accuracy, an accurate determination of Q_E and Q_H is necessary if one is to obtain reliable results from the Heat-Budget analysis. Therefore, one can assume that the values obtained for Q_E and Q_H during the previously mentioned study were in error, and these errors caused the computed stream temperature to vary from the measured stream temperature. The reason for these errors lies in the equation used to compute evaporative heat losses.

Furthermore, if errors are made in the computation of Q_E, then errors are also made in computation of Q_H, since these two terms are intimately related by the Bowen Ratio. In fact, Q_H is computed from Q_E by employing the Bowen Ratio. The Bowen Ratio, R, is equal to the conductive heat loss, Q_H, divided by the evaporative heat loss, Q_E, (i.e. - $R = Q_H / Q_E$). Expressed in terms of the ratio of sensible heat loss to latent heat loss, the Bowen Ratio becomes, according to Duttweiler, et al (19):

$$R = C_B \frac{T_o - T_a}{e_o - e_a} \frac{P}{1000} \qquad (2)$$

where

R = the Bowen Ratio;

C_B = a coefficient which ranges from 0.58 to 0.66 depending on surface roughness and atmospheric conditions; 0.61 is used most commonly;

T_o = water surface temperature, °C;

T_a = ambient air temperature, °C;

e_o = saturation vapor pressure at the temperature of the water surface, millibars;

e_a = vapor pressure of the ambient air, millibars;

P = atmospheric pressure, millibars.

Therefore, the Bowen Ratio can be computed without a specific knowledge of either Q_E or Q_H. The sign of the Bowen Ratio indicates the direction of flow of the sensible and latent heat. If the sign is positive, both Q_H and Q_E are operating in the same direction, and, conversely, if the sign is negative Q_H and Q_E are operating in opposing directions.

Three cases are possible under specific conditions:

1) $T_o > T_a$, $e_o > e_a$, R is positive.
Evaporation occurs, thus the latent heat flows from the water to the air; the conductive heat flow is also from the water to the air.

2) $T_o < T_a$, $e_o > e_a$, R is negative.
Evaporation occurs, thus the latent heat flows from the water to the air; the conductive heat flows in the opposite direction, from the air to the water.

3) $T_o < T_a$, $e_o < e_a$, R is positive.
Condensation occurs, thus the latent heat flows from the air to the water; the conductive heat flow is also from the air to the water.

It should be noted that the case of $T_o > T_a$ and $e_o < e_a$ can never occur, since if the water temperature exceeds the ambient air temperature, the saturation vapor pressure at the water temperature will always exceed the vapor pressure of the ambient air, even if the air is saturated.

Since, as previously mentioned, the values of Q_H and Q_E are the only terms in the Heat-Budget Equation which can not be obtained with good accuracy, and since Q_H can be computed from a knowledge of Q_E and the Bowen Ratio, it is evident that one must have an accurate measure of Q_E in order to obtain a balanced Heat-Budget. Since Q_E can be obtained directly from a value of evaporation rate, one can therefore state that an accurate determination of evaporation rate is essential to the successful analysis of any Heat-Budget Equation applied to streams.

Several methods of predicting or computing evaporation are available. These include:

a) Pan Evaporation,

b) Heat-Budget Analysis, and

c) Mass Transfer Analysis.

Pan evaporation techniques involve the correlation between the evaporation from a standard pan and that from another body of water. While such a method may be applicable to lakes, ponds, and other standing bodies of water, its use as a tool for computing evaporation from streams is highly questionable. If it were possible to simulate in a pan the type of water movement associated with a stream and various Heat-Budget parameters, then the pan evaporation method might be applicable to stream evaporation prediction. As of this time, however, such a method has not even been investigated in more than a cursory manner.

The Heat-Budget Method is a powerful tool for predicting evaporation from lakes and reservoirs. Anderson's (6) work on Lake Hefner is a classic example. This method, however, presupposes a knowledge of the water temperature. Since the reason for employing the Heat-Budget Method on streams is the evaluation of stream temperature, obviously one must use another method for predicting the heat loss due to evaporation.

The shortcomings of the above methods leave mass transfer analysis as the only approach now available with which one can hope to obtain an accurate measure of evaporation rates from streams, when the heat loss due to evaporation is to be incorporated into a Heat-Budget Equation for predicting stream temperature.

PURPOSE AND SCOPE

Several types of mass transfer equations, both theoretical and experimental, have been developed for evaporation from lakes and reservoirs. These equations account for such factors as air and water temperature, humidity gradients, velocity gradients, atmospheric pressure, surface roughness parameters, and a myriad of other meteorological and hydrological parameters. There has not yet been developed, however, a method which relates specific stream parameters, such as surface configuration and stream turbulence, to evaporation. Therefore as an initial step in the search for needed knowledge, this thesis undertakes as its purpose the evaluation of the effect of surface configuration on the magnitude of evaporation from a modeled stream surface.

The study will be conducted in a low speed wind tunnel using saturated porous stream models of several surface configurations. The analysis of the data obtained during the study will have two parts:

1. Some existing evaporation equations will be evaluated and compared to establish their utility as tools for estimating stream evaporation.

2. The data will be analyzed to develop a relationship between surface configuration and stream evaporation.

MASS TRANSFER THEORY AS APPLIED TO WATER SURFACES

Three types of mass transfer equations are commonly used for the prediction of evaporation. They are:

1. the general mass transfer equation which employs Dalton's relationship between evaporation and vapor pressure differences together with a correction for wind velocity,
2. the equation based on the mixing length or discontinuous mixing approach, and
3. the equation based on the continuous mixing theory.

General

In the early nineteenth century, Dalton established a relationship between evaporation and vapor pressure differences. It can be expressed as:

$$E = x(e_s - e_a) \qquad (3)$$

where,

E = evaporation rate;

e_s = saturation vapor pressure at the temperature of the water;

e_a = vapor pressure of the ambient air;

x = empirical coefficient.

This equation is valid only in the absence of wind, and therefore has little practical value. However it does emphasize that a difference in vapor pressure is the driving force for the mass transfer of water vapor commonly expressed as evaporation.

If a wind velocity correction is added to this equation, the resulting formula assumes a more useful form:

$$E = (A + Bu)(e_s - e_a) \qquad (4)$$

where,

E, e_s, e_a = previously defined;
u = wind velocity;
A, B = empirical coefficients.

Several equations of this type have been developed. Among the most well known are the equations of Meyers (28, p. 168), Horton (28, p. 168), and Rohwer (41, p. 21). These equations are listed in the Appendix.

Horton's equation is especially interesting in that it uses a power function of the wind speed. It is similar to the following equation:

$$E = a(u)^b (e_s - e_a) \qquad (5)$$

where,

E, u, e_s, e_a = previously defined;
a, b = empirical coefficients.

Equations 4 and 5 are general mass transfer equations which, with minor changes, have been used extensively for evaporation prediction. It should be emphasized, however, that the solution of these types of equations requires that the wind speed always be taken at the same height above the water surface. If this is not done, the computed evaporation can not be expected to be consistent with the actual water vapor transfer, since wind velocity changes with vertical elevation. Due to this relationship and the fact that mass transfer coefficients are empirically derived, such equations are not generalized and the use of a specific formulation like 4 or 5 can not be expected to give accurate results when applied to every situation.

Atmospheric Structure

As a prelude to considering the discontinuous and continuous mixing approaches to evaporation, it is necessary to discuss briefly the structure of the atmosphere above land and water surfaces. For air flow over land, three layers are believed to exist. They are, from the land upward:

1. the laminar layer,
2. the turbulent boundary layer, and
3. the outer layer of frictional influence.

The processes of mass transfer occur in the first two layers. In the laminar layer, only a few millimeters thick, wind velocity, humidity, and temperature vary linearly with height. The mass transfer of water vapor through this layer has been described as a molecular process. In the turbulent boundary layer, wind speed, humidity, and temperature vary exponentially with height. The mass transfer of water vapor through this layer is a turbulent process.

When the air flow is over water, a more complicated situation arises. Due to the waves generated by the wind, various investigators (7) feel that another layer occurs near the tops of the waves. This "intermediate layer" is positioned between the laminar and turbulent layers.

In determining the wind profile in the turbulent boundary layer it is necessary to know whether the flow is smooth or rough from a hydrodynamic standpoint. A hydrodynamically smooth surface exists when roughness elements do not protrude upward through the laminar layer, when they do the surface is said to be hydrodynamically rough. For a "smooth" surface, Sutton (44, p. 80) gives the equation for the velocity distribution in the turbulent layer:

$$\frac{u_z}{u_*} = \frac{1}{k_o} \ln z + \text{constant} \qquad (6)$$

where,

u_z = mean velocity of the air at height z, ft/sec;

u_* = shear velocity, ft/sec;

z = height above the surface, ft;

k_o = von Karman's constant = 0.4.

Sutton (44, p. 82) reports the equation for the velocity distribution in the turbulent boundary layers under hydrodynamically rough conditions as:

$$\frac{u_z}{u} = \frac{1}{k_o} \ln \left(\frac{z}{z_o}\right) \qquad (7)$$

where,

u_z, u_*, k_o, z = previously defined;

z_o = roughness parameter, ft.

By substituting logarithms to the base ten for the natural logarithms and substituting the value for k_o in equation 7, Cermak and Koloseus (13, p. 8) obtain:

$$\frac{u_z}{u_*} = 5.75 \log\left(\frac{z}{z_o}\right). \tag{8}$$

Two of the terms in the proceeding equations, u_* and z_o, require further discussion. The shear velocity, sometimes called the friction velocity is defined as:

$$u_* = \sqrt{\tau_{o/\rho}} \tag{9}$$

where,

u_* = shear velocity, ft/sec;

τ_o = shearing stress at the surface, $\mathrm{lb/ft^2}$;

ρ = air mass density, $\frac{\mathrm{lb - sec^2}}{\mathrm{ft^4}}$.

According to Sutton (44), this relationship comes from the fact that in turbulent motion the mean velocity is proportional to the square root of the shearing stress.

The roughness parameter, z_o, is related to the size of the roughness elements, but the nature of this relationship is, as yet, undefined. However, roughness relationships have been explored by Nikuradse, in his work on pipe flow, which related z_o to equivalent sand roughness (13, p. 9):

$$z_o = \epsilon/30 \tag{10}$$

where,

z_o = roughness parameter, feet;

ϵ = equivalent sand roughness, feet.

This relationship requires knowledge of ϵ, which is a relative measure of roughness. Since z_o can vary for different wind conditions over the same surface, to call it a roughness parameter is misleading since a surface of the same "roughness" can exhibit several values of z_o under various wind conditions. By plotting the logarithm of height versus velocity for a specific velocity profile, one can extrapolate the linear portion of the resulting curve (i.e. - the turbulent boundary region) to the point where the velocity is zero. The value of the intercept at this point is z_o. Thus, z_o is merely a value of height whose magnitude satisifies the theoretical requirements of the wind laws in the turbulent boundary region.

Discontinuous Mixing

The discontinuous mixing approach to evaporation is based on turbulence theory developed by Prandtl and Schmidt. According to Anderson, Anderson, and Marciano (7, p. 5):

> Prandtl visualizes mixing as a discontinuous process, whereby a mass of fluid called an eddy leaves its environment and moves to a new level, there mixing with its new surroundings and eventually losing its identity. The mean distance traveled by the eddy during this

> process, the hydrodynamical counterpart of the molecular free path, is regarded as the mixing length.

This theory is the basis for the equations describing vertical wind profiles in the turbulent layer under conditions of adiabatic stratification (see equations 6, 7, and 8).

Several researchers give evidence which supports the theory that close to the ground the diffusion of water vapor and momentum are nearly the same (7, p. 5, 38, p. 10-12). The mixing length theory can be used to analyze the transfer of momentum, and an analogy between water-vapor transfer and momentum transfer has been established. These relationships have permitted work to proceed in developing equations from the mixing length theory suitable for computation of evaporation.

The basic evaporation equation based on the mixing length approach is (7, p. 6):

$$F = \frac{-0.623\, \rho K_z}{P} \frac{\partial e}{\partial z} \qquad (11)$$

where

F = point evaporation per unit area, gm/cm^2 - sec;

ρ = density of the air, gm/cm^3;

K_z = eddy vapor diffusivity in the vertical direction, cm^2/sec;

P = atmospheric pressure, gm/cm-sec^2;

e = vapor pressure, gm/cm-sec^2;

z = height above the surface, cm;

$\frac{\partial e}{\partial z}$ = vapor pressure gradient.

The solution of this equation requires a definition of K_z and an estimation of $\frac{\partial e}{\partial z}$.

Several different approaches to the solution of equation 11 have been taken, including the work of Sverdrup (46), Norris (32), and Thornthwaite and Holzman (49). The work of both Sverdrup and Norris culminated in essentially equivalent equations, so for the sake of brevity, the equation of Norris will be given in lieu of Sverdrup's work. Sverdrup's equation can be found in the Appendix.

Norris developed the following evaporation equation for a water surface roughened by waves (32, p. 8):

$$E = \rho k_o \gamma_a \Gamma_b (q_s - q_b) u_a \qquad (12)$$

where,

E = evaporation rate, lb/ft^2-sec;

ρ = air density, lb/ft^3;

k_o = von Karman's constant, 0.4;

q_s = specific humidity at the temperature of the water;

q_b = specific humidity at a height b above the surface;

u_a = wind speed at a height a above the surface, ft/sec;

$$\gamma_a = \frac{u_*}{u_a} \quad \text{(smooth surface);}$$

$$\gamma_a = \frac{k_o}{\ln\left(\frac{a}{z_o}\right)} \quad \text{(rough surface);}$$

$$\Gamma_b = \left(\ln \frac{b}{z_o}\right)^{-1} \text{(smooth surface);}$$

$$\Gamma_b = \left(\ln \frac{b}{\alpha z_o}\right)^{-1} \quad \text{(rough surface);}$$

where $\alpha = 2.41$.

The subscripts a and b denote heights above the water surface within the turbulent boundary region. It should also be noted that $(q_s - q_b)$ is directly proportional to $(e_s - e_b)$.

Thornthwaite and Holzman's equation is given by Anderson, Anderson, and Marciano as (7, p. 25):

$$F = \frac{0.623\rho\, k_o^2\, (e_1 - e_2)\, (\overline{u}_2 - \overline{u}_1)}{P \ln \frac{z_2}{z_1}\; \ln \frac{z_2\,(1 - sz_1)}{z_1\,(1 - sz_2)}} \qquad (13)$$

where,

F, P, ρ, k_o = previously defined;

e_1, e_2 = vapor pressure at heights z_1 and z_2, gm/cm - sec^2;

$\overline{u}_1$, $\overline{u}_2$ = average wind speed at heights z_1 and z_2, cm/sec;

z_1, z_2 = height above water surface, cm;

s = atmospheric stability parameter .

The subscripts 1 and 2 denote heights above the water surface within the turbulent boundary region.

Although equations 12 and 13 were both derived from the same basic discontinuous mixing evaporation equation (equation 11), there is a substantial difference in their final form. Norris (32) developed his equation using a vapor pressure difference, $(q_s - q_b)$ or $(e_s - e_b)$, between the water surface and a point in the turbulent boundary region as the driving force for evaporation. Thornthwaite and Holzman (49), however, used as a driving force the difference in vapor pressure, $(e_1 - e_2)$, existing between two points within the turbulent boundary layer. The effect of these two different forms of the evaporation driving force on the computed evaporation will be discussed later in this thesis.

Continuous Mixing

While the discontinuous mixing theory assumes the existence of three layers over a water surface (i.e. - laminar, intermediate, and turbulent), the continuous mixing approach assumes that only the turbulent layer exists. This layer is assumed to extend down to the water surface. According to Sutton (45, p. 702):

> The basic idea of the present treatment (i.e. - continuous mixing) is that mixing by turbulence should not be regarded as the kind of "explosive" action contemplated in these theories (i.e. - mixing length theories), but rather as a continuous process which takes place along the whole path of the eddy.

Anderson, Anderson, and Marciano (7, p. 5) state that:

> The continuous mixing theory considers an eddy as a mass of fluid which moving as a discrete body, blends continuously with its surroundings. There is no waiting before mixing takes place. As the surroundings change there is a continuous sharing of the transferable property and a gradual change in the excess or deficit originally possessed by the eddy, until it is indistinguishable from its surroundings and mixing is complete. Since the process is continuous, an eddy may move up through a level, momentarily lose its identity at that level, and continue upward as a new eddy, never having been at rest relative to its environment.

The major work on the continuous mixing approach to evaporation has been done by Sutton (45) who considers his contribution to be an extension of Taylor's analysis of "Diffusion by Continuous Mixing" (48). According to Sutton (45, p. 702), Taylor's Theory, based on turbulence statistics, considers eddy motion to be a ". . . succession of connected movements" instead of " . . . a series of independent impulses."

Anderson, Anderson, and Marciano give the basic evaporation equation of continuous mixing in integral form as (7, p. 6):

$$E = \int_o^x \int_o^y F(x)\, d\,x\, dy \qquad (14)$$

where,

E = total evaporation from a rectangular strip of downwind length x and crosswind length y.

The evaporation function, F (x) is:

$$F(x) = \lim_{z \to 0} \left(- K_z \, \partial\psi/\partial z \right) \qquad (15)$$

where,

F, K_z, z = previously defined;

ψ = water vapor content of the air, gm/cm^3.

The solution of equations 14 and 15 is, to the non-mathematician, extremely complicated. By using modified Bessel functions and Weber's exponential integral, Pasquill (34) expanded on Sutton's work yielding a set of equations involving incomplete Gamma functions. These equations, suitable for evaporation computation, are reported by Anderson, Anderson, and Marciano as (7, p. 10):

$$E(x_o, y_o) = G\bar{u}_1^{(2-n)/(2+n)} x_o^{2/(2+n)} y_o \qquad (16)$$

where,

$E(x_o, y_o)$ = evaporation from a strip x_o by y_o, gm/sec;

x_o = downwind length of the evaporating surface, cm;

y_o = crosswind length of the evaporating surface, cm;

$\bar{u}_1$ = average wind speed at height z, where z is within the linear range of the log-wind profile;

n = a number indicating the degree of turbulence or atmospheric stability.

Also:

$$G = (\psi_o - \psi_i)\left(\frac{2+n}{2-n}\right)^{\left(\frac{2+n}{2-n}\right)} \left(\frac{2+n}{2\pi}\right) \sin\frac{2\pi}{2+n}\, \Gamma\left(\frac{2}{2+n}\right) a^{\left(\frac{2}{2+n}\right)} z_1^{\left(\frac{-n^2}{4-n^2}\right)} \qquad (17)$$

where,

ψ_o = water vapor content of the air at the water surface, gm/cm^3;

ψ_i = water vapor content of the ambient air, gm/cm^3;

z_1 = height above the water surface, cm;

Γ = Gamma function.

And,

$$a = \frac{(\frac{1}{2}\pi\, k_o^2)\ (2-n)^{(1-n)}\, n^{(1-n)}}{(1-n)\ (2-2n)^{(2-2n)}}\ \nu^n\, z_1^{\left(\frac{n^2-n}{2-n}\right)} \qquad (18)$$

where,

k_o = von Karman's constant = 0.4;

ν = kinematic viscosity of the air, cm^2/sec.

This set of equations is applicable to a hydrodynamically smooth surface. Marciano and Harbeck (31, p. 60) indicate that to make these equations suitable for a hydrodynamically rough surface the term for "a" should be expanded to read;

$$a = \frac{(\frac{1}{2}\pi\, k_o^2)(2-n)^{(1-n)}\, n^{(1-n)}}{(1-n)\ (2-2n)^{(2-2n)}}\ z_1^{\left(\frac{n^2-n}{2-n}\right)}\ (\nu + u_* z_o)^n. \qquad (19)$$

The difference between equations 18 and 19 is that the term ν^n in equation 18 is expanded to $(\nu+u_* z_o)^n$ in equation 19. Thus if $z_o = 0$, equations 18 and 19 would be identical.

From the appearance of equations 16-19, it first seems that the continuous mixing approach to evaporation computation is mathematically untenable. A close examination of these equations, however, reveals a heavy dependence on the stability parameter, n. Thus if n can be evaluated, these equations are relatively easy to solve. In a wind tunnel, where adiabatic stratification occurs, n has a value of 0.25 (7, p. 10). Thus, by substituting a value of $n = 0.25$ into these equations, a greatly simplified set of new equations is obtained. These simplified equations will be presented later in this thesis.

Surface Roughness of Lakes and Streams

Even though a great deal of work has been done on computing evaporation from free water surfaces as found in lakes, almost no work has been concerned with evaporation from streams. In order to apply the results of research on lake evaporation to streams, it is first necessary to delineate the difference between lakes and streams with respect to the physical aspects of evaporation.

As previously mentioned, the process of evaporation depends upon the characteristics of the water surface and on the turbulent region immediately above the water surface. The turbulent layer which occurs above the water surface is caused by meteorological factors (i.e. - wind, temperature, atmospheric stability), and its form is affected by the water surface roughness. Since the meteorology of a region is dependent on external factors, the roughness of the water surface is the major evaporation parameter which is a characteristic of the evaporating body. Therefore, the differences in the types of surface roughness of lakes and streams should be examined.

The surface roughness of any body of water is, of course, caused by surface waves. In lakes or ponds the waves which occur are caused by wind. In streams the waves are caused by hydraulic factors, characteristic of the stream itself, and also wind, but in most cases the hydraulic factors are the most important.

In discussing wind waves, it should be recognized that if heavy winds occur, the waves turn into "whitecaps" and the process of water loss includes aerosol separation in addition to evaporation. For purposes of simplicity only winds of less than storm intensity need to be considered, since water lost by aerosol separation is not involved in evaporative heat transfer. According to The Oceans (47, p. 523):

> If a wind blows, waves of all different sizes are present, varying in form from long, gently sloping ridges to waves of short and sharp crests. Superimposed on the gentler waves, which may or may not run in the direction of the wind, series of deformations of the surface appear which, from the point of view of physics, can be termed 'waves' only by stretching the definition.

Thus, there is no easy way of characterizing the surface roughness of a wind swept surface using a clear, concise mathematical formula. Because of this problem, some of the preceding evaporation equations use a hypothetical roughness parameter, z_o, to characterize the water surface. This term does not define surface roughness on the basis of waves, but is derived from the velocity profile above the water surface.

The surface waves of streams are just as complex as the wind waves mentioned above, though their cause is different. Even during periods of no wind, surface waves are present, and in many cases the wind intensity has little or no effect on the form of a stream's waves. For example, a stream flowing through a rocky, mountain gorge has an extremely complicated surface wave pattern which is completely independent of wind. The waves found in such streams are a result of such factors as the slope of the stream bed, the roughness of the channel, and the quantity of water flowing. Here again, there is no mathematical model available which can be used to describe a stream's surface waves using hydraulic parameters.

Thus, both the wind waves on lakes and the waves on streams are difficult to deal with mathematically. In this respect they are similar, but they are not similar with respect to their methods of formation. The waves on lakes are dependent on the wind, while those on streams are not. In considering evaporation, this difference in wave formation is of extreme importance. Since a lake's wave pattern varies with wind speed, surface roughness is not independent of wind velocity. But on a stream, often the surface waves are not affected by wind, and thus true surface roughness is independent of (or only slightly dependent on) wind speed. Therefore while a change in wind velocity over a lake will also change the lake's roughness, this same velocity change will have little or no effect on the roughness of a stream.

It has previously been pointed out that the roughness parameter, z_o, is neither independent of wind speed nor a true indicator of surface roughness. Thus, even though the true surface roughness of a stream may not be affected materially by a change in wind speed, z_o will change. Therefore, a change in z_o does not necessarily indicate a change in surface roughness with respect to streams.

Computation of Stream Evaporation

In the past, researchers (39, 50, 17, 18, 51) have computed stream evaporation using experimental equations developed from studies on lakes and reservoirs. Raphael (39), in a study of stream temperature prediction, used an evaporation equation developed from Lake Hefner (6, p. 67):

$$E = 0.00177\, u(e_o - e_a) \qquad (20)$$

where,

E = evaporation rate, inches/day;

u = wind speed, miles/hr;

e_o = saturation vapor pressure at the water temperature, mb;

e_a = vapor pressure of ambient air, mb.

The mass transfer coefficient of this equation was derived empirically by using wind and humidity readings from an airport 13 miles south of Lake Hefner and evaporation measurements made on Lake Hefner. Thus, the constant, 0.00177, is valid only for these conditions. Any attempt to apply the same empirically derived mass transfer coefficient to another situation could very well lead to erroneous results. The mass transfer equation used to predict evaporative heat loss during the 1963 study on the coast fork of the Willamette River mentioned in the introduction was also derived from equation 20 (17, p. 60). Therefore it is not surprising that the results obtained were in error.

In attempting to evaluate the effect of evaporative heat loss on the temperature of a stream, Duttweiller (18, p. 22-29) compared the mass transfer coefficients of several equations which were empirically developed from lake studies. Commenting on these comparisons, Duttweiler stated (18, p. 28):

> The agreement between these values is none too good. This is partially explained by the variation of u with height above the surface and also by the fact that the individual expressions do not, of course, precisely fit the observations upon which they are based, i.e. there is, perhaps, considerable error in the individual formulations. Furthermore, the observations on

> which they are based are difficult to make with any real accuracy.

Even though most experimentally derived evaporation equations are developed from evaporation measuring spans of days or weeks, Harding (21, p. 70) states:

> To give accurate results a formula that correctly represents the factors controlling evaporation would need to be applied to short periods, such as hours, within which there is a slight variation in the factors involved. A correct formula of this sort cannot be expected to give accurate results when applied to monthly or annual means of its factors . . . . For such long periods only general agreement between the computed and the actual evaporation should be expected . . . .

Therefore, the use on rivers of mass transfer coefficients empirically derived from lake studies should be tempered with a knowledge of their assumptions, restrictions, and limitations. One of the assumptions of an equation for lake evaporation is that under conditions of no wind there is no roughness. This assumption is invalid with respect to streams. In addition, even though the atmosphere is still, the stream's velocity of flow imparts to the surface some motion relative to the overlying air.

As stated in the scope of this thesis, some existing evaporation equations will be evaluated to establish their utility for use on streams, and equations will be experimentally developed which will best describe the model evaporation. It is felt that the use of equations based on sound theory, such as those developed from the mixing length theory and the continuous mixing theory, has received too little attention with respect to stream evaporation. Therefore, two equations (equations 12 and 13) based on the mixing length concept and a set of equations (equations 16-19) developed from continuous mixing theory are to be used with the data obtained during the course of this study.

Since the shortcomings of experimental equations include inaccuracy of measurements and extended periods of observation, the reduction of error caused by these two factors is of value. This study has been carried out in a wind tunnel environment so that the necessary measurements for developing empirical mass transfer coefficients should be of fairly high accuracy. Harding's objections (21) concerning meteorological variations with time can also be overcome in wind tunnel studies, since the length of an observation period may be adjusted to any desired limit.

With these factors in mind, it was decided to develop three experimental equations based on the model study. These equations take the form of equations 4 and 5 and the following equation:

$$E = B'u(e_s - e_a) \qquad (21)$$

where,

E, u, e_s, e_a = previously defined;

B' = empirical mass transfer coefficient.

It is recognized that these developed equations will not be directly applicable to real streams, but it is hoped that the various magnitudes of their mass transfer coefficients will shed some light on the relationship between stream evaporation and surface configuration. It is also hoped that this work will provide additional knowledge on the difference between evaporation from lakes and from streams.

SELECTION OF RESEARCH MODE

Previous Use of Saturated Surfaces

Although there has been extensive experimental work done in the past on evaporation from free water surfaces, only a few researchers have used saturated surfaces for evaporation studies. Powell (36) proved that the evaporation rate from saturated surfaces was equivalent to the rate of evaporation from free water surfaces. After comparing the vapor pressure of a saturated surface of moistened filter paper against a free water surface of the same temperature, Powell stated (36, p. 46):

> These tests showed conclusively that the vapour pressure at the surface of moistened filter paper and similar materials does not differ to any appreciable extent from that of a free water surface at the same temperature.

Pasquill (34) also indicated that evaporation rates were equivalent for saturated surfaces and free liquid surfaces.

Table 2 lists some of the previous uses of saturated surfaces in evaporation experiments.

Table 2. Previous Use of Saturated Surfaces

Investigator	Date	Type of Surface	Reference
Powell and Griffiths	1935	linen	37
Powell	1940	linen, filter paper, gelatin impregnated with water	36
Pasquill*	1942	filter paper	34
Albertson	1948	porous porcelain	1
Cermak and Koloseus	1953-1954	Plaster of Paris	13

*Pasquill used bromobenzene instead of water.

It should be emphasized that this is only a partial list, but it does indicate the range of materials which have been used successfully as evaporating surfaces.

Of the studies listed in Table 2, only the investigation of Cermak and Koloseus was actually a model study. In conjunction with a massive research project on Lake Hefner, Oklahoma, Cermak and Koloseus constructed a model of Lake Hefner in a large wind tunnel at Colorado A. and M. College in Fort Collins, Colorado. According to Cermak and Koloseus (13, p. 2):

> The Lake Hefner study presented an opportunity to investigate the possibilities of duplicating by means of a model the prototype evaporation and wind structure. Prior to the Lake Hefner undertaking, a model study of this nature would have had very limited application because of the scarcity of accurate substantiating prototype data. If it were possible to evaluate the evaporation and wind structure by means of model studies,

models may be used to determine the evaporation and wind structure for situations which as yet are too complex for theoretical analysis.

The method of analysis used in this study involved the relationship between two dimensionless parameters. Hickox (22, p. 10), using an analogy between mass transfer and heat transfer, proposed the following relationship:

$$N = \alpha R_*^{\beta} \qquad (22)$$

where,

N = a dimensionless number similar to the Nusselt number used in heat transfer;

R_* = a dimensionless number analagous to the Reynolds number;

α, β = empirical constants.

Albertson (3) also reported an equation of this form. Using methods of dimensional analysis involving the principles of the Buckingham π theorem, Cermak and Koloseus (13, p. 10) developed a similar relationship which defined N and R_*:

$$N = E\sqrt{A}/\nu_e \, \Delta C \qquad (23)$$

where,

N = form of Nusselt number;

E = average rate of evaporation, lb/ft^2-day;

A = area of evaporating surface, ft^2;

ν_e = coefficient of molecular diffusion for water vapor, ft^2/sec;

ΔC = difference between the absolute humidity of the air in contact with the evaporating surface and the absolute humidity of the ambient air, lb/ft^3.

$$R_* = \frac{u_* \sqrt{A}}{\nu_e} \qquad (24)$$

where,

R_* = form of Reynolds number;

u_* = shear velocity, ft/sec;

A, ν_e = previously defined.

After completing the Lake Hefner model study, Cermak and Koloseus (14, p. 62) state that:

> . . . N may be related to a form of Reynolds number R_* for both the model and the prototype.

This success of Cermak and Koloseus in achieving a comparison of prototype and model evaporation provides an important approach to model studies using saturated evaporating surfaces. The methods of research used for the completion of this thesis were developed, to a large extent, using the study of Cermak and Koloseus as a guide. Furthermore, by substantiating the theory of Hickox (22) and Albertson (3), Cermak and Koloseus have made the relationship between N and R_* a valuable analytical tool. Therefore, a solution for the empirical coefficients in equation 22 should be an important step in the evaluation of the effect of surface configuration on the evaporation from a porous stream model.

Preliminary Investigations

Prior to undertaking the study, several preliminary investigations were carried out. These included the selection of the model size and configuration, tests to confirm previous assumptions, and the selection of proper instrumentation.

In selecting the size of the model, the most important consideration was the availability of a suitable wind tunnel. A low velocity wind tunnel located in the Aero Laboratory of the Department of Mechanical Engineering was made available, and consequently the size of the models used was made consistent with the size of this wind tunnel's test section. The test section is approximately 2-1/2 feet wide and 3-1/2 feet long, thus giving a plane area of slightly more than 8-1/2 square feet available for evaporating surfaces. It was decided to use three separate evaporating surfaces, each one foot by two feet. The three surfaces would be arranged to give a total evaporating surface with a downwind dimension of three feet, a crosswind dimension of two feet, and an area of six square feet.

The selection of three separate surfaces was based on several factors. Albertson (1) discussed the formation of a "vapor blanket" starting at the leading edge of a saturated, porous evaporating surface and increasing to a maximum some distance downwind. This means that the rate of evaporation changes with down stream movement. Many other investigators have also reported similar results.

Powell and Griffiths (37) give an expression for evaporation which includes the downwind dimension to a power less than one, thus indicating a change in evaporation rate with down stream movement. With this in mind, it was decided that the use of a "buffer" surface just upwind of the test surface would prevent a change in evaporation over the test section. Albertson (1) used "buffer" surfaces on the sides of a test surface to reduce the effect of lateral diffusion of water vapor from the test surface, so the use of a "buffer" surface is not unprecedented.

Instead of one large test section placed downwind of the "buffer" section, it was felt that two smaller sections would be more advantageous, since two test sections would make it possible to obtain two separate evaporation rates for each test run. These two rates could then be compared against one another and significant errors in observation would become evident. With a single test surface, there would be no such reference. Another reason for employing two test sections was that of practical fabrication. It was felt that the casting of two one by two surfaces would be much easier than casting a single two by two surface. The same reasoning can be applied to the fabrication of the molds and the model containers. More information on fabrication will be given later in this thesis.

The selection of the type of surface configuration to be used on the models posed several problems. The type of configuration chosen would have to be made up of roughness elements comparable to those found on a stream, thus giving a "wavy" profile which imposes a surface roughness not caused by wind. These roughness elements would have to be easy to define mathematically and also practical to duplicate on a model. Several possible profiles were available. These include:

1. saw tooth profile (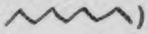),
2. sharp wave profile (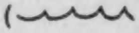),
3. square wave profile (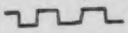),
4. sine wave profile (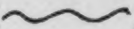),
5. complex wave pattern, and
6. random wave pattern.

Of these six, only 1, 2, and 4 satisfied both the criteria of being mathematically definable and easy to duplicate and fabricate. The fifth choice could be defined mathematically, for example, using a Fourier expansion, but its construction would be very difficult. The sixth choice probably best represents what occurs on a real stream, but both its mathematical definition and model reproducibility would be impossible with the analytical tools available at the present time.

In order to simplify the problems of mathematics and construction, a sine wave was selected as the basic model configuration. Although this admittedly is an extreme simplification of a real stream situation, the use of a sine wave certainly has a theoretical basis.

The basic equation describing a water wave is given by Sverdrup, Johnson, and Fleming (47, p. 517) as:

$$y = \frac{H}{2} \sin \frac{2\pi t}{T} \qquad (25)$$

where,

y = height of water surface at time t,

H = wave height,

T = wave period.

This, of course, is a simple harmonic function describing a sine wave. Sears (42) describes a simple traveling wave in the same manner. Clark's work on the speed of waves in a ripple tank also assumes a simple sine wave as the basic water wave (16). Therefore, the simplest form of a water wave is a sine wave, and it is easily defined mathematically. The sine wave is also easy to duplicate on a model.

A total of five separate surface configurations were selected for model investigation. Four of these had sine wave profiles, the other being flat. Table 3 lists the selected configurations.

In selecting the configuration of the "buffer" surface, it was decided to use a sine wave configuration (Series B) rather than a flat surface. This sine wave configuration would develop an initial level of turbulence over the downwind test sections. Using the same "buffer" surface configuration for all test conditions would give consistent

Table 3. Surface Configurations

Model Surface	Wave Height	Wave Length
A (Flat)	0	∞
B	1/4"	2"
C	1/4"	1"
D	1/2"	2"
E	1/2"	4"

turbulence levels at the leading edge of the test sections for each test velocity. Thus the "buffer" section would perform two functions, acting as a pre-evaporator and as an initiator of turbulence.

The basic assumption on which the use of saturated evaporating surfaces is based is the equality of evaporation from both saturated surfaces and free water surfaces. Several investigators have effectively shown that this equality exists (36, 34). In order to further substantiate this assumption, a simple experiment was performed. A flat saturated surface and a free water surface of the same size and shape were each used as evaporation surfaces for a period of one week. During each of these weekly experiments, readings were taken periodically noting the amount of water evaporated. Concurrently, readings were also taken from a porous porcelain spherical atmometer. An atmometer is a hollow bulb of porous material whose exterior face acts as an evaporating surface (29). Equal readings from such a device indicate an equal potential for water vapor transfer by evaporation. The evaporation rates from both the saturated and free water surfaces which corresponded to equal atmometer rates were then compared. This comparison showed no significant differences between the evaporation rates from the saturated and free water surfaces.

Another assumption that is made concerning the use of porous saturated surfaces, is that no vertical temperature gradient exists within the surface. This is important, since the temperature of the water surface is a significant evaporation parameter, and it is necessary to obtain true surface water temperature. If no vertical temperature gradient exists in a saturated model, the water temperature probes can be placed at any level within the model instead of at the air-water interface.

Cermak and Koloseus (13) used copper-constantan thermocouples at the air-water interface of the Plaster of Paris surface. At one position thermocouples were inserted at the surface and at a lower level within the model. In order to test whether a difference in temperature existed between the two levels, a statistical test was performed using the method of "paired observation" described by Li (27). This method employs the t-distribution. A total of 111 paired observations were available, giving a t value of 0.123. A two-tailed test at the five percent level of significance gives limits of t for 110 degrees of freedom equal to ± 1.98. Since the computed t of 0.123 is close to zero, and well within the t limits of ± 1.98, it can be stated that no significant difference in temperature existed between the two levels tested.

A separate and independent investigation was conducted on a small Plaster of Paris model to further substantiate the assumption of no vertical temperature gradients within a saturated surface. Three thermistors were inserted at different levels within the model, and periodic readings for five days failed to show any difference in temperature between the three points. The results of this model test together with the data of Cermak and Koloseus confirmed the assumption of zero vertical temperature differences within a saturated porous surface. Therefore, no errors should be introduced due to the placement of the water temperature probes a small distance below the air-water interface, instead of directly at it.

The success of any model study hinges ultimately on the accuracy and precision of the data obtained, and because of this fact, proper instrumentation must be employed. The use of inadequate measuring devices would easily defeat the purpose of a study, regardless of how carefully these devices are used. In approaching the selection of instruments several factors were considered, including precision, accuracy, versatility, operating characteristics, and cost. The model study undertaken for this dissertation required instruments for measurement of wind velocity, water and air temperature, relative humidity, and evaporation.

Several methods are available for the measurement of air speed. Cup and vane anemometers, pitot tubes, and hot-wire anemometers have all been used by previous investigators. Of these instruments the hot-wire anemometer best satisfies the requirements of accuracy at low velocities and small size. An additional advantage of the hot-wire anemometer is that it can be used as an indicator of air turbulence. The two types of hot-wire anemometers available operate with either constant temperature or constant current. A constant temperature hot-wire anemometer was selected for use, because this type is best adapted to studies involving low velocities.

The common devices used for temperature measurement include thermometers, thermocouples, and thermistors. Both thermocouples and thermistors have the advantage of being able to be read at some distance from the sensing element. Thermistors have an advantage over thermocouples in that they require no reference junction. The development of thermistors in the past few years has made available a selection of very accurate and precise sensing elements of various shapes and sizes. Thermistors were chosen for this study because of these reasons and because the Civil Engineering Department had on hand most of the required equipment.

In selecting equipment for measuring the relative humidity in the air above the model surface it was necessary to find an instrument with a small sensing element, since relative humidity readings were to be taken at small increments of vertical distance. This requirement ruled out the use of dew point apparatus, even though this method is more accurate than all others. A combination wet and dry bulb determination, as employed in a sling psychrometer, is the most common method in use today. However, a psychrometer, whether sling or fan-aspirated, could not be used to make separate readings at small increments of distance. Cermak and Koloseus (13) employed wet and dry thermocouples, and it was felt that wet and dry thermistors would work equally well. Tests conducted using a small glass bead thermistor with a cloth wick as the wet bulb showed that it was possible to obtain relative humidity readings within one percent of values received from a hand held, fan-aspirated psychrometer. Because of this good accuracy, the small size of the sensing element, and the availability of equipment, wet and dry thermistors were selected for measuring relative humidity.

Perhaps the most important determination required for this model study was the measurement of the quantity of water evaporated from the saturated model surfaces. This can be accomplished either volumetrically or by weight. Due to the large size of the models involved, a weight measurement was deemed impractical.

Cermak and Koloseus (13) had an opening in the model surface which was designated as the "lake stage indicator." A point gauge was installed to check the level of the free water surface in the opening. If the water level in the opening dropped from the level of the point gauge, the amount of water added to the surface to bring the water level back up to the point gauge was considered equal to the amount of water evaporated from the saturated surface. Since the total model area was 25.01 square feet, a small one inch opening did little to disrupt the evaporation pattern. However, the size of the model surfaces for the study under discussion here is only two square feet, thus it was felt that an opening in the model surface would be detrimental to the successful operation of the saturated surfaces. For this reason, another method had to be found to volumetrically measure evaporation. Tests were conducted using various arrangements of water level indicator tubes. These tubes were connected by plastic tubing directly to the water supply inlet of a model surface. The water level changes in the tubes acted as an indicator of the changes in the amount of water in the model surface. Thus, when a point gauge was installed above an indicator tube, the tube served the same purpose as the "lake stage indicator" of Cermak and Koloseus. The water level indicator tube also had the added advantage of being able to be placed outside the wind tunnel, thus making its reading much more convenient. The accuracy of the arrangement ultimately selected was estimated to be plus or minus one to two milliliters.

It should be pointed out here that the preceding discussion has dealt only with the selection of proper equipment. The next section of this thesis will deal with descriptions of the experimental apparatus.

DESCRIPTION OF EXPERIMENTAL FACILITIES

Porous Stream Model

Selection of material for the porous stream model was governed by several limiting criteria. The material had to be porous enough to allow water fed in from the bottom to reach the surface by capillary action. It also had to be smooth, so that surface irregularities would not create a rough surface. Cermak and Koloseue (13) investigated five different materials:

a) fine sand with no binding material,
b) fine gravel with a clay binder,
c) gravel with a cement binder,
d) glass beads with a plastic binder, and
e) Plaster of Paris.

In their studies Plaster of Paris was selected as being most applicable for use as an evaporating surface.

After examining the use of a porous porcelain surface, which was rejected because of prohibitive cost, Plaster of Paris was also selected as the material to be employed for fabricating the porous model surfaces to be used in the present study.

Preliminary investigations were made to determine the best plaster to water ratio which could be obtained. After experimenting with plaster to water ratios of 1:0.5, 1:0.6, 1:0.7, and 1:0.65, a mix was selected which consisted of one part dry plaster of 0.65 parts of distilled water by weight. This mixture gave good workability, and when a plaster model was removed from its mold, the surface of the model was very smooth. The plaster used for the models was "Red Top Gypsum Casting Plaster" manufactured by the U. S. Gypsum Company.

Model surfaces were fabricated by pouring the plaster mix into a mold. The molds were made of a sheet metal base, which was formed into the desired surface configuration, surrounded by wood sides. The molds were constructed so that the height of the wooden sides was equal to the depth of the model surface. The interior wooden sides of the mold were coated with silicone stopcock grease prior to the plaster pouring to prevent the finished model from sticking to the inside of the mold. A period of at least three hours was allowed to elapse before the model surface was removed from its mold.

The porous model surfaces were installed in plastic boxes in the wind tunnel. These boxes were constructed of acrylic plastic sheeting with 1/8 inch thickness for the sides and 3/8 inch thickness for the bottoms. The inside dimensions of the boxes were one foot by two feet by 2-1/8 inches. Each box had a one inch (inside diameter) tube inserted through the bottom to accommodate the water supply tubing. The two boxes to be instrumented for water temperature also had 1/2 inch (inside diameter) tubes installed, through which the thermistors could be inserted.

A layer of gravel was used to support the model surfaces installed in these boxes. This gravel, pre-washed to prevent clogging of the porous models, was placed in the box at a depth which allowed the model surface to be installed flush with the level of the box.

The installation of the model surfaces is shown in Figure 1. This figure shows the front buffer zone of sine wave surface configuration and two flat test sections. Photographs showing the four sine wave surface configurations are given in the Appendix.

Wind Tunnel

The wind tunnel used, located in the Aero Laboratory of the Department of Mechanical Engineering, is a low velocity, recirculating type. The wind source is a variable pitch aircraft propeller which is driven through belts and pulleys by an electric motor. Prior to the model installation, the tunnel's test section was 3-1/2 feet long, 2-1/2 feet wide, and 3-1/2 feet high. The models reduced the height by about two inches. Figure 2 shows the test section after the models had been installed.

A preliminary pilot tube survey indicated that a well controlled velocity range of 15 to 60 feet per second could be obtained in the test section by varying the pitch of the propeller. Since the minimum speed of 15 feet per second was too high, the velocity in the test section was reduced by placing a screen of wire and fabric just upwind

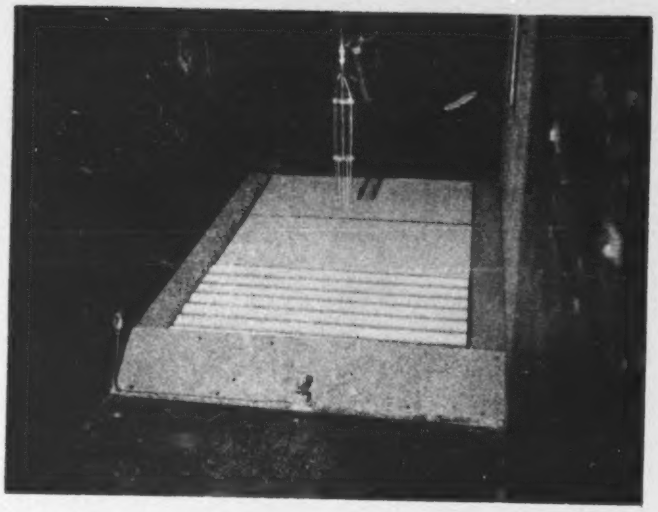

Figure 1. Installed Model Surfaces

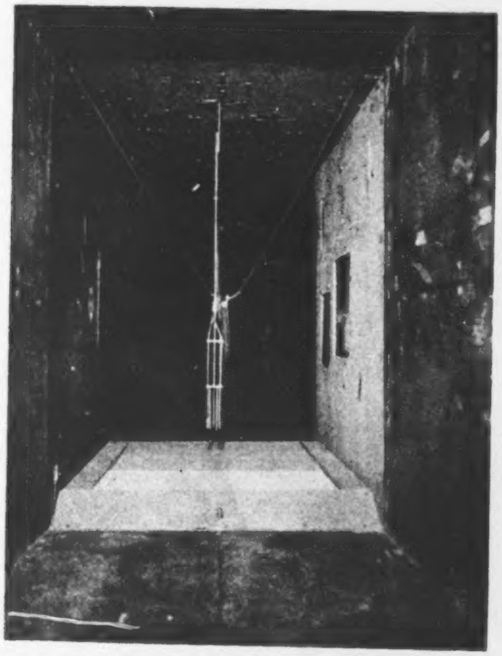

Figure 2. Wind Tunnel Test Section

of this section. After the insertion of this screen, the minimum velocity in the test section dropped to about six feet per second.

Velocity Instrumentation

Velocity profiles were measured up from the surface of the model by a constant temperature hot-wire anemometer. The hot-wire anemometer was selected for this purpose since it is one of the most sensitive instruments yet devised to measure low velocities in an air stream. The constant temperature hot-wire anemometer determines the amount of current necessary to maintain a constant wire temperature, and this current is a measure of the air velocity. A rather sophisticated electronic system is necessary for amplifying and measuring the system output. This study employed a DISA model 55A01 hot-wire anemometer with a miniature hot-wire probe, model 55A25. The active element of the probe (i.e. - the hot-wire) is a platinum coated tungsten wire with a diameter of five microns. Further data on the hot-wire anemometer can be found in the Appendix.

Velocity determinations were also made using a pitot tube extending from the top of the tunnel.

Temperature Instrumentation

Water and air temperatures were measured with "Yellow Springs" thermistor probes used with a model 4002 twelve point switch box and a model 43TJ Tele-Thermometer. Air temperatures were obtained with "model 405" probes and water temperatures were measured with "model 401" probes.

Water temperature thermistors were inserted into holes drilled in the bottom of the plaster models. Each of the two test sections had four such thermistors, and an additional thermistor was located at the point where the water entered section two. Two air temperature thermistors were installed in the tunnel, with one at the bottom, upwind of the test section and the other at the top, downwind of the test section.

Relative Humidity Instrumentation

Relative humidity information was obtained from a combination of wet and dry bulb thermistors. The dry bulb thermistor was a Yellow Springs model 401 probe. A small glass bead thermistor with a cloth wick was used as the wet bulb. The wick was kept wet by water fed through a small plastic tube which egressed from an inverted Erlenmeyer flask mounted on the top of the tunnel.

The wet and dry thermistors were mounted on the shaft of the hot-wire anemometer probe. Figure 3 shows this arrangement. The wet thermistor is located on the far left with the dry thermistor on the far right. The middle projection is the hot-wire probe. The other two rods are merely stops to prevent the hot-wire probe from contacting the model surface. These stops are placed so that the hot-wire probe is 0.05 inches above the surface when the stops are resting on the surface. Figure 3 also shows a large plastic tube leaving the top of the probe assembly. This tube carried the wet and dry thermistor lead wires and the water supply tube for the wet thermistor. The whole unit was stabilized by a guy wire which prevented excessive vibrations. This guy wire is shown in the upper center of Figure 3.

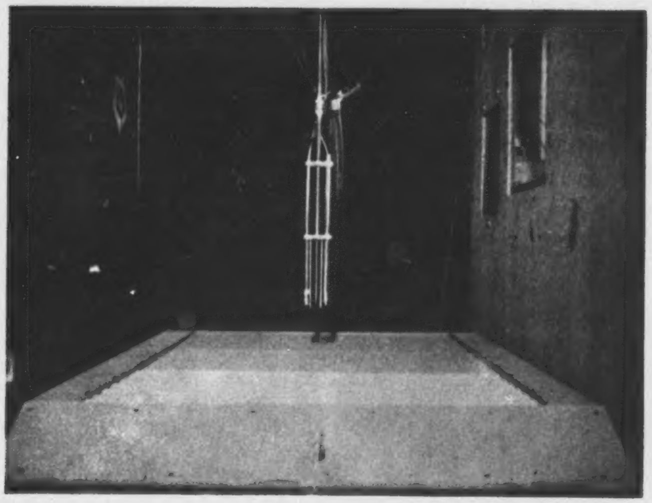

Figure 3. Hot-wire and Relative Humidity Probe

Water Supply

Distilled water was supplied to the model surfaces from two burettes. A 1000 ml. burette was used to supply water before a test run, and a 25 ml. burette was used to supply water during a testing period. The water was distributed by gravity to each surface through plastic tubes. Figure 4 is a schematic sketch of the water distribution and evaporation measuring system.

Evaporation Measurement

A water level indicator tube for each model surface was mounted on the outside of the tunnel. These indicator tubes were connected by plastic tubing to the water inlet of each model container, as indicated in Figure 4. A wire point gauge was installed above each tube. The amount of water evaporated during a test run was obtained by noting how much water was added to bring the water level in the tubes up to a pre-set level indicated by the point gauges. Figure 5 shows the arrangement of the plastic tubing beneath the wind tunnel. Figure 5 also shows the two pieces of tubing which contain the thermistor leads for water temperature in model sections two and three.

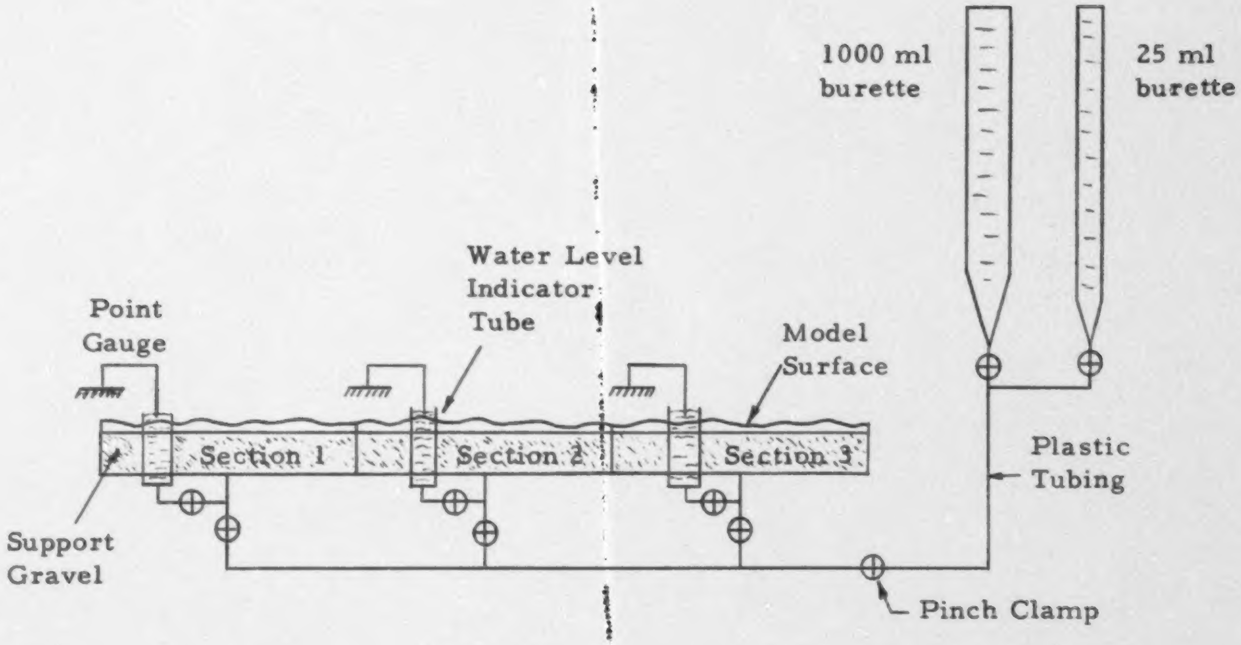
1000 ml
burette
25 ml
burette
Water Level
Indicator
Tube
Point
Gauge
Model
Surface
Section 1
Section 2
Section 3
Plastic
Tubing
Support
Gravel
Pinch Clamp

Figure 4. Water Distribution and Evaporation Measuring System

Other Instruments

In order to obtain velocity profiles up from the surface of the model, a Moseley Model 135A X-Y recorder and a linear potentiometer were used in conjunction with the hot-wire anemometer. By placing the hot-wire probe at the end of a shaft which was connected to the linear motion potentiometer, it was possible to obtain a trace of height versus hot-wire output on the X -Y recorder. This was done by connecting the output from the potentiometer to the Y- axis of the recorder and the output from the hot-wire anemometer to the X - axis. By using the calibration curves which relate hot-wire output to velocity, it was then possible to obtain a velocity for any height on the trace.

A Bourns Model 108 linear motion potentiometer with a four inch travel was used with a nine volt battery as a power source. Figure 6 shows the linear motion potentiometer and its specially designed holder on top of the tunnel. This figure also shows the reservoir for the wet bulb thermistor on the far right and the pitot tube on the left. The wire egressing from the shaft in the center of the photo is the coaxial cable leading from the hot-wire probe. The picture also shows the position of the "sampling points" as indicated by a number and a letter.

A Tektronix type 533A oscilloscope with a Type B plug-in unit

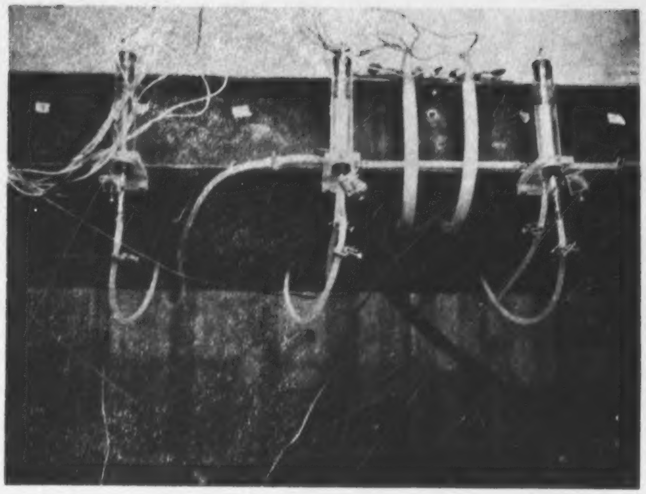

Figure 5. Arrangement of Tubing for Water Supply and Evaporation Measurement

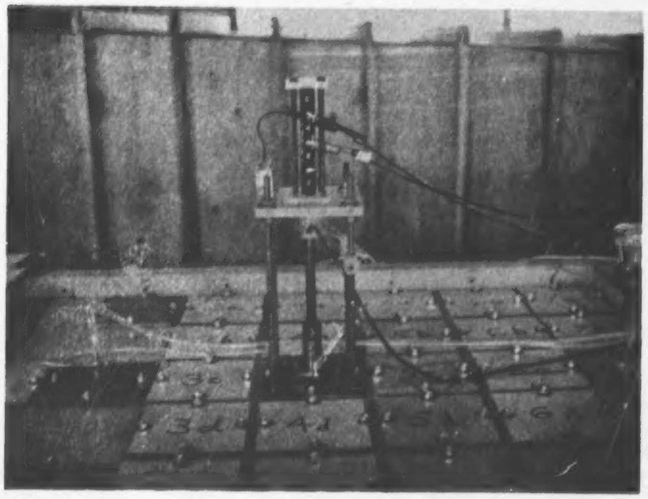

Figure 6. Holder for Linear Motion Potentiometer

was used for checking the stability of the hot-wire probe and also as a visual display of the levels of turbulence above the model surfaces.

Figure 7 shows an overall view of the test facilities.

Figure 7. Overall View of Test Facilities

EXPERIMENTAL PROCEDURES

A total of five wind speeds were used to evaluate evaporation from each surface configuration. Each wind speed was used twice for every configuration, allowing separate data to be obtained for each of the two test surfaces. During a test, vertical profiles of relative humidity and velocity were taken over the model surface under investigation. Table 4 presents the total number of profile data sets which were taken. A profile set includes one velocity profile and one relative humidity profile.

Table 4. Number of Profile Sets

Propeller Hub Position	4"		4-1/16"		4-1/8"		4-3/16"		4-1/4"	
Approximate wind speed, ft/sec	6		12		17		21		24	
Test Surface	2	3	2	3	2	3	2	3	2	3
Series A	2	2	2	2	3	2	2	2	2	2
Series B	2	2	2	2	3	2	2	2	2	2
Series C	2	2	2	2	3	2	2	2	2	2
Series D	2	2	2	2	3	2	2	2	2	2
Series E	2	2	2	2	3	2	1	2	-	-

As indicated in Table 4, 100 velocity and 100 relative humidity profiles were taken during 48 separate wind tunnel tests.

For sampling purposes, the two test surfaces were each divided into two hypothetical half-sections, one foot by one foot square. For the tests where two profile sets were obtained, the readings were taken over the centroid of each half-section. When three profile sets were taken, the additional readings were obtained over the centroid of the whole model surface. The reason for taking three profile sets in some cases was to check whether the velocity or relative humidity profiles changed with cross-wind distance from the model edges. In all five cases where this procedure was used, the averages of the three profile sets were comparable to those averages obtained when only two profile sets were taken, thus indicating that two profile sets were sufficient.

Each wind tunnel test was conducted using the following sequence:

1. The propeller pitch was set at the desired angle by adjusting a hub, which could be moved back and forth along a threaded shaft. The distance from the edge of this hub to the end of the shaft was designated as the propeller hub position (PHP). Preliminary tests showed that PHP's of 4, 4-1/16, 4-1/8, 4-3/16, and 4-1/4 inches corresponded to wind velocities in the test section of 6, 12, 17, 21, and 24 feet per second respectively.
2. The mechanism consisting of the hot-wire probe and the wet and dry bulb thermistors was installed in the desired position on the tunnel top. The holder shown in Figure 6 was designed so that it could be securely fastened to the tunnel top at any one of the 28 "sampling points."
3. Water was added from the 1000 ml. burette to wet the model surfaces.
4. The hot-wire anemometer was made operational following the steps prescribed in its instruction manual. Since a detailed account of these steps is provided in the manual, they are not restated here, however, it should be mentioned that the determination of both the cold and operating resistances of the hot-wire

probe was necessary. These parameters varied from probe to probe, and since several probes were employed during the course of this research, the successful operation of the anemometer depended on a knowledge of these two resistance values.

5. The wind tunnel was turned on, and a period of 15 - 30 minutes was allowed to elapse before data acquisition began. This lag time allowed thermal equilibrium to occur in the test section.
6. The pitot tube's manometer was read, and the velocity, as obtained from a calibration curve, was recorded. This velocity was then compared to that obtained from the hot-wire anemometer in order to check the hot-wire probe.
7. The dry and wet thermistors were read, and a value of relative humidity was obtained from a table. This value was checked using the hand-held, fan-aspirated psychrometer. The Erlenmeyer flask serving as a reservoir for the wet thermistor was then checked to see if enough water was available. The wick of the wet thermistor was saturated so that a small drop of water was hanging from the thermistor tip. The water fed to the wick was adjusted so that the drop remained for about one minute before falling. If the water was fed too fast or too slow, inaccurate readings would occur. In addition, the battery used with the wet thermistor was checked at this time. Since this thermistor was calibrated at a battery voltage of 1.55 volts, any change in battery output would result in erroneous wet

thermistor readings. It was not necessary to check the battery voltage of the "Yellow Springs Tele-Thermometer" since it had a compensating circuit which could be adjusted to provide uniform output voltage.

8. The point gauges for the water level indicator tubes were set for all three model surfaces, and the time was recorded. This step had to be done carefully, since these gauges gave the reference levels for all evaporation measurements. Before the gauges were set, care had to be taken to assure a high water level in the indicator tubes. This was done by filling the model containers to the point where a small amount of free water appeared on the saturated surfaces. This free water was then removed by absorbent paper towels, and the point gauges were set. This procedure assured a high water level in the indicator tubes. Preliminary investigations revealed that if the point gauges were set at lower levels in the water indicator tubes, the sensitivity of the gauges was very low. The test section had two access panels in the front face which had to be closed when the point gauges were set. This was necessary, because the water level indicator tubes acted as manometers and opening the access panels changed the velocity in the test section. This change in velocity caused a fluctuat on in the level of the water in the indicator tubes.

It should be mentioned at this point that steps 1 - 7 were preliminary, and step 8 was the start of the actual testing.

9. The barometric pressure obtained from a mercury Torricelli barometer hanging on the outside of the tunnel was recorded.
10. The air temperature thermistors in the test section were read and the values recorded.
11. The water temperatures in model surfaces two and three were read and recorded along with the time.
12. Relative humidity readings were obtained at distances above the surface of approximately 4, 3, 2, 1, 3/4, 1/2, 1/4, and 1/20 inches. Dry thermistor temperatures were taken from the Tele-Thermometer and wet thermistor readings were obtained from a separate volt meter. The Y - axis of the X - Y recorder was used to indicate the height of the sensing elements above the model surface. After the thermistors were positioned at a new level, about one minute was allowed to elapse before readings were made. This was to allow for thermistor stabilization. The time constant for the thermistors was about seven seconds, and five time constants (i.e. - 35 seconds) are required for the probe to react to 99 percent of a temperature change.
13. Water was added to each section from the 25 ml. burette. The amount of water added to bring the level in the indicator tube up

to the pre-set point gauge and the time were recorded. The water temperatures were also recorded at this time (i.e. - repeat Step 11).

14. A velocity profile was traced by the X - Y recorder. This was done by manually moving the shaft of the hot-wire probe, thus actuating the linear motion potentiometer. A trace of height versus hot-wire output was obtained, as previously explained. Since the hot-wire probe measures resultant velocity, care had to be taken to make the vertical motion of the shaft very slow. If this movement was too fast, the vertical component of velocity would increase the resultant velocity, thus giving a hot-wire output indicating a horizontal wind speed higher than that actually in the tunnel. The air temperature in the tunnel was recorded at this time, since the velocity taken from the hot-wire calibration curves is temperature dependent.
15. The relative humidity in the test section was obtained with the probe about four inches above the surface. This value was checked using the hand-held psychrometer.
16. The barometric pressure, air temperature, and time were recorded. This step concluded the data acquisition necessary for the completion of one profile set.
17. Step 13 (evaporation measurement) was repeated.
18. Step 2 (positioning of probes) was repeated, with the anemometer

in the stand-by position. If the hot-wire probe were disconnected from the shaft with the anemometer in the operating position, damage to the probe and "black box" could occur.

19. Steps 9 - 16 were repeated.
20. Step 13 (evaporation measurement) was repeated so that all the readings were taken at the same time. This step concluded the data acquisition.
21. The wind tunnel and all of the instruments, except the anemometer, were shut off.
22. The hot-wire anemometer was checked to make sure that the cold probe and operating resistance had not changed. Some slight drift in these values was noted, but at no time was this drift of sufficient magnitude to cause significant error.

Although this sequence of steps was followed in most test runs, some circumstances required that it be altered. For example, when the rate of evaporation was very high, it was necessary to take evaporation measurements (Step 13) more often. Also, when three profile sets were taken, Steps 18 and 19 were repeated.

Originally it was planned to measure the longitudinal pressure drop through the test section. However this was not done, since Cermak and Koloseus (13), using a Wahlen gauge which was capable of measuring pressure differences of 0.00028 lb/in^2, showed that this pressure drop was insignificant.

When the velocity and relative humidity profiles were taken over the sine wave surfaces, they were obtained over the top of the waves, thus making the wave crest the zero reference level. This was done, because the position of the "sampling points" on the tunnel top and the layout of the model surfaces prevented one from obtaining profiles over the wave trough unless the shaft holding the hot-wire probe was angled slightly. Preliminary tests were conducted by taking velocity profiles over both the wave crest and the wave trough using configuration B. A comparison of these profiles showed that the profile taken over the wave top gave the same velocity at a specific height as that taken over the trough, when both profiles used the wave trough as the zero reference level. Therefore, no significant difference in velocity profiles occurs when the wave crest instead of the wave trough is used as the zero reference height.

As a final note on experimental procedures, it should be pointed out that the experimenter was unable to control all the physical aspects of the research project. For example, even though this research was carried out inside a building, the weather played a most important role. During the heat of the summer, the temperature in the test section often exceeded 100°F, and when colder weather arrived, a furnace was used to maintain building heat. Variations in building heating gave fluctuating thermal conditions in the wind tunnel's section. Mechanical problems were also encountered in the wind tunnel. The sleeve bearing which supported the propeller shaft changed its characteristics during the months of testing. This caused the same propeller pitch to give slightly lower wind speeds with each successive test run. This did not cause any major problems until finally the bearing became worn to the point that the final two test runs were curtailed, as shown in the last row and column of Table 4. Even with these difficulties, it is felt that the equipment and instruments operated satisfactorily and that the testing procedures yielded data of sufficient accuracy to be used in the computations and analyses that follow.

COMPUTATIONS AND RESULTS

Data Reduction

Before any computations or statistical analyses could be made on the laboratory data, it had to be reduced to a usable form. Data reduction for the various parameters measured proceeded in the following manner.

1. Evaporation Data

The evaporation rate for each test was obtained by plotting the total evaporation (grams of water per square foot of plane surface area) versus time (minutes). The best straight line was drawn through the points, and the slope of the line was equal to the evaporation rate in gm/ft^2 - min.

2. Relative Humidity Data

The raw data for relative humidity consisted of the dry thermistor temperature and a voltage reading from the wet thermistor. These values were recorded for specific heights above the model surface. First, the wet thermistor voltages were converted to temperatures by using a calibration curve, and then the relative humidity in percent was obtained from appropriate tables of wet and dry bulb temperatures.

3. Water Temperature Data

The raw data for water temperature consisted of readings from eight thermistors every time water temperatures were recorded. Each surface had four thermistors, and the water temperature for each model surface was obtained by averaging the four thermistor readings. A plot of this average water temperature (degrees Centigrade) versus time was made for the model surface under investigation. The average water temperature over the test run was then obtained by a visual examination of the best curve constructed through the plotted points.

4. Velocity Data

The trace of height (inches) versus hot-wire output (D. C. volts) made on the X - Y recorder was analyzed to determine wind speed. Due to the turbulence in the air stream, a "jagged" trace was obtained. A smooth line was drawn through this "jagged" trace so that the average velocity at any height could be obtained from calibration curves. These curves showed the relationship between the D. C. voltage output of the hot-wire anemometer and the air velocity in feet per second. A set of curves was constructed for each of the hot-wire probes employed. Each set consisted of several curves, with each one being for a specific air temperature. The temperatures selected covered the complete temperature range to be encountered during the months of testing. Visual interpolation between the curves was necessary when the air temperature in the tunnel fell between two of the specific values for which calibration curves had been constructed.

Preliminary Calculations

Prior to computing evaporation rates from several existing equations and before developing specific experimental equations it was necessary to perform some preliminary calculations. They are as follows.

1. Graphical Determination of Roughness Parameter, z_o

As explained previously, the roughness parameter, z_o, is obtained graphically from the relationship of the logarithm of height versus wind speed. A plot of this type was made for every test run using four cycle semi-log paper. Velocities were obtained from the X - Y recorder trace, and points were plotted for heights of 0.05, 0.3, 0.6, 0.9, 1.2, 1.8, 2.4, and 3.6 inches above the zero reference level. These heights in inches correspond to heights in feet of 0.00417, 0.025, 0.05, 0.075, 0.10, 0.15, 0.20, and 0.30 respectively. The heights were evaluated in units of feet because the value of z_o was required in units of feet. Points of this type were plotted for as many velocity profiles (i.e. - two or three) as were taken during the test run. For each velocity profile, a straight line was drawn through those points which exhibited a linear relationship (i.e. - the turbulent boundary region). As a rule, this hypothetical turbulent boundary region extended from about 0.3

inches to approximately 1.2 inches above the model surface. The height at which the straight line intersected the Y-axis was equal to the roughness parameter, z_o. Often times, each velocity profile would yield a slightly different value for z_o. Therefore, z_o was evaluated for each wind tunnel test as the logarithmic average of the separate values obtained from each velocity profile.

2. Calculation of u_*

The shear velocity, u_*, was computed from equation 8, which becomes:

$$u_* = u_z / 5.75 \log (z/z_o). \qquad (8)$$

z_o was obtained as prescribed above. The height z had to be within the turbulent boundary region, and a value of 0.075 feet (i.e. - 0.9 inches) was selected, because for all velocity profiles obtained, this height was within the limits of the turbulent boundary region. The magnitude of u_z was obtained by using the semi-log plot and taking the velocity corresponding to a height of 0.075 feet.

3. Calculation of N

When equation 23 was converted so that it would be consistent with respect to the units of evaporation measured in the research, it became:

$$N = E\sqrt{A} \,/\, (2.72 \times 10^4)\, \nu_e \Delta C \qquad (26)$$

where,

N, A, ν_e ΔC = previously defined;

E = evaporation rate, gm/ft^2 - min.

The evaporation rate was obtained experimentally from a model surface of plane area A; therefore the values of E and A are readily available.

The evaluation of the coefficient of molecular diffusion for water vapor, ν_e, requires some mathematical manipulation. This term is equal to the kinematic viscosity of air divided by the Prandtl number:

$$\nu_e = \nu/\sigma \qquad (27)$$

where,

ν_e = previously defined;

ν = kinematic viscosity of air, ft^2/sec;

σ = the Prandtl number, 0.6 for the evaporation of water into air, dimensionless.

Furthermore,

$$\nu = \eta/\rho \qquad (28)$$

where,

ν, ρ = previously defined;

η = absolute viscosity, lb/sec - ft.

Thus the evaluation of ν_e required a knowledge of both the absolute viscosity and density of the air.

The determination of ΔC required a knowledge of air and water temperatures and the relative humidity of the overlying air.

$$\Delta C = C_s - C_a \tag{29}$$

where,

ΔC = previously defined;

C_s = absolute humidity of the air in direct contact with the evaporating surface, lb/ft^3;

C_a = absolute humidity of the ambient air, lb/ft^3.

C_s was obtained directly as the mass of water vapor in saturated air at the temperature of the water. C_a was obtained by multiplying the mass of water vapor in saturated air at the temperature of the ambient air by the relative humidity of this ambient air.

4. Calculation of R_*

R_* was computed using equation 24. The evaluation of terms included in this equation was completed during the calculation of N.

Computations Using Existing Equations

A total of five existing evaporation prediction methods were used to compute evaporation rates from the data obtained during the course of this research. They included two equations based on the discontinuous mixing approach, a set of equations based on the continuous mixing theory, an equation empirically derived from a lake study, and a method based on the relationship between N and R_*

developed from a wind tunnel study. The equations used in these methods were reduced to make them consistent with respect to the units of evaporation used in this research. The equations in their reduced form are as follows:

1. Discontinuous Mixing Approach by Norris (Equation 12)

For a hydrodynamically smooth surface, equation 12 becomes:

$$E = (2.72 \times 10^4) k_o \rho u_* (q_s - q_z)/\ell n (z/z_o) \qquad (30)$$

where,

E = evaporation rate, gm/ft^2-min;

k_o, ρ, u_*, q_s, q_z, z, z_o = previously defined.

For a hydrodynamically rough surface, equation 12 becomes:

$$E = (2.72 \times 10^4) k_o^2 \rho u_z (q_s - q_z)/\ell n (z/z_o)(\ell n (z/z_o) - 0.88) \qquad (31)$$

where,

E = evaporation rate, gm/ft^2 - min;

k_o, ρ, u_z, q_s, q_z, z, z_o = previously defined.

An examination of equation 12 shows that two heights a and b within the turbulent boundary region were used for wind speed and specific humidity levels. For purposes of simplification, a height z was used for both a and b in equations 30 and 31. This should not change the equation's effectiveness, since the theory from which Norris developed his equations assumes the same exponential vertical gradient for wind speed and vapor pressure. Sverdrup (46) also used a single height, z, within the turbulent boundary region.

2. Discontinuous Mixing Approach by Thornthwaite and Holzman (Equation 13)

Equation 13 becomes:

$$E = (5.54 \times 10^{3})\rho(e_1 - e_2)(\bar{u}_2 - \bar{u}_1)/ P\left(\ell n\frac{z_2}{z_1}\right)^2 \qquad (32)$$

The atmosphere stability parameter, s, in equation 13 is set at zero for neutral (i.e. - adiabatic) conditions (7, p. 25).

3. Continuous Mixing Approach by Sutton (Equations 16-19)

By substituting a value for n of 0.25, equation 18 becomes:

$$a = (0.1276)(\nu)^{0.25} \qquad (33)$$

and equation 19 becomes:

$$a = (0.1276)(\nu + u_* z_0)^{0.25} \qquad (34)$$

The equation for G (equation 17) becomes:

$$G = (0.1585)(\psi_0 - \psi_i)a^{0.888} \qquad (35)$$

The value of $(\psi_0 - \psi_i)$ is equal to the value of ΔC (see equation 29) converted to units of gm/cm^3.

Finally, the equation for evaporation rate (equation 16) becomes:

$$E = (5.71 \times 10^{4})G\bar{u}_1^{0.778} \qquad (36)$$

where,

E = evaporation rate, gm/ft^2 - min.

All of the other terms in equations 33-36 have been previously defined.

4. Empirical Equation by Delay and Seaders

Delay and Seaders (17, p. 60) developed an equation for the heat loss due to evaporation from an equation reported by Rapheal (39). Raphael, in turn, took the equation directly from the Lake Hefner study (6, p. 67). This equation has been given previously as equation 20. The equation of Delay and Seaders is as follows:

$$Q_E = M\,u\,(e_o - e_a)\,\theta \qquad (37)$$

where,

Q_E = energy loss due to evaporation, BTU/ft^2;

θ = time, hrs;

e_o, e_a, u = as defined for equation 20;

M = empirical mass transfer coefficient, M = 0.34 for lakes and 0.57 for rivers.

For evaporation rates in gm/ft^2 - min., equation 37 becomes:

$$E = \frac{M u (e_o - e_a)}{0.262\,L} \qquad (38)$$

where,

L = latent heat of vaporization of water, cal/gm.

This method was used in the aforementioned 1963 study on the coast fork of the Willamette River. In evaluating equation 38, the values for u and e_a were taken above the turbulent boundary region in the wind tunnel.

5. Experimental Relationship by Cermak and Koloseus (Equation 22)

Cermak and Koloseus (14) developed values for α and β such that equation 22 becomes:

$$N = 0.256\, R_*^{0.87} \tag{39}$$

where,

N, R_* = previously defined.

Evaporation rates are obtained from this relationship by first solving for R_* using equation 24, then solving for N from equation 39, and finally solving for E by using a form of equation 26, since equation 26 can be rearranged to give a direct solution for E if all the other terms are known.

Evaporation rates were computed for each test run using the five methods outlined above. For each method, a plot of computed evaporation versus measured evaporation was made. These plots are given in figures 8 - 12. The data from which these figures were made is given in the Appendix.

A set of computations for one test run, including original data, data reduction, preliminary calculations, and the use of existing equations, is also given in the Appendix.

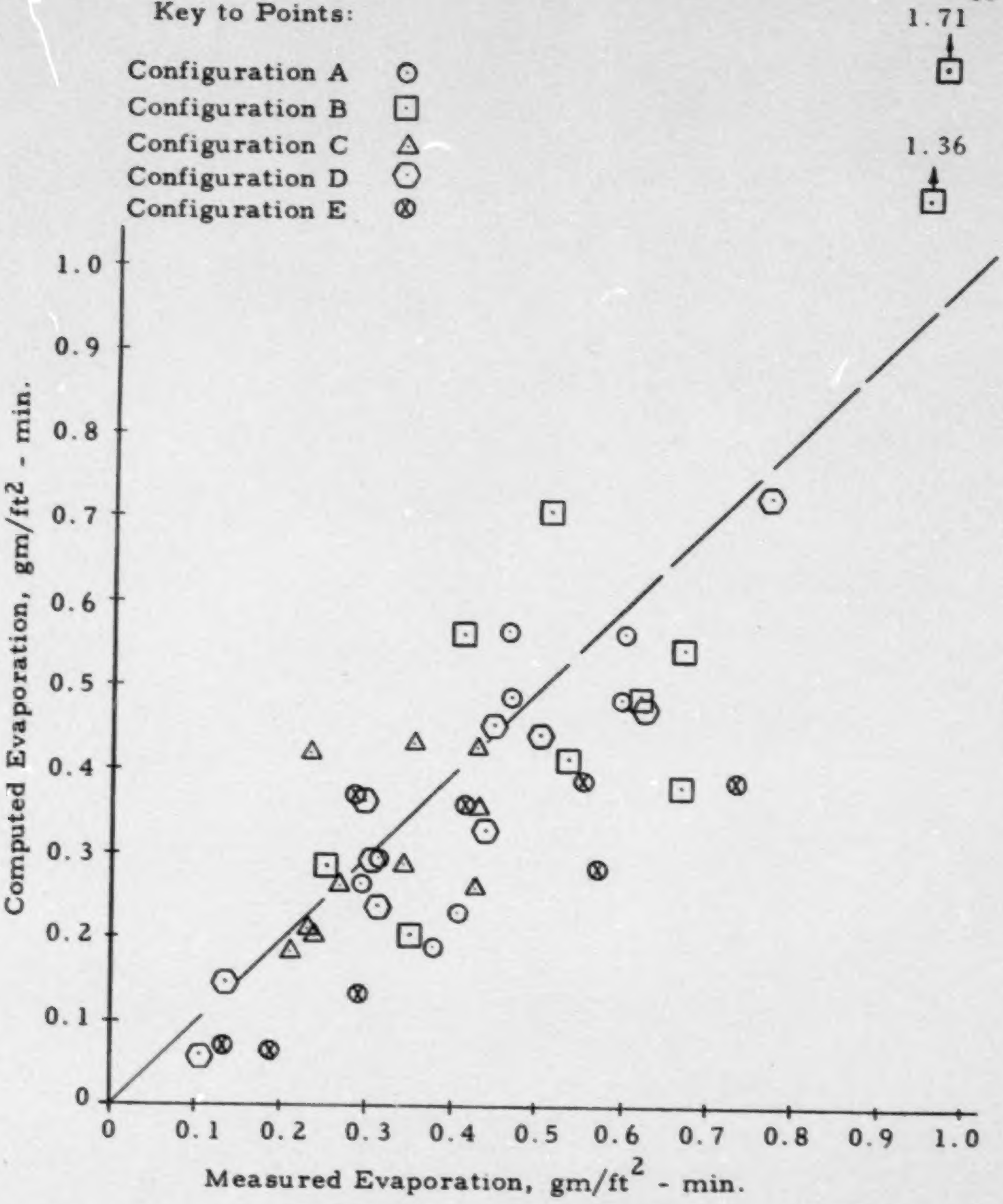

Figure 8. Evaporation Computed Using the Equations of Norris vs. Measured Evaporation

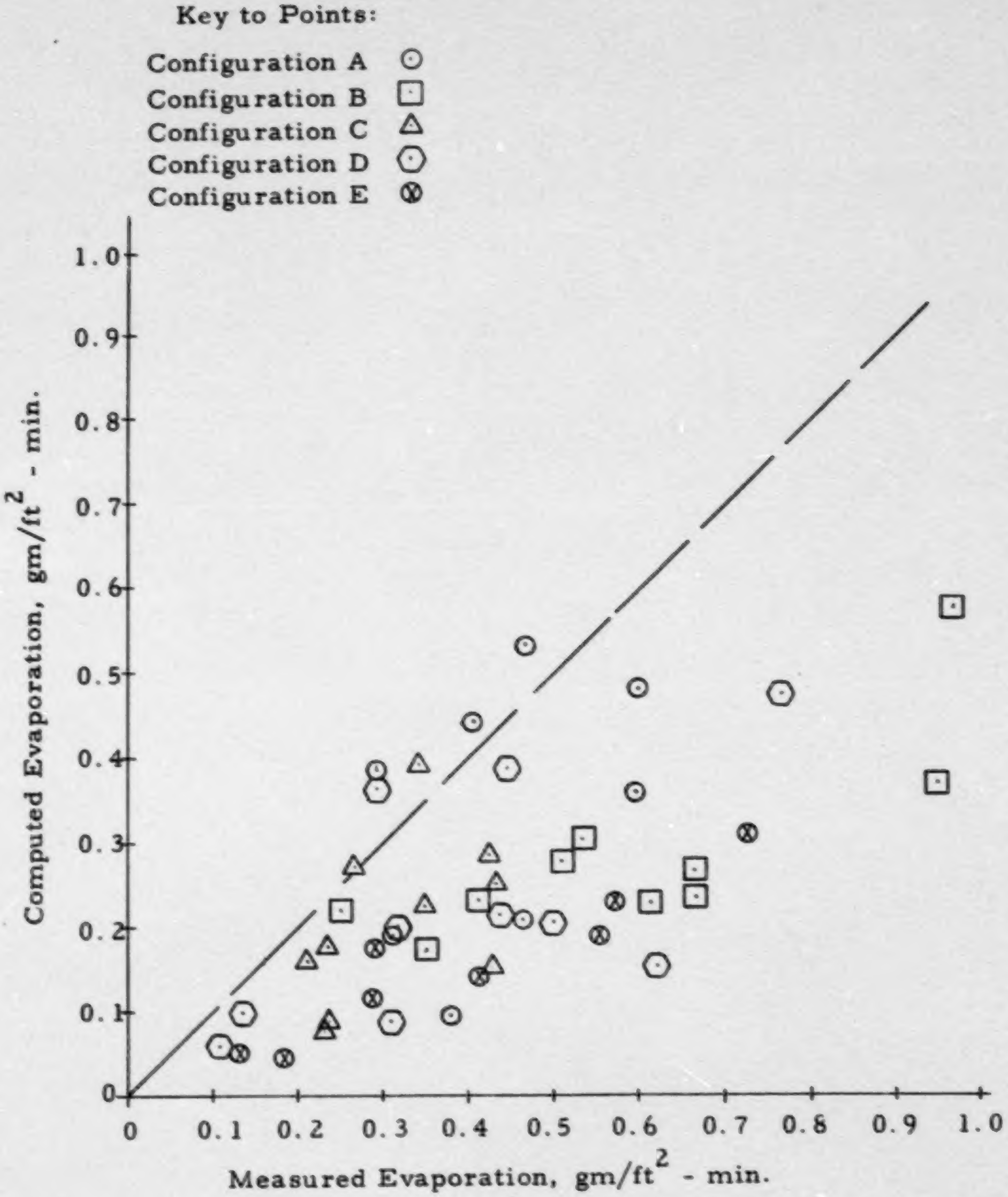

Figure 9. Evaporation Computed Using the Equation of Thornthwaite and Holzman vs. Measured Evaporation

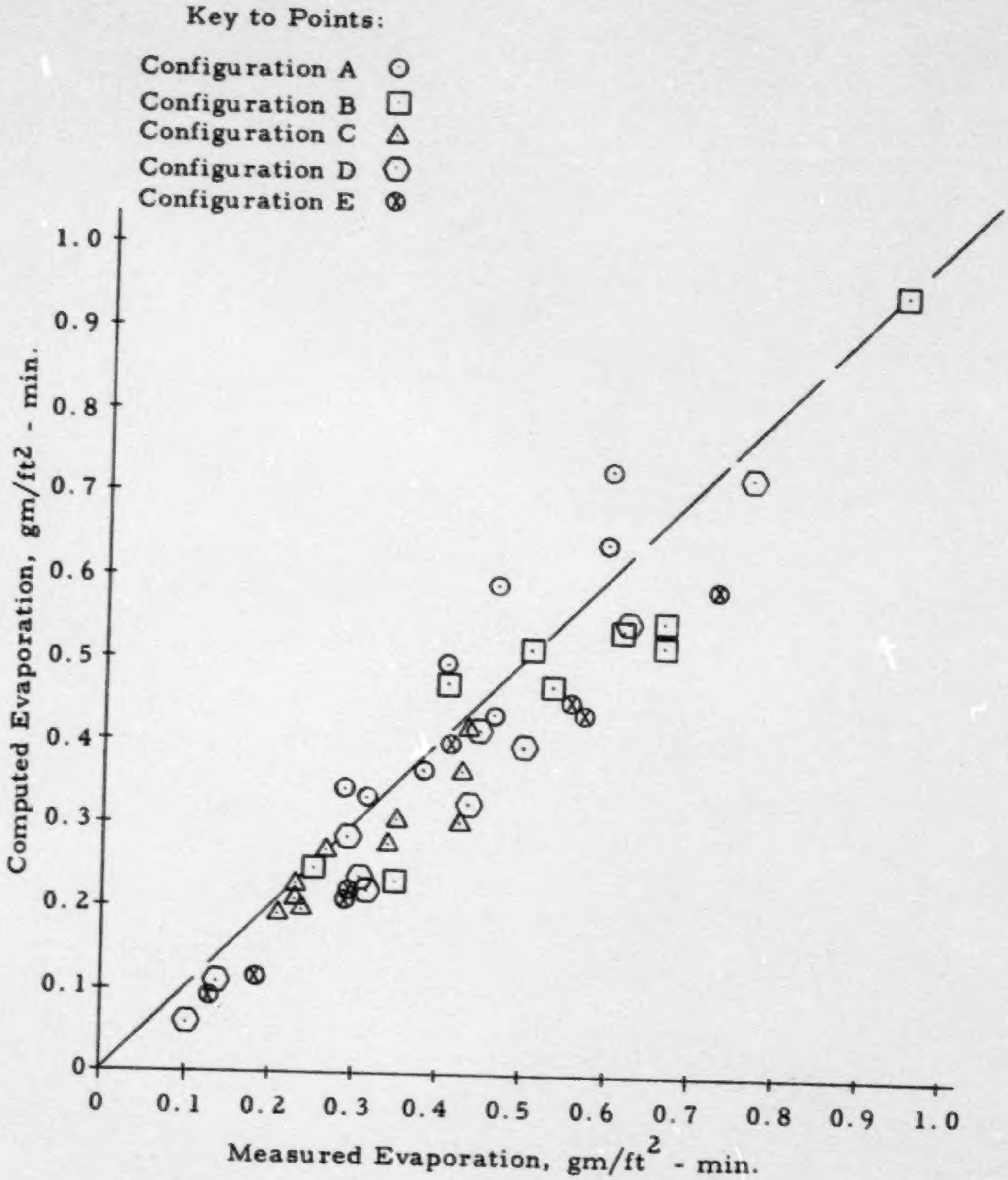

Figure 10. Evaporation Computed Using the Equations of Sutton vs. Measured Evaporation

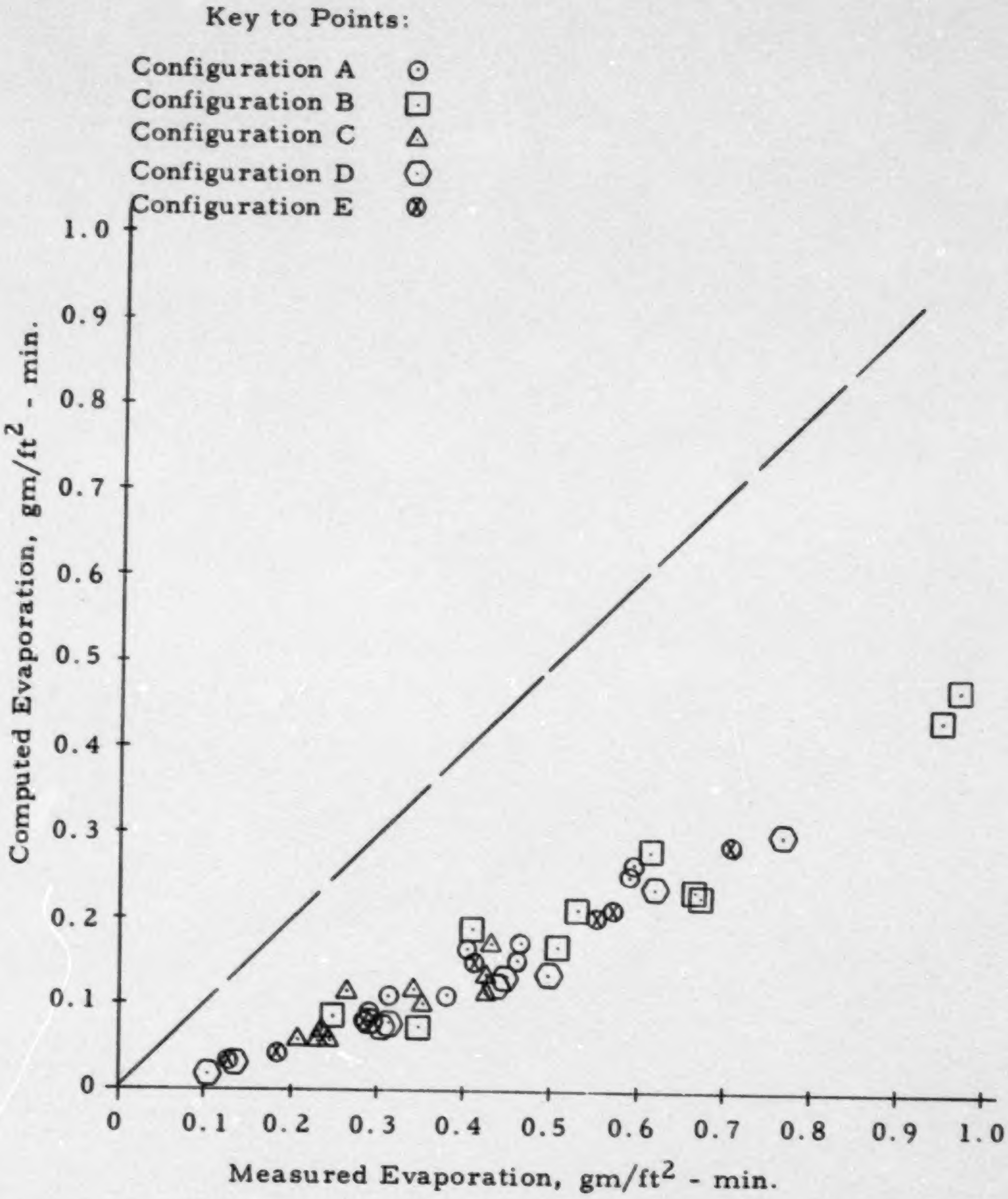

Figure 11. Evaporation Computed Using the Equation of Delay and Seaders vs. Measured Evaporation

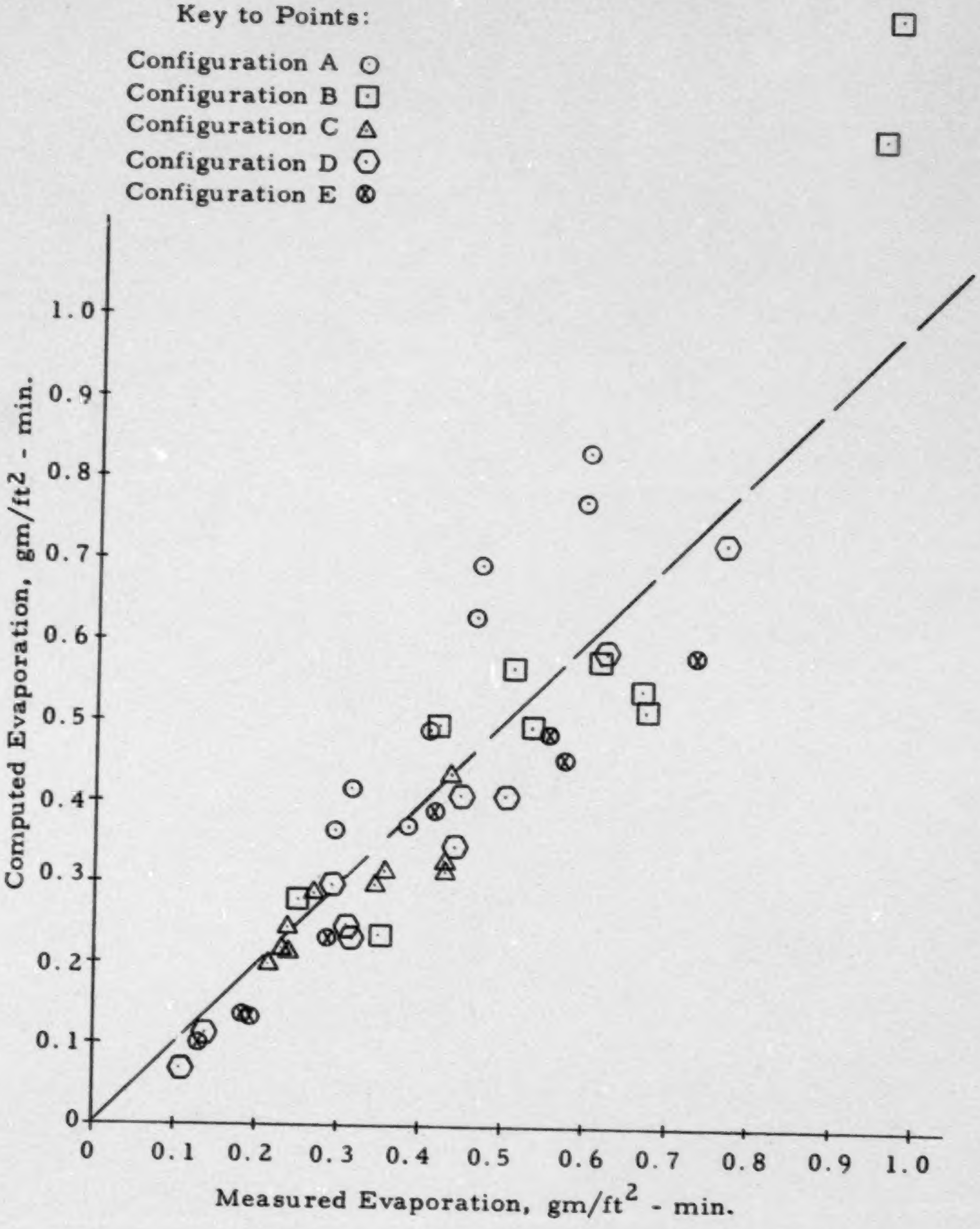

Figure 12. Evaporation Computed Using the Equations of Cermak and Koloseus vs. Measured Evaporation

Development of Experimental Equations

Four sets of experimental equations were developed to predict the evaporation rates from the model surfaces. Each set of equations consisted of empirical coefficients for each of the five surface configurations. These equations took the form of equations 4, 5, 21, and 22.

Equation 4,

$$E = (A + Bu)(e_s - e_a) \tag{4}$$

is a general mass transfer equation, where A is an empirically derived coefficient of molecular diffusion (i.e. - evaporation in the absence of wind) and B is an empirically derived mass transfer coefficient.

For each surface configuration, a plot was made of $E/(e_s - e_a)$ versus u, where e_a and u were taken in the ambient air stream above the turbulent boundary layer. Linear regression techniques employing the method of least squares, as described by Li (27), were used to evaluate the best straight line through these points. The equation of this line took the form:

$$E/(e_s - e_a) = A + Bu .$$

Thus, A was equal to the y-intercept at zero wind speed, and B was equal to the slope of the line.

Equation 21,

$$E = B'u\,(e_s - e_a) \qquad (21)$$

is probably the most common type employed. It differs from equation 4, because at zero wind speed the evaporation rate is also zero.

Using the same plot of $E/(e_s - e_a)$ versus u as mentioned above, the best straight line was constructed through the points and also through the origin. Thus, B' was merely the slope of this line. It was not possible to use Li's (27) method of least squares for this equation, since the form of the equation did not conform to that for which Li's method was developed.

The least squares method of linear regression requires that the residual sum of squares be minimized. Using an equation of the form:

$$y_i = \beta' x_i \,. \qquad (40)$$

The residual sum of squares (SS) is equal to:

$$\text{Residual SS} = \Sigma\,(y_i - \beta' x_i)^2.$$

Taking the partial derivative of this Residual SS with respect to β' yields:

$$\frac{\partial \text{ Res. SS}}{\partial \beta'} = -2\,\Sigma\,(y_i - \beta' x_i)\,(-x_i).$$

Setting this equal to zero gives:

$$\Sigma\,(y_i - \beta' x_i)\,(-x_i) = 0$$

$$\Sigma x_i y_i - \beta' \Sigma x_i^2 = 0.$$

Therefore,

$$\beta' = \frac{\Sigma x_i y_i}{\Sigma x_i^2}. \tag{41}$$

If x_i equals u, and $y_i = E/(e_s - e_a)$, then,

$$B' = \frac{\Sigma (u) \frac{E}{e_s - e_a}}{\Sigma u^2} \tag{42}$$

is an unbiased estimate of β', the slope of the regression line. Therefore, equation 42 was used to determine the best straight line which satisfied equation 21 for each surface configuration.

The development of the empirical coefficients in equation 5,

$$E = a (u)^b (e_s - e_a), \tag{5}$$

required a logarithmic transformation of the data prior to the use of Li's method of least squares. The logarithm of $E/(e_s - e_a)$ versus the logarithm of u was plotted using linear coordinates. The regression line thus took the form of:

$$\log[E/(e_s - e_a)] = a' + b \log u \tag{43}$$

where,

b = slope of regression line;

a' = intercept at u = 0.

Converting equation 43 back to the form of equation 5 yields:

$$E/(e_s - e_a) = (\text{antilog } a')(u)^b$$

$$E = (\text{antilog } a')\,(u)^b\,(e_s - e_a)$$

$$E = a\,(u)^b\,(e_s - e_a) \qquad (5)$$

where,

b = slope of the logarithmic regression line,

a = antilog of a'.

The evaluation of the empirical coefficients for equation 22,

$$N = \alpha R_*^{\beta}, \qquad (22)$$

followed the same steps as prescribed above for equation 5, but in this case plotting the logarithm of N versus the logarithm of R_*. Therefore, α = antilog of the intercept of the logarithmic regression line at $R_* = 0$, and β = the slope of this regression line.

The empirical coefficients obtained for these four equations and correlation indexes, r', are given in Table 5 for each surface configuration.

The correlation index is a measure of the closeness of fit of the plotted points to the estimated line of regression. It can be defined as:

$$r' = \frac{\text{Regression SS}}{\text{Total SS}} \qquad (44)$$

For equations 4, 5, and 22, this correlation index, r', is equivalent to the square of what Li calls the "correlation coefficient" r (27, p. 265). However, only in the context of Li's evaluation of

Table 5. Empirical Coefficients and Correlation Indexes

Surface Configuration	Equation 4			Equation 21		Equation 5			Equation 22		
	$E = (A + Bu)(e_s - e_a)$			$E = B'u(e_s - e_a)$		$E = a(u)^b(e_s - e_a)$			$N = \alpha R_*^{\beta}$		
	A	B	r'	B'	r'	a	b	r'	α	β	r'
A	0.018	4.72×10^{-3}	0.911	5.64×10^{-3}	0.871	0.00941	0.830	0.953	0.181	0.878	0.966
B	-0.0071	9.68×10^{-3}	0.907	9.29×10^{-3}	0.904	0.01243	0.890	0.895	0.011	1.234	0.855
C	0.0264	10.63×10^{-3}	0.863	12.01×10^{-3}	0.847	0.01952	0.834	0.931	0.097	0.992	0.934
D	0.0867	7.20×10^{-3}	0.678	12.28×10^{-3}	0.297	0.0439	0.554	0.810	2.24	0.637	0.846
E	0.0621	6.60×10^{-3}	0.908	10.55×10^{-3}	0.532	0.0356	0.575	0.954	1.64	0.672	0.956

Notes:

1. Budyko (9) reported values of b ranging from 0.5 to 1.0.
2. Hickox (22) reported $\alpha = 0.013$ and $\beta = 0.75$.
3. Albertson (3) reported $\alpha = 0.5$ and $\beta = 0.8$.
4. Cermak and Koloseus (14) reported $\alpha = 0.256$ and $\beta = 0.87$.

regression lines with the form,

$$\mu_{y \cdot x} = \alpha + \beta (x - \overline{x}),$$

can r' be considered equivalent to r^2. Thus, for equation 21, which was developed from a regression line of another form, r' does not equal r^2. The values of r' can range up to one, with an r' value of one indicating a perfect correlation (i.e. - all the points lie on the regression line).

Figures 13 - 16 are plots of evaporation rates computed from the experimentally developed equations versus measured evaporation. The reason for constructing such plots is to illustrate the difference in closeness of fit between the four experimental equations. The data from which these figures were derived can be found in the Appendix.

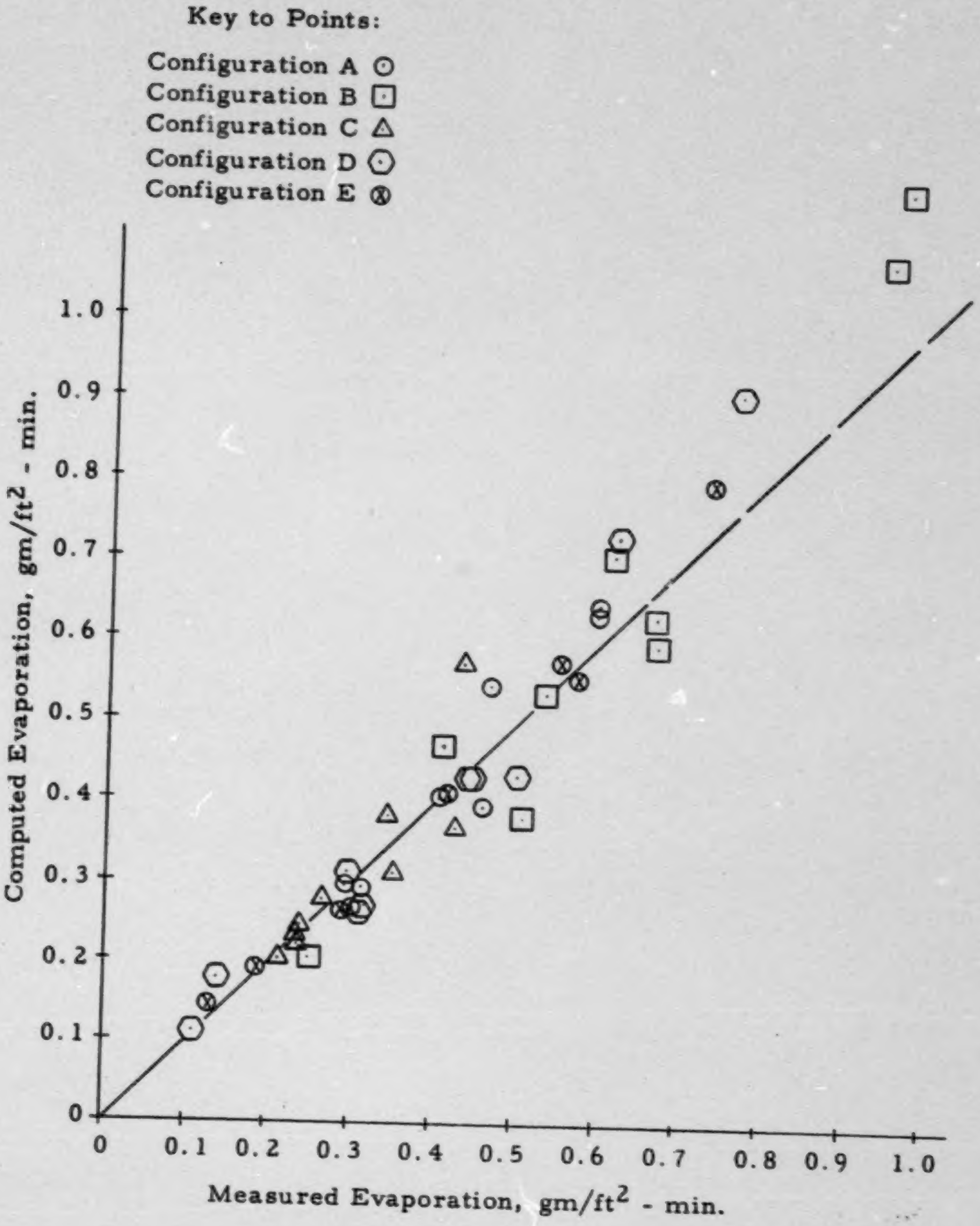

Figure 13. Evaporation Computed Using Equation 4 $[E = (A + Bu)(e_s - e_a)]$ vs. Measured Evaporation

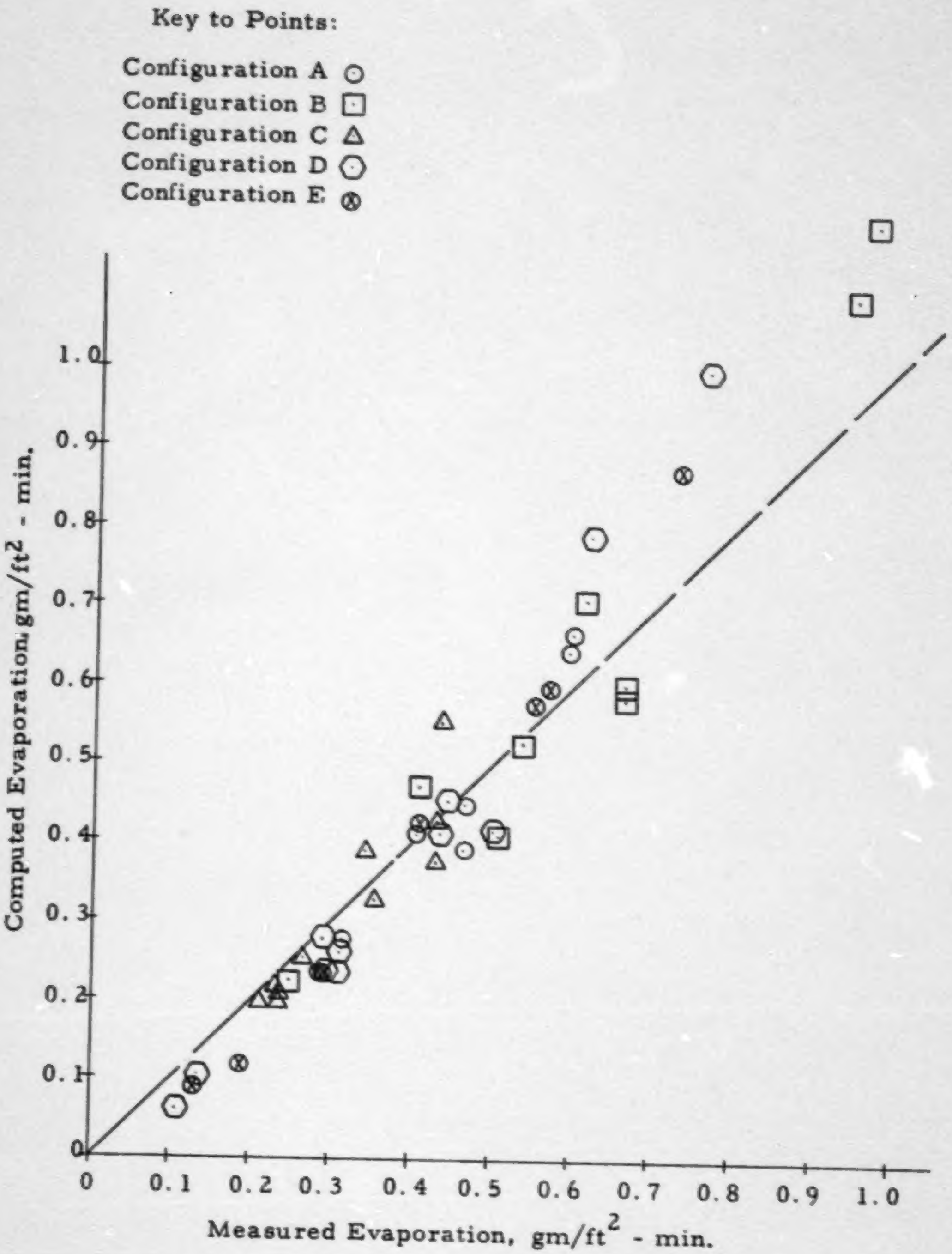

Figure 14. Evaporation Computed Using Equation 21
$[E = B'u(e_s - e_a)]$ vs. Measured Evaporation

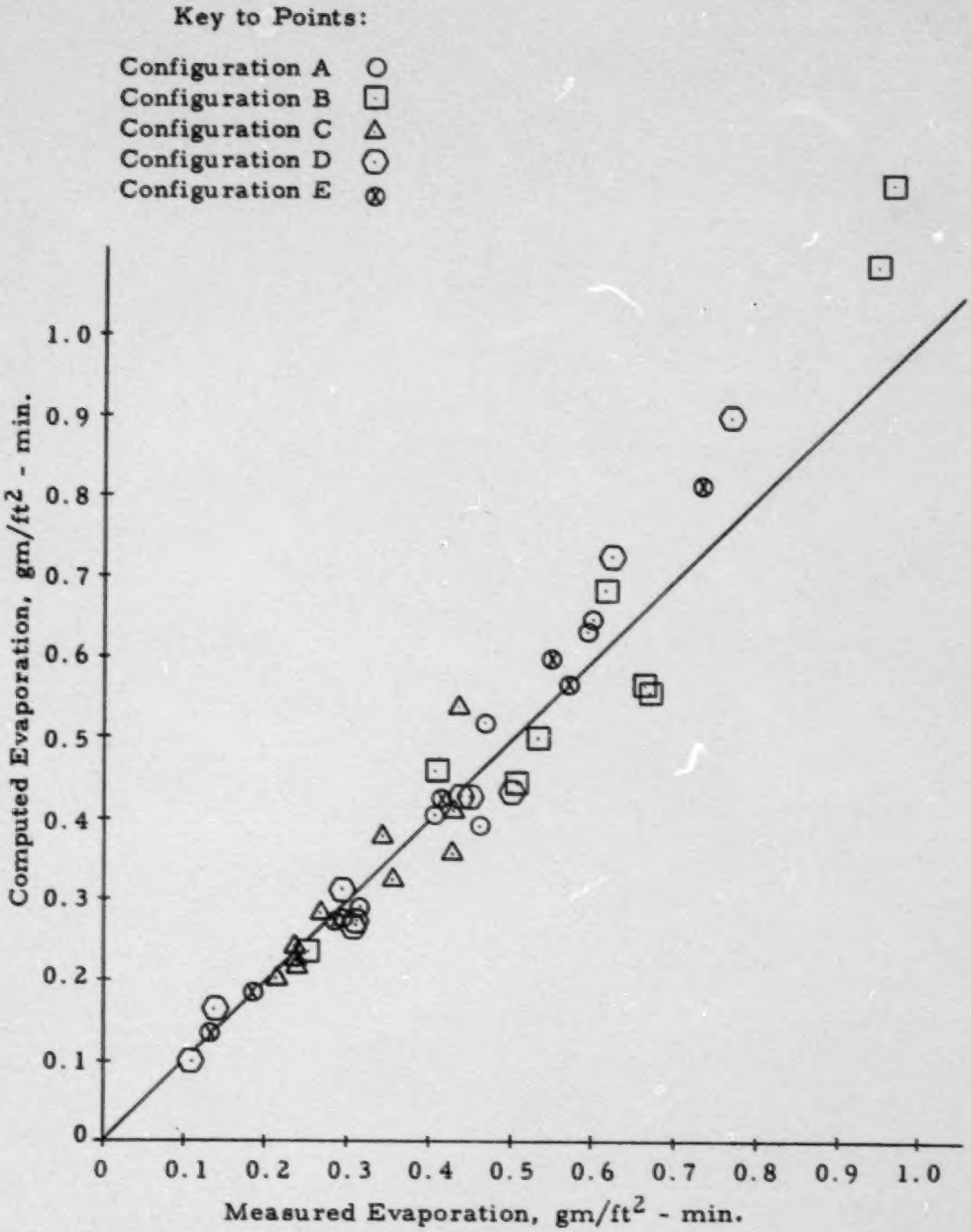

Figure 15. Evaporation Computed Using Equation 5 $[E = a(u)^b(e_s - e_a)]$ vs. Measured Evaporation

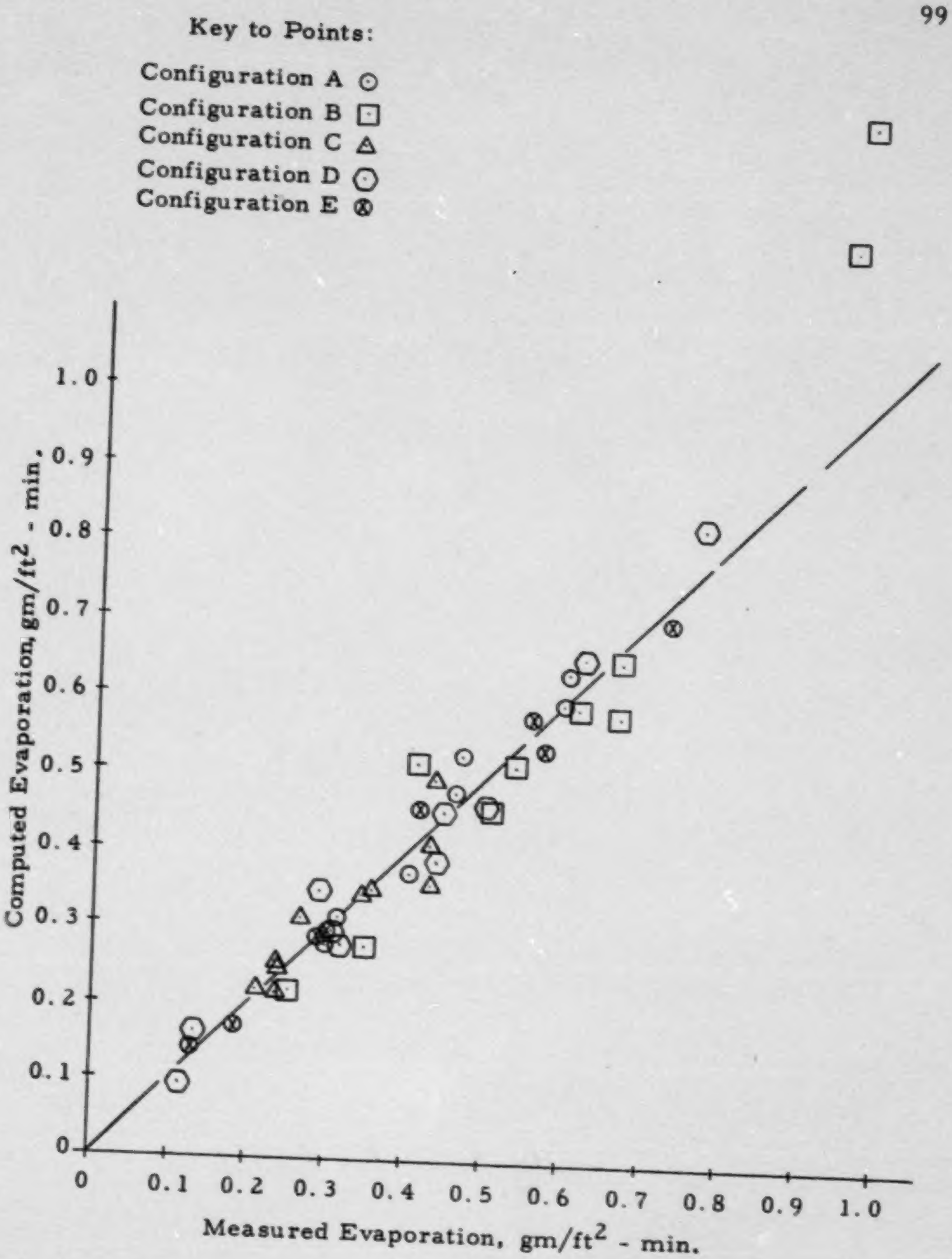

Figure 16. Evaporation Computed Using Equation 22 $[N = \alpha R_*{}^{\beta}]$ vs. Measured Evaporation

ANALYSIS AND DISCUSSION OF RESULTS

As stated in the scope of this thesis, the analysis of results is in two parts, including the comparison of existing equations and the development of a relationship between surface configuration and evaporation. The following section presents these analyses and a discussion of results obtained.

Comparison of Existing Equations

Figures 8 - 12 show the relationship between the evaporation rates as measured during the wind tunnel tests and those computed from existing equations. The 45 degree line extending from the origin of these graphs indicates the line of perfect correlation (i.e. - computed evaporation equals measured evaporation). In order to compare the five methods, it was necessary to establish a numerical measure of the closeness of fit of the plotted points to this line. Since this line is not a regression line, the correlation index, r', is not applicable. The numerical value which was employed is equal to the residual sum of squares (SS) divided by the total number of plotted points. The residual SS is found by summing the squares of the deviations of the points from the line. Since the equation of the line is simply $y = x$, where y = computed evaporation and x = measured evaporation, the residual SS can be defined as:

$$\text{Res. SS} = \Sigma(\text{computed E} - \text{measured E})^2.$$

Table 6 gives the values for Res. SS/n for each of the equations used (figures 8 -12) and for the plots involving the experimentally developed equations (figures 13 - 16).

Table 6. $\frac{\text{Res. SS}}{n}$ for Figures 8 - 16

Figure	Investigator(s)	Equation(s)	Res. SS
8	Norris	30, 31	30.94×10^{-3}
9	Thornthwaite and Holzman	32	59.87×10^{-3}
10	Sutton	33 - 36	8.04×10^{-3}
11	Delay and Seaders	38	86.78×10^{-3}
12	Cermak and Koloseus	39	13.09×10^{-3}
13	———	4	4.06×10^{-3}
14	———	21	6.07×10^{-3}
15	———	5	3.98×10^{-3}
16	———	22	6.00×10^{-3}

A low value for Res. SS/n indicates a better correlation than a high value, therefore, in order of their effectiveness, these five existing methods of evaporation prediction may be rated as follows:

1st - Sutton,

2nd - Cermak and Koloseus,

3rd - Norris,

4th - Thornthwaite and Holzman, and

5th - Delay and Seaders.

The high accuracy of Sutton's continuous mixing approach is not unusual since previous investigators have also found this method to be very effective (31). The reason that this method is not employed more extensively to field problems lies in the necessity of evaluating the stability parameter, n (see equations 16 - 19). As was mentioned previously, the wind tunnel environment of this research gave an n value of 0.25, however, under field conditions, the evaluation of n is often very difficult. Since field conditions involve changing atmospheric structure, the value of n also changes.

The reason for the relatively high ranking of the equation of Cermak and Koloseus must be attributed, in large part, to luck. Since this method involves empirical parameters developed under wind tunnel conditions for a specific model surface, its application to another model of different characteristics is questionable.

The two methods based on the discontinuous mixing theory are rated third and fourth. The failure of Thornwaite and Holzman's equation to give results of the same accuracy as obtained from the equations of Norris lies in their respective form. As mentioned previously, Norris (equation 12) developed his equation using a vapor pressure difference, $(q_s - q_b)$ or $(e_s - e_b)$, between the water surface and a point in the turbulent boundary region as the driving force for evaporation. Thornthwaite and Holzman (equation 13), on the other hand, used as a driving force the difference in vapor pressure,

$(e_1 - e_2)$, existing between two points within the turbulent boundary region. Although, theoretically, both of these methods should give equally valid results, the physical process of vapor pressure measurement makes the method of Thornthwaite and Holzman subject to error. Since the magnitude of $(e_s - e_b)$ is usually much greater than that of $(e_1 - e_2)$, more latitude of measurement error is allowed in the first case. This means that using instruments of the same accuracy, the value for $(e_s - e_b)$ would be more accurate than the value for $(e_1 - e_2)$ since the same experimental error will affect $(e_1 - e_2)$ more than $(e_s - e_b)$. Several investigators (31, 9) have commented on their failure to apply the equation of Thornthwaite and Holzman, because of a lack of the instrumentation necessary to measure $(e_1 - e_2)$ accurately. In this research, it was also difficult to measure $(e_1 - e_2)$ accurately as is evident from an examination of Figure 9.

The complete failure of the equation of Delay and Seaders to give accurate results lies in the fact that it was derived from an experimental equation with an empirical mass transfer coefficient which is only applicable to a specific set of conditions. An examination of Figure 11 reveals, however, that predictions based upon this equation are quite uniform. Thus, the basic equation appears to be valid, but the empirically derived mass transfer coefficient does not. Since this was the equation used in the 1963 study mentioned previously, it is significant that the low evaporation rates obtained using this equation further substantiate the assumption that the reason for the poor comparison of computed to measured stream temperature during the night lies in an erroneous evaluation of evaporative heat loss.

An evaluation of the two methods based on discontinuous mixing and Sutton's method based on the continuous mixing theory leads one to the conclusion that theoretical methods of evaporation prediction vary widely in their simplicity and accuracy. Sutton's equations give reliable results, but are generally avoided because of their complexity. On the other hand, the equations of Norris (or Sverdrup) yield results of lower accuracy but are more amenable to solution using field data. Finally, the equation of Thornthwaite and Holzman is sound theoretically, but instruments of sufficient accuracy to measure the required vapor pressure deficit have not yet been perfected, so the method itself is of limited usefulness.

Since these three theoretical methods were developed using the structure of the turbulent boundary region as their basis, there is no provision for analyzing the effect of surface configuration on evaporation. Since different surface configurations can be expected to produce wind speed profiles of different shapes under similar conditions of ambient air flow, the effect of surface configuration will be taken into account in the evaluation of such parameters as z_o and u_*. In other words, different surface configurations will produce turbulent boundary regions of different characteristics under the same wind tunnel conditions, and these different boundary region characteristics will be accounted for in the solution of the theoretical equations. Thus, the theoretical evaporation equations require knowledge concerning the structure of the overlying air, but they do not require information about the surface configuration of the water body.

Analysis of Experimentally Developed Equations

The reason for developing the four types of experimental equations, as described in a preceding section, was to gain an insight into the pattern of evaporation from the five different model surfaces. As can be seen from the last four Res. SS/n values in Table 6, each experimentally developed equation was about equally effective in predicting measured evaporation rates. The equations are given in curve form in Figures 17 - 20. Data points are omitted in the figures in the interest of clarity. The Appendix contains the data upon which the figures are based. It should be noted that Figures 19 and 20 are plotted on linear coordinates, while the regression lines from which they were derived were logarithmic.

A series of statistical tests were performed on these regression lines in an effort to relate surface configuration to evaporation rates.

1. Test of Homogeneity of Regression Coefficients

This test, as described by Li (27, p. 344-349), was used to determine if the regression coefficients (i.e. - the slopes of the

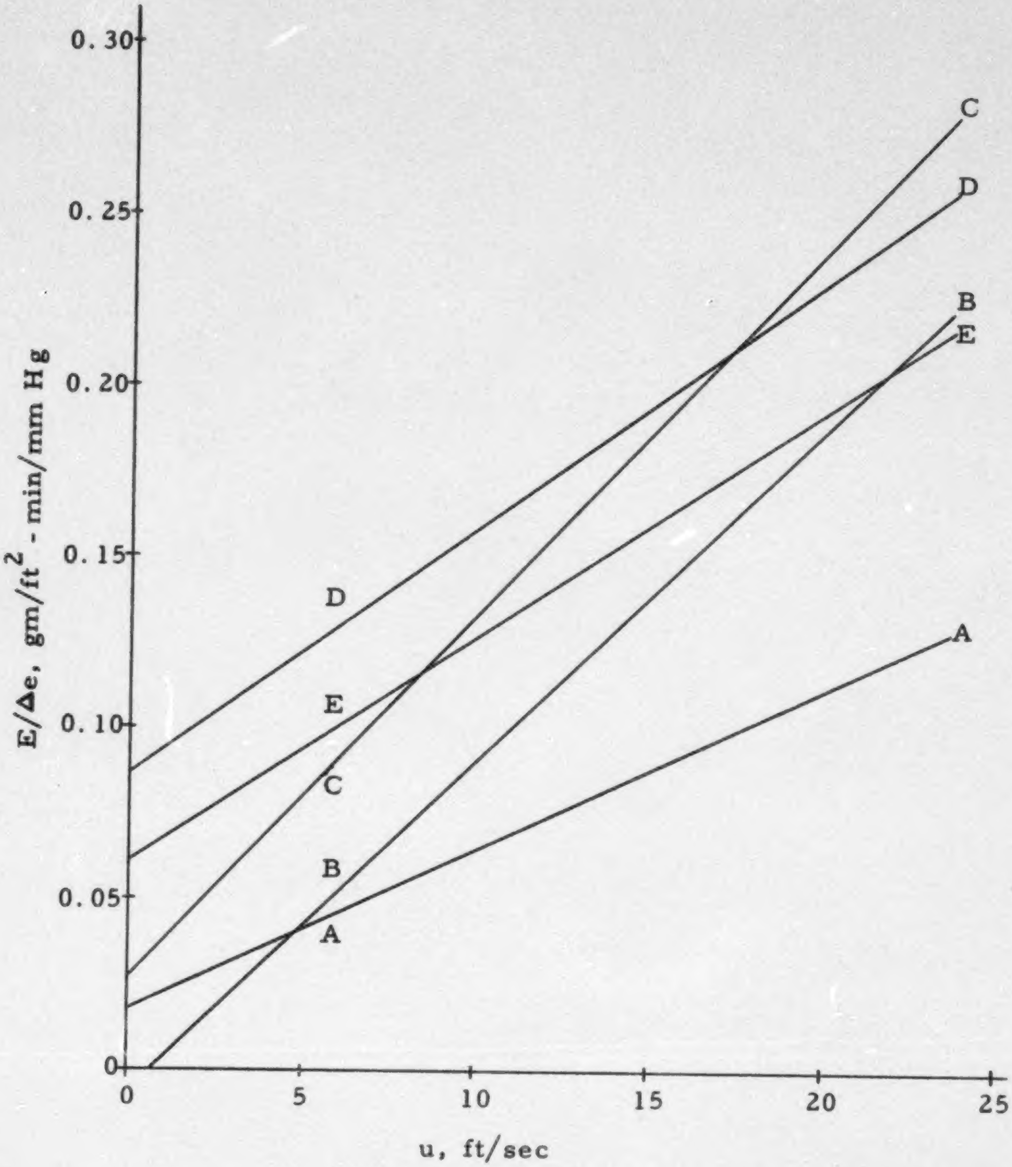

Figure 17. Curves of $E = (A + Bu)(\Delta e)$ for the Five Model Surfaces

Note: $\Delta e = (e_s - e_a)$

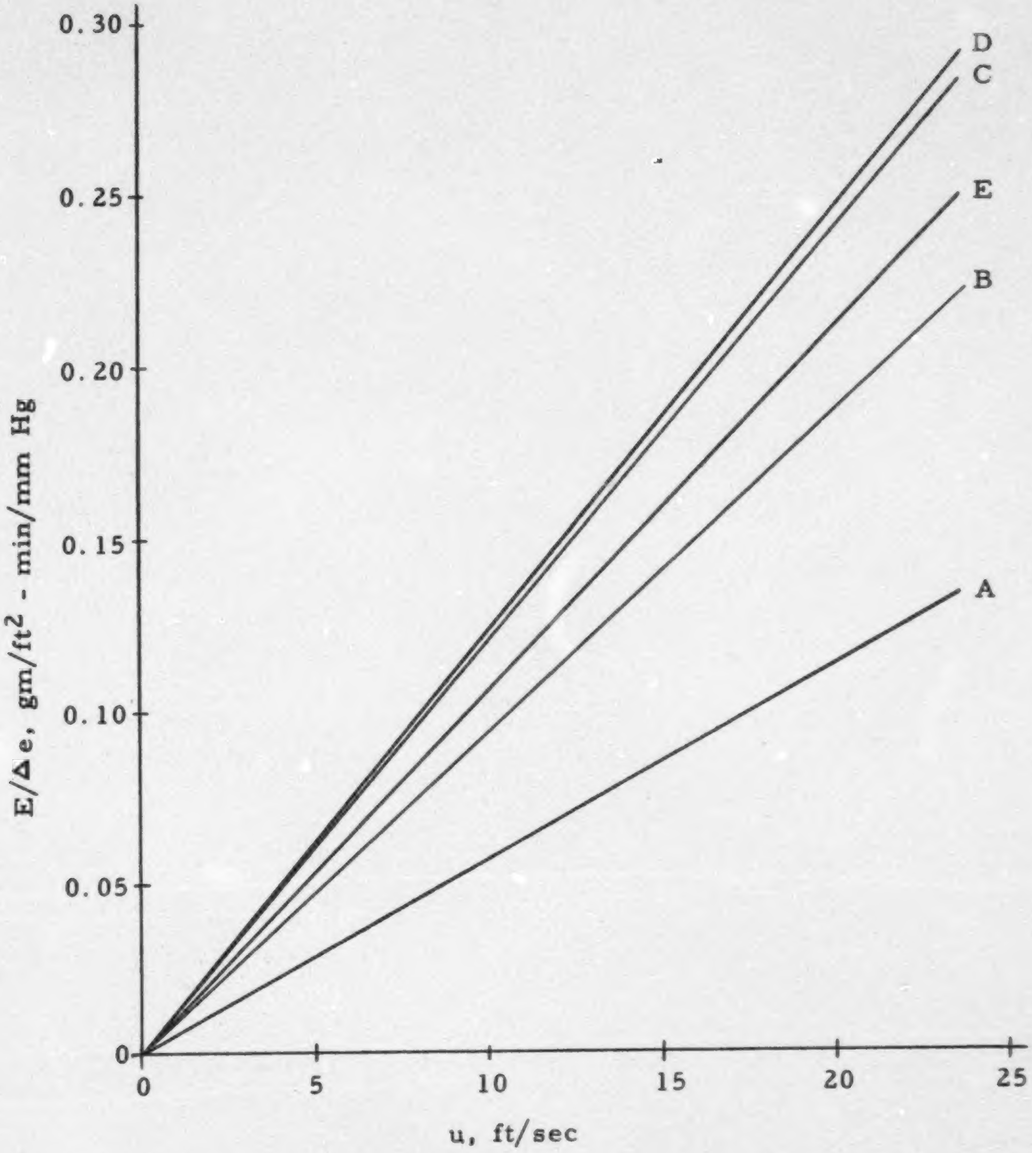

Figure 18. Curves of $E = B'u(\Delta e)$ for the Five Model Surfaces

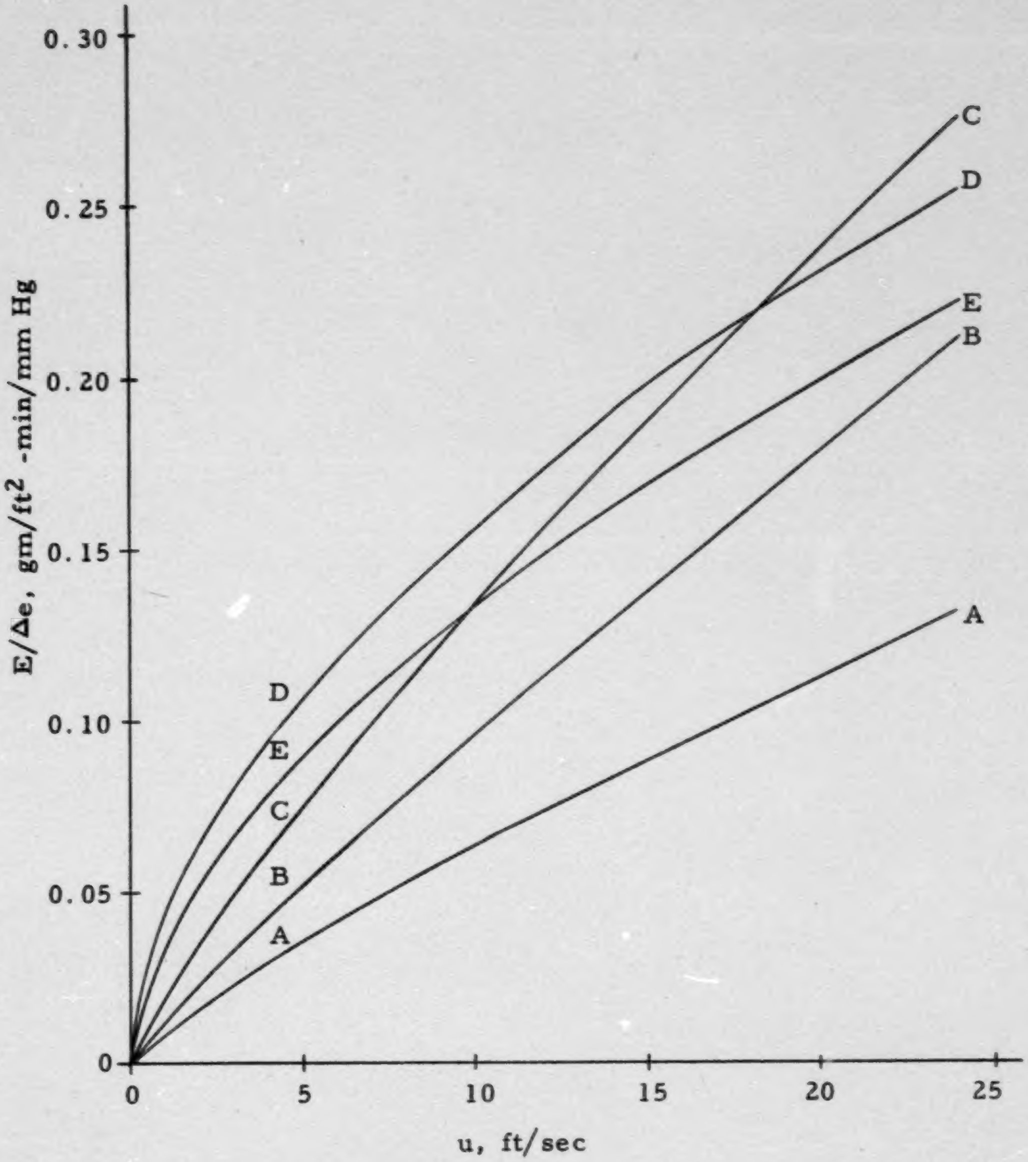

Figure 19. Curves of $E = a(u)^b(\Delta e)$ for the Five Model Surfaces

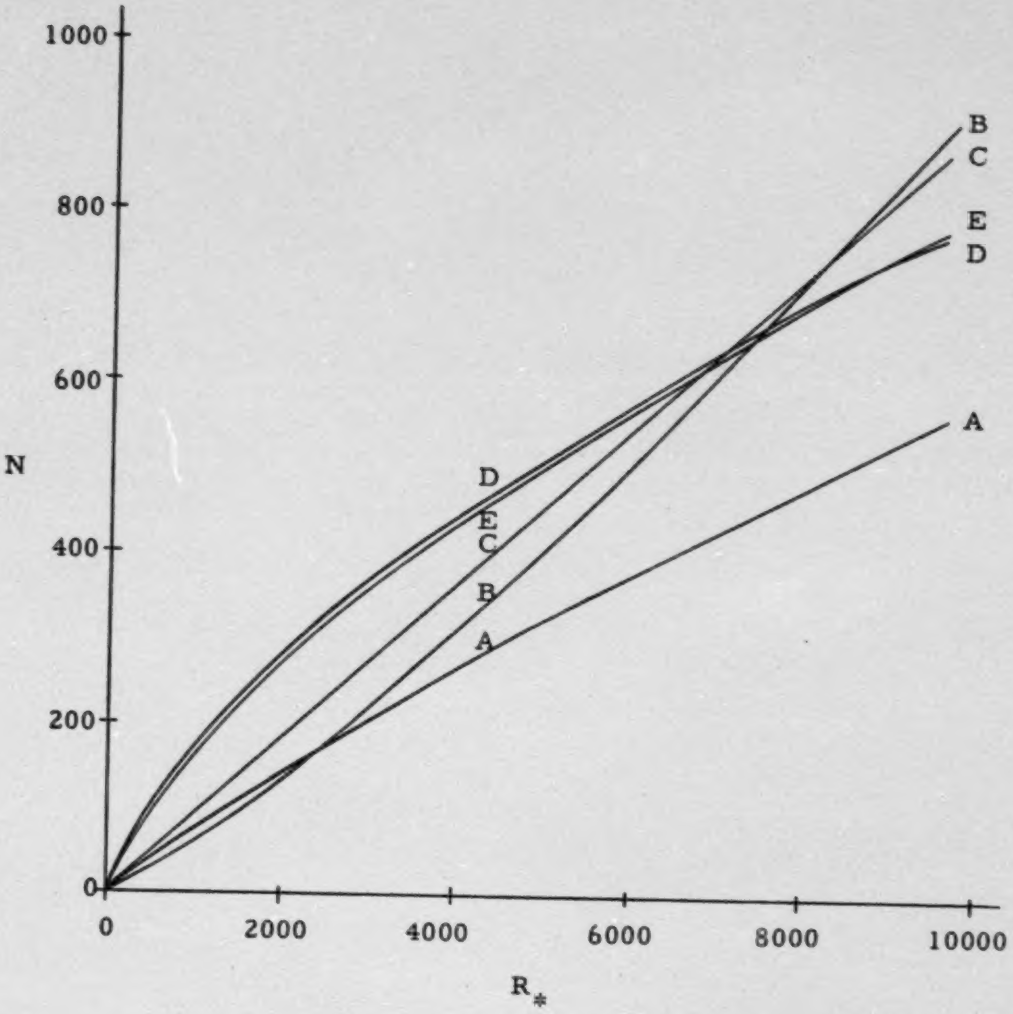

Figure 20. Curves of $N = \alpha R_*^{\beta}$ for the Five Model Surfaces

regression lines) were equal for the five curves of each experimental equation. The method uses an F - test, where the F value is equal to a modified regression mean square divided by the pooled residual mean square. All the tests were performed at the five percent level of significance, and the tests were one-tailed on the right. The results of the statistical analyses are summarized in Table 7.

As can be seen from this table, all of the hypotheses were rejected. This means that there is a statistically significant difference between the slopes of the individual regression lines established for the four experimental equations.

2. Analysis of Covariance for Testing the Homogeneity of Adjusted Means.

This test (27, p. 353-356) is used to determine if the y values of a set of regression lines are equal at any value of x. In terms of the experimental equations under discussion, the test was used to determine if the intercepts of the regression lines at an x value of zero were all equal for each equation. This method is similar to that used for testing the homogeneity of regression coefficients. The F value is determined by dividing a weighted mean square due to variation among the adjusted means by the pooled residual mean square. The test is one-tailed on the right. Table 8 summarizes the results of the statistical analyses.

This table shows that at the five percent level of significance all

Table 7. Tests of Homogeneity of Regression Coefficients

Equation	Hypothesis	Regression Degrees of Freedom	Residual Degrees of Freedom	5% F Limit	Computed F Ratio	Conclusions
$E = (A + Bu)(e_s - e_a)$	$B_A = B_B = B_C = B_D = B_E$	4	34	2.65	3.33	Reject Hypothesis
$E = B'u(e_s - e_a)$	$B'_A = B'_B = B'_C = B'_D = B'_E$	4	34	2.65	19.04	Reject Hypothesis
$E = a(u)^b(e_s - e_a)$	$b_A = b_B = b_C = b_D = b_E$	4	34	2.65	3.24	Reject Hypothesis
$N = a R_*^{\beta}$	$\beta_A = \beta_B = \beta_C = \beta_D = \beta_E$	4	35	2.64	4.94	Reject Hypothesis

Note: The subscripts on the regression coefficients refer to the model surfaces.

Table 8. Tests of Homogeneity of Adjusted Means

Equation	Hypothesis	Adjusted Mean Degrees of Freedom	Residual Degrees of Freedom	Level of Significance	F Level	Computed F Ratio	Conclusions
$E = (A+Bu)(e_s - e_a)$	$A_A = A_B = A_C = A_D = A_E$	4	34	5%	2.64	2.72	Reject Hypothesis
$E = (A+Bu)(e_s - e_a)$	$A_A = A_B = A_C = A_D = A_E$	4	34	2-1/2%	3.19	2.72	Accept Hypothesis
$E = a(u)^b(e_s - e_a)$	$a_A = a_B = a_C = a_D = a_E$	4	34	5%	2.64	7.03	Reject Hypothesis
$N = \alpha R_*^{\beta}$	$\alpha_A = \alpha_B = \alpha_C = \alpha_D = \alpha_E$	4	35	5%	2.65	5.34	Reject Hypothesis

of the hypotheses were rejected, thus indicating that a statistically significant difference exists between the adjusted means at x equals zero for the individual regression lines developed for the three experimental equations. However, at the 2-1/2 percent level of significance, the hypothesis is accepted for $E = (A + Bu)(e_s - e_a)$. This means that at this level of significance there is no significant difference between the A values for each model surface configuration.

3. t-tests for A Values

Since the test of homogeneity of adjusted mean values indicated that the values of A in the equation $E = (A + Bu)(e_s - e_a)$ are all equal at the 2-1/2 percent significance level, five t-tests were performed to determine if the A values were equal to zero. A two-tailed t-test based on the distribution of adjusted means (27, p. 287) was used. The results of these t-tests are indicated in Table 9.

An examination of this table shows that at the five percent significance level the A values for all the surface configurations except E are not significantly different from zero. For configuration E, this same conclusion is reached at a level of significance of two percent.

4. Tests Using Individual Degrees of Freedom

The individual degree of freedom may be used to test specific hypotheses concerning parameters of linear regression lines. A series of tests using individual degrees of freedom was performed on

Table 9. t-Tests for A Values Equal to Zero

Surface Configuration	Hypothesis	Degrees of Freedom	Level of Significance	t Limits	Computed t Value	Conclusions
A	$A_A = 0$	5	5%	± 2.57	0.13	Accept Hypothesis
B	$A_B = 0$	7	5%	± 2.37	-0.14	Accept Hypothesis
C	$A_C = 0$	8	5%	± 2.31	0.34	Accept Hypothesis
D	$A_D = 0$	8	5%	± 2.31	1.14	Accept Hypothesis
E	$A_E = 0$	6	5%	± 2.45	2.88	Reject Hypothesis
E	$A_E = 0$	6	2%	± 3.14	2.88	Accept Hypothesis

the regression coefficient, B', of the equation $E = B'u(e_s - e_a)$. As described by Li (27, p. 359-363), the method involves a one-tailed F test, with the F ratio equal to the individual degree of freedom divided by the pooled residual mean square. Table 10 summarizes the results of the tests, which were all performed at the five percent significance level. With 34 residual degrees of freedom, the F_{34}^{1} limit equals 4.12.

At this point conclusions can be drawn with regard to the effect of surface configuration on evaporation rates from the model surfaces. An examination of the equation $E = B'u(e_s - e_a)$ reveals that the mass transfer coefficient, B', is related to some characteristic of the model surfaces. If this were not true, then there would be no significant difference between the B' values for the five different surface configurations. However, the test of homogeneity of regression coefficients proved that there is a significant difference between these values (see Table 7). The tests of individual degrees of freedom, however, indicates that certain relationships do exist between the B' values. The conclusions reached in Table 10 can be summarized in the following manner, with the subscript letter indicating the model surface type described in Table 3:

1) $B'_C = B'_D$

2) $B'_B = B'_E$

Table 10. Tests of Individual Degrees of Freedom of B'

Specific Hypothesis	Computed F Ratio	Conclusions
$B'_C = B'_A$	0.11	Accept Hypothesis
$B'_B = B'_E$	1.72	Accept Hypothesis
$B'_C + B'_D = B'_B + B'_E$	14.89	Reject Hypothesis
$B'_A = \frac{1}{2}(B'_B + B'_E)$	27.13	Reject Hypothesis

3) $B'_C + B'_D \neq B'_B + B'_E$ and

4) $B'_A \neq 1/2(B'_B + B'_E)$.

Also, if one examines the magnitudes of the B' values in Table 5, one can establish the following inequalities:

B'_C and $B'_D > B'_B$ and $B'_E > B'_A$.

One characteristic of surface configuration is wave steepness, where wave steepness equals the ratio of wave height to wave length (i.e. - H/L). Table 3 indicates H and L for the five model surfaces. Wave steepness values computed from this table give the following results, along with B' values for comparison:

Model Surface	H/L	B'
A (flat plate)	0	5.64×10^{-3}
B (rippled)	1/8	9.29×10^{-3}
C (rippled)	1/4	12.01×10^{-3}
D (rippled)	1/4	12.28×10^{-3}
E (rippled)	1/8	10.55×10^{-3}

By using these H/L values, one can draw the conclusion that B' values increase as wave steepness increases. Taking this one step further, since B' is the only empirical constant in the equation $E = B'u(e_s - e_a)$, one can conclude that evaporation rates increase as wave steepness increases.

This conclusion is, of course, limited in that it was obtained from an analysis of only one of the four experimentally developed equations. The use of this equation, however, is based on several factors. First of all, it should be recognized that this form of simplified experimental equation is the type most widely used. For example, Delay and Seaders used a similar equation (see equation 20) to develop their method. Another factor worthy of note is that the equation $E = (A + Bu)(e_s - e_a)$ is not significantly different from the equation which was used to draw the preceding conclusion. The analysis of covariance for testing the homogeneity of adjusted means (Table 8) showed that the A values were not significantly different for the five surface configurations. A series of t-tests (Table 9) further showed that the A values did not vary significantly from zero. Thus, if A equals zero, the equation $E = (A + Bu)(e_s - e_a)$ becomes $E = Bu(e_s - e_a)$, which is essentially the same as $E = B'u(e_s - e_a)$. The physical significance of the A values being zero is that there is assumed to be no evaporation in the absence of wind. Although a small amount of water vapor is lost by molecular diffusion under these conditions, this assumption can be regarded as valid for practical conditions encountered in the field.

The two equations represented by Figures 19 and 20 present a somewhat more complicated picture than Figure 18. Only within a certain range of u values (i.e. - 10 to 15 ft/sec.) does Figure 19 exhibit the same characteristics as Figure 18. Furthermore, an interesting phenomenon occurs in Figure 20 at a modified Reynolds number, R_*, value of about 7500. At this point it appears that all the lines intersect, except for the line of model surface A. At R_* values below 7500 Figure 20 displays trends similar to Figure 18, but above these values a different relationship between evaporation rates and surface configuration emerges.

A possible explanation for this reversal may lie in what could be called the sheltering effect of waves. Since the waves on the model surfaces were solid, static bodies, it is possible that at some wind speed eddies were formed behind each wave. This is shown schematically in Figure 21.

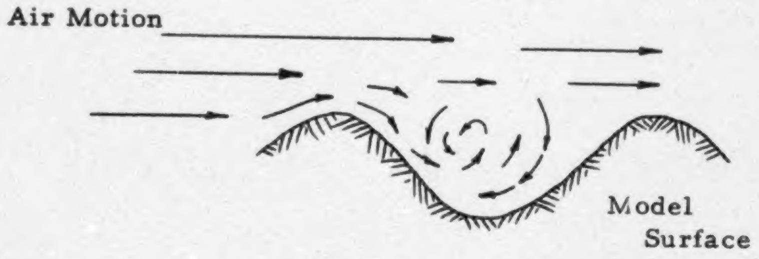

Figure 21. The Sheltering Effect

The eddies formed behind the wave would give increased turbulence, but the effect of this increase in turbulence would be more than compensated for by the increase in moisture content of the air being recirculated in the eddies. Therefore, within this eddy zone the evaporation rate would decrease, because the eddies tend to recirculate the same air. This would maintain a high vapor concentration over this region, and thus lower the vapor pressure driving force. This phenomenon has been explained in a somewhat different manner by Albertson (2).

Although it is likely that this phenomenon occurred over the model surfaces, no quantitative evaluation of its effect is possible. It does appear, however, that thereis a critical modified Reynolds number range where this effect occurs. There also may be a relationship between the decrease in evaporation due to the sheltering effect and the steepness of the waves, but data is not now available to evaluate this relationship.

No conclusions regarding the relationship between surface configuration and evaporation rates can be drawn from Figures 19 and 20. However, it is interesting to note that in the lower absicissa ranges both figures exhibit the same pattern.

In summarizing the analysis of the experimentally developed equations, it can be said that when a simple equation of the form $E = B'u(e_s - e_a)$ is employed, there is a general relationship between surface configuration and evaporation. When more complex forms are employed, however, this relationship is unclear due, at least in part, to a phenomenon called the sheltering effect.

Application of Results to Real Streams

Cermak and Koloseus (14) developed a relationship between the dimensionless ratios N and R_* so a correlation could be made between model results and prototype data. Their analysis of similitude indicated that the equation $N = \alpha {R_*}^{\beta}$ is valid for both model and prototype when R_* values ranged from 10^3 to 10^9. Since all the R_* values obtained in the research carried out for this thesis were in the lower part of this range, the relationships established between N and R_* might be applicable to a prototype situation. No R_* data is available for field conditions on streams, but data taken over Lake Hefner gave R_* values exceeding 10^8 (14). Therefore, it is reasonable to expect that R_* values for streams would not exceed 10^9. As was stated previously, however, the empirical coefficients of the relationships between N and R_* which were developed for the model streams could not be related to surface configuration, hence an application of this method to a prototype situation would have little significance in the context of this research.

An application of the empirical coefficients of the other equations to a real stream is, of course, impossible. Since all three of these equations are based on velocity and vapor pressure measurements above the turbulent boundary layer, the physical problems of measurement in the field are, at present, insurmountable.

These equations were not developed for prototype application, however, and their real value lies in the conclusions reached from an analysis of the various empirical coefficients. The next step in the total research program would be to develop a means of relating the surface configuration of a flowing stream to some measureable hydraulic parameter. If such were attainable, the results of this model study could be applied to a real stream. Until that time, the results obtained in this thesis can not be applied directly to a dynamic situation. It is felt, however, that the conclusion reached regarding evaporation rates and model wave steepness is a significant contribution which is useful for the solution of the total problem.

Until valid techniques for applying empirical coefficients to general situations are available, the computation of evaporation rates from streams should be made using the equations based on the transfer of water vapor in the turbulent boundary region. These theoretical equations are preferable to experimental methods, unless the experimental techniques are developed for the specific conditions under investigation. The reason for the reliance of field personnel on empirical relationships lies in the simplicity of their mathematics and in the relatively small amount of data necessary for their solution. Therefore, in any evaporation determination, the expedience of experimental methods must be weighed against the higher accuracy of theoretical equations, even though the cost of using the latter might be high.

In conclusion, it can be said that despite the seemingly unending and unlimited quantities of equations, data, and experimental relationships concerned with the evaporation from free water surfaces, there is, in truth, a glaring paucity of data and information which can be used to relate specific stream parameters to evaporation. This void of research includes the relationship between stream evaporation and surface configuration. It is hoped that this research project has filled at least a small part of this empty space.

CONCLUSIONS

1. The mass transfer coefficient in the experimentally developed equation $E = B'u(e_s - e_a)$ is related to model surface configuration. Using wave steepness, H/L, as a characteristic of model surface configuration, B' increases as H/L increases. Therefore, when this specific equation is used, evaporation rate increases as wave steepness increases.

2. The term for molecular diffusion, A, in the equation $E = (A + Bu)(e_s - e_a)$ appears to be essentially equal to zero.

3. A phenomenon called the sheltering effect appears to influence evaporation rates from the model surfaces. This effect seems to occur in a certain range of modified Reynolds number values, and it also may be a function of wave steepness.

4. Equations based on the structure of the overlying air may be used to predict evaporation rates, without any specific knowledge concerning stream surface configuration.

5. Of the three theoretical methods tested, Sutton's method gave the best correlation between computed and measured evaporation rates. The method of Norris was next, followed by the equation of Thornthwaite and Holzman.

6. The equation of Thornthwaite and Holzman failed to give good results, because the instrumentation for measuring the vapor

pressure deficit is not accurate enough.

7. The failure during the 1963 study made on the coast fork of the Willamette River to compute accurate stream temperatures during nighttime periods can be attributed, at least in part, to errors in underestimating the evaporation rates as computed from the equation of Delay and Seaders.

8. Surface configuration does affect evaporation rates from streams, but its full quantitative evaluation awaits further research. A few suggestions on areas of needed research follow in the succeeding section.

RECOMMENDATIONS FOR FUTURE RESEARCH

1. Research should be carried out in attempt to correlate stream surface configuration to some measurable hydraulic parameter.

2. Work needs to be done to correlate the results of this model study to a dynamic model or prototype stream.

3. Investigations should be made on the sheltering effect of waves.

4. Any further model studies should be instrumented for digital read-out, so computer techniques could be employed in data reduction and analysis of results.

5. Further static model studies should be made using many values of wave steepness, so a more quantitative evaluation of this wave characteristic could be made with respect to evaporation rates.

6. Research should be carried out to evaluate the effect of a flowing stream's motion relative to the overlying air.

BIBLIOGRAPHY

1. Albertson, Maurice L. Analysis of evaporation as a boundary-layer phenomenon. Ph. D. thesis. Iowa City, Iowa University, 1948. 58 numb. leaves.

2. Albertson, Maurice L. Discussion on evaporation. Transactions of the American Society of Civil Engineers 111:55-62. 1946.

3. Albertson, Maurice L. Evaporation in relation to friction velocity. Comptes Rendus de l'Academie des Sciences, Paris. 239:529-531. 1954.

4. Albertson, Maurice L. Extension of the Reynold's analogy to evaporation. Comptes Rendus de l'Academie des Sciences, Paris. 239:474-476. 1954.

5. Albertson, Oran L., Bruce A. Tichenor, John Seaders and Fred J. Burgess. Stream temperature prediction by digital computer techniques. Corvallis, Oregon State University, Department of Civil Engineering, 1963. 27 numb. leaves.

6. Anderson, Ernest R. Energy budget studies. In: Water-loss investigations: Lake Hefner studies. Washington, 1954. p. 71-119. (U. S. Geological Survey Professional Paper no. 269).

7. Anderson, Ernest R., L. J. Anderson and J. J. Marciano. A review of evaporation theory and development of instrumentation. Interim report: Lake Mead water loss investigations. San Diego, U. S. Navy Electronics Laboratory, 1950. 71p. (Report 159).

8. Boyer, Peter B. Method of computing average reservoir temperature. In: Proceedings of the Twelfth Pacific Northwest Symposium on Water Pollution Research, Corvallis, Oregon, 1963. Corvallis, U. S. Public Health Service, Pacific Northwest Water Laboratory. p. 78-97.

9. Budyko, M. I. Evaporation under natural conditions. Jerusalem, Israel Program for Scientific Translations, 1963. 130 p. (Translated from Russian).

10. Burt, Wayne V. A second forecast of temperature conditions in Brownlee Reservoir and in the Snake River below Brownlee Dam. Corvallis, 1957. 10 numb. leaves. (U. S. Fish and Wildlife Contract: Water Temperature Studies on the Snake River. Reference 57-5. Technical Report no. 4).

11. Burt, Wayne V. Heat budget terms for middle Snake River reservoirs. Corvallis, 1958. 23 numb. leaves. (U. S. Fish and Wildlife Contract: Water Temperature Studies on the Snake River. Reference 58-7. Technical Report no. 6).

12. Calder, K. L. Eddy diffusion and evaporation in flow over aerodynamically smooth and rough surfaces. Quarterly Journal of Mechanics and Applied Mathematics 2:153-176. 1949.

13. Cermak, J. E. and H. J. Koloseus. Lake Hefner model studies of wind structure and evaporation: Final Report - Part I. Fort Collins, Colorado A. and M. College, 1953. 151 p. (Report no. 54 JEC 20).

14. Cermak, J. E. and H. J. Koloseus. Lake Hefner model studies of wind structure and evaporation: Final Report - Part II. Fort Collins, Colorado A. and M. College, 1954. 123 p. (Report no. 54 JEC 22).

15. Chemical Rubber Publishing Co. Handbook of chemistry and physics. Cleveland, 1956. 3206 p.

16. Clark, C. B. Speed of straight waves in a ripple tank. American Journal of Physics 27:478-483. 1959.

17. Delay, William H. and John Seaders. Temperature studies on the Umpqua River, Oregon. In: Proceedings of the Twelfth Pacific Northwest Symposium on Water Pollution Research, Corvallis, Oregon, 1963. Corvallis, U. S. Public Health Service, Pacific Northwest Water Laboratory. p. 57-75.

18. Duttweiler, David William. A mathematical model of stream temperature. Ph. D. thesis. Baltimore, John Hopkins University, 1963. 139 numb. leaves. (Microfilm).

19. Duttweiler, David William et al. Heat dissipation in flowing streams. Report of the 1960-1961 Advanced Seminar. Baltimore, John Hopkins University, 1962. 80 numb. leaves.

20. Harbeck, G. Earl, Jr. et al. Water-loss investigations: Lake Mead studies. Washington, 1958. 100 p. (U. S. Geological Survey Professional Paper no. 298).

21. Harding, S. T. Evaporation from free water surfaces. In: Hydrology, ed. by O. E. Meinzer. New York, McGraw-Hill, 1942. p. 56-82.

22. Hickox, G. H. Evaporation from a free water surface. Transactions of the American Society of Civil Engineers 111:1-33. 1946.

23. Holzman, B. The influence of stability on evaporation. Annals of the New York Academy of Sciences 44:13-18. 1943.

24. Jaske, R. T. Some comments on the effects of heat rejection processes on lakes and streams. Paper presented at the Water Resources Seminar, Water Research Institute, Oregon State University, Corvallis, Oregon, November 11, 1964. 10 numb. leaves.

25. Laberge, Ronald H. Thermal discharges. Water and Sewage Works 106:536-540. 1959.

26. Lamoreux, W. W. Modern evaporation formula adapted to computer use. Monthly Weather Review 90:26-28. 1962.

27. Li, Jerome C. R. Introduction to statistical inference. Ann Arbor, Michigan, Edwards Brothers, 1957. 568 p.

28. Linslev, Ray K., Jr., Max Kohler and Joseph L. H. Paulhus. Applied hydrology. New York, McGraw-Hill, 1949. 689 p.

29. Livingston, Burton E. Atmometers of porous porcelain and paper, their use in physiological ecology. Ecology 16:438-472. 1935.

30. McAlister, W. Bruce. Unpublished research on Rogue River temperature prediction. Corvallis, Oregon State University, Department of Oceanography, 1961.

31. Marciano, J. J. and G. Earl Harbeck, Jr. Mass-transfer studies. In: Water-loss investigations: Lake Hefner studies. Washington, 1954. p. 46-70. (U. S. Geological Survey Professional Paper no. 269).

32. Norris, Ramalingam. Evaporation from extensive surfaces of water roughened by waves. Quarterly Journal of the Royal Meteorological Society 74:1-12. January 1948.

33. Oregon State Water Resources Board. Preliminary report on water temperature prediction and control study - Umpqua River basin. Salem, June 1963. 14 numb. leaves.

34. Pasquill, F. Evaporation from a plane, free-liquid surface into a turbulent air stream. Proceedings of the Royal Society of London, Ser. A, 182:75-95. 1943.

35. Pasquill, F. Some further considerations on the measurement and indirect evaluation of natural evaporation. Quarterly Journal of the Royal Meteorological Society 76:287-301. 1950.

36. Powell, R. W. Further experiments on the evaporation of water from saturated surfaces. Transactions of the Institution of Chemical Engineers 18:36-50. 1940.

37. Powell, R. W. and Ezer Griffiths. The evaporation of water from plane and cylindrical surfaces. Transactions of the Institution of Chemical Engineers 13:175-198. 1935.

38. Priestly, C. H. B. Turbulent transfer in the lower atmosphere. Chicago, University of Chicago Press, 1959. 130 p.

39. Raphael, Jerome M. Prediction of temperatures in rivers and reservoirs. Proceedings of the American Society of Civil Engineers, Journal of the Power Division 88 (PO2):157-181. July 1962.

40. Raphael, Jerome M. Temperature phenomena and control in reservoirs. In: Proceedings of the Twelfth Pacific Northwest Symposium on Water Pollution Research, Corvallis, Oregon, 1963. Corvallis, U. S. Public Health Service, Pacific Northwest Water Laboratory. p. 76-77.

41. Rohwer, Carl. Evaporation from free water surfaces. Washington, 1931. 96 p. (U. S. Department of Agriculture Technical Bulletin no. 271).

42. Sears, Francis W. Mechanics, heat, and sound. Cambridge, Mass., Addison-Wesley, 1950. 527 p.

43. Stanier, Roger Y., Michael Doudoroff and Edward A. Adelburg. The microbial world. Englewood Cliffs, N. J., Prentice-Hall, 1963. 753 p.

44. Sutton, O. G. Micrometeorology. New York, McGraw-Hill, 1953. 333 p.

45. Sutton, O. G. Wind structure and evaporation in a turbulent atmosphere. Proceedings of the Royal Society of London, Ser. A, 146:701-722. 1934.

46. Sverdrup, H. U. On the evaporation from the oceans. Journal of Marine Research 1:3-14. 1937.

47. Sverdrup, H. U., Martin W. Johnson and Richard H. Fleming. The oceans. Englewood Cliffs, N. J., Prentice-Hall, 1942. 1087 p.

48. Taylor, G. I. Diffusion by continuous movements. Proceedings of the London Mathematical Society, Ser. 2, 20:196-211. 1922.

49. Thornthwaite, C. W. and B. Holzman. The determination of evaporation from land and water surfaces. Monthly Weather Review 67:4-11. 1939.

50. Velz, C. J. and J. J. Gannon. Forecasting heat loss in ponds and streams. Journal of the Water Pollution Control Federation 32:392-416. 1960.

51. Zeller, Robert. Summary of current theories and studies relating to temperature prediction. In: Proceedings of the Twelfth Pacific Northwest Symposium on Water Pollution Research, Corvallis, Oregon, 1963. Corvallis, U. S. Public Health Service, Pacific Northwest Water Laboratory. p. 111-156.

A. Thermistor Placement

The twelve "Yellow-Springs" thermistors were placed in the following positions:

Thermistor Number	Position
1	Dry thermistor for relative humidity
2	Air temperature - Top of tunnel
3	Air temperature - Bottom of tunnel
4	Water temperature - Section 2
5	Water temperature - Section 2
6	Water temperature - Section 2
7	Water temperature - Section 2
8	Water temperature - Inlet to Section 2
9	Water temperature - Section 3
10	Water temperature - Section 3
11	Water temperature - Section 3
12	Water temperature - Section 3

The following section will use a subscripted T to denote the number of the thermistor (i.e. - T_2 refers to the reading from thermistor number two).

B. Example of Computational Methods

The following is an example of the computational methods given in the section entitled "Computations and Results." The Handbook of Chemistry and Physics (15) was the source of much of the physical information required.

1. Test Information

Date: November 1, 1965

Surface Configuration: C

Model Test Section: 2

Propeller Hub Position: 4-1/4 inches

2. Wind Tunnel Data and Reduction

a) First Profile Run

Hot-Wire Position: 4d

Pitot Tube Velocity: 23 ft/sec

Time - Start: 8:13 p.m.
End: 8:28 p.m.

Barometric Pressure - Start: 30.01" Hg
End: 30.02" Hg

Air Temperature - T_2 - Start: 16.6°C
End: 16.6°C

T_3 - Start: 17.2°C
End: 17.2°C

Psychrometer Relative Humidity, 69%

Relative Humidity Profile Data:

Height above surface inches	Wet Bulb Thermistor Voltage D. C. volts	Wet Bulb Temperature °C	T_1 °C	Relative Humidity %
4.01	0.599	13.9	17.3	69
3.06	0.599	13.9	17.3	69
1.98	0.599	13.9	17.3	69
1.02	0.599	13.9	17.2	70
0.76	0.599	13.9	17.2	70
0.52	0.599	13.9	17.1	70
0.05	0.599	13.9	17.0	71

Velocity Profile (as obtained on the X-Y recorder):

Cold Probe Resistance = 3.44 Ω
Operating Resistance = 6 23 Ω
Air Temperature = 17° C

X-Y Recorder Trace

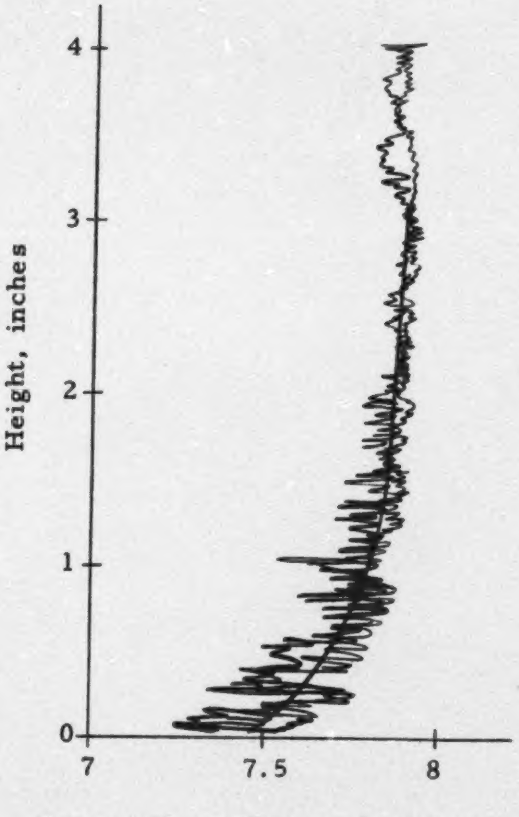

b) Second Profile Run

Hot-Wire Position: 4b

Pitot Tube Velocity: 23 ft/sec

Time - Start: 8:56 p.m.
End: 9:13 p.m.

Barometric Pressure - Start: 30.02 " Hg
End: 30.03 " Hg

Air Temperature - T_2 - Start: 17.6°C
End: 17.3°C

T_3 - Start: 18.1°C
End: 17.9°C

Psychrometer Relative Humidity: 69%

Relative Humidity Profile Data:

Height above surface	Wet Bulb Thermistor Voltage	Wet Bulb Temperature	T_1	Relative Humidity
inches	D.C. volts	°C	°C	%
4.01	0.616	14.9	18.2	70
2.93	0.616	14.9	18.2	70
2.00	0.616	14.9	18.1	71
0.98	0.616	14.9	18.0	72
0.72	0.616	14.9	18.0	72
0.50	0.616	14.9	17.9	73
0.05	0.616	14.9	17.7	75

Velocity Profile (as obtained on the X - Y recorder):

Cold Probe Resistance = 3.44Ω
Operating Resistance = 6.23Ω
Air Temperature = 18°C

X-Y Recorder Trace

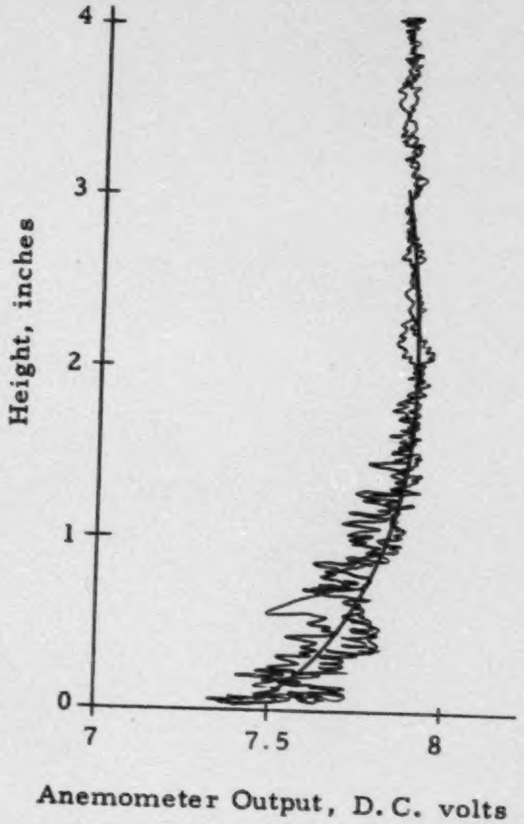

c) Evaporation Data

Section 1			Section 2			Section 3		
Time	Evap. Increment	Total Evap.	Time	Evap. Increment	Total Evap.	Time	Evap. Increment	Total Evap.
p.m.	ml	ml	p.m.	ml	ml	p.m.	ml	ml
8:12	--	0	8:12	--	0	8:12	--	0
8:32	11	11	8:33	16½	16½	8:34	15½	15½
8:51	15	26	8:52	15½	32	8:53	14½	30
9:30	30	56	9:30	34	66	9:30	32	62

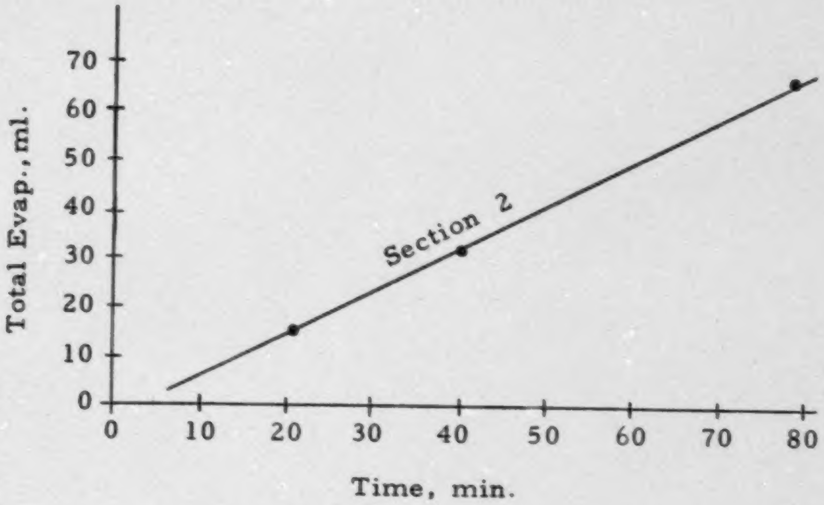

Evaporation Rate = Slope of line/Area

Evaporation Rate = $\underline{0.429 \text{ gm/ft}^2 \text{ - min}}$

d) Water Temperatures (°C):

Time	T_4	T_5	T_6	T_7	T_8	T_9	T_{10}	T_{11}	T_{12}	Section Average 2	Section Average 3
8:12 p.m.	13.7	13.7	13.7	13.7	14.1	13.9	13.9	13.8	Non-operable	13.7	13.9
8:35	13.8	13.7	13.7	13.8	14.4	13.8	13.9	13.8		13.7	13.8
8:55	13.9	13.9	13.9	13.9	14.5	13.9	14.0	14.0		13.9	14.0
9:30	14.0	14.0	13.9	14.0	14.5	14.0	14.0	14.0		14.0	14.0

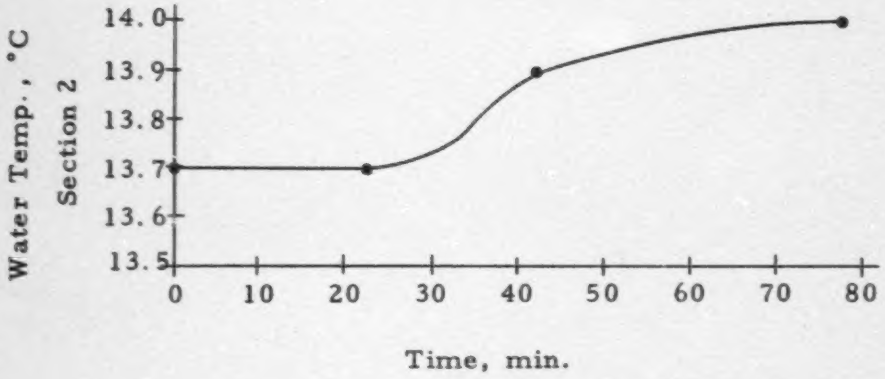

Average water temperature for Section 2
over the test run = 13.8°C

3. Preliminary Calculations

a) Graphical Determination of z_o

Plot of log z vs. u

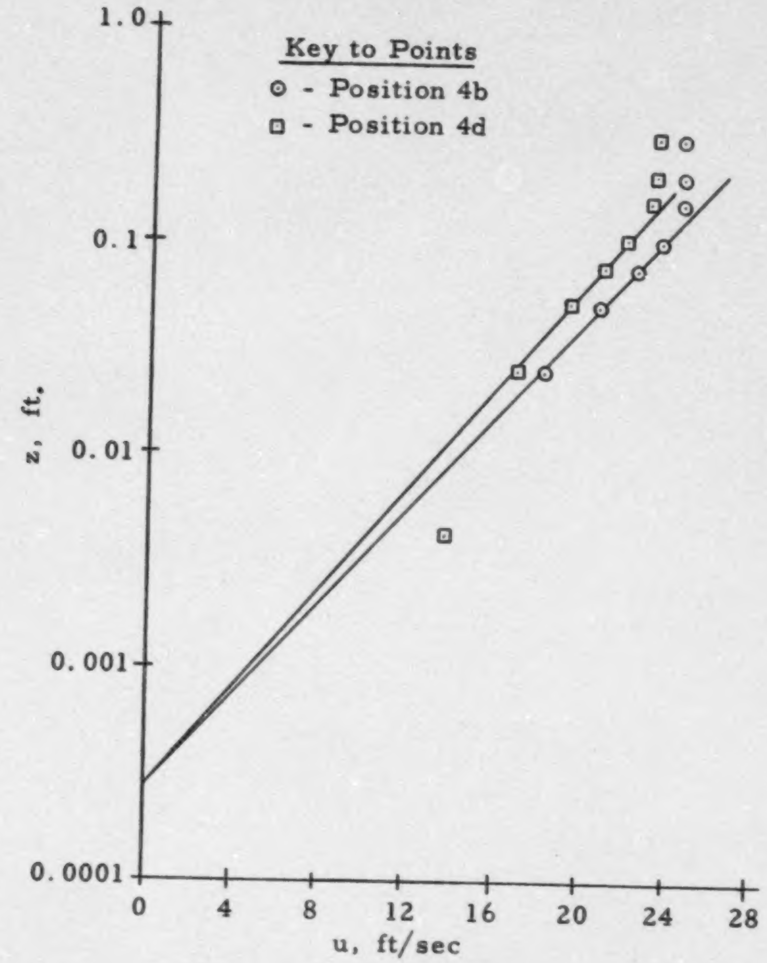

$z_o = 2.75 \times 10^{-4}$ ft

b) **Calculation of u_***

$$\underline{u_* = u_z/5.75 \log (z/z_o)} \qquad (8)$$

$$z_o = 2.75 \times 10^{-4} \text{ ft}$$

$$z = 7.5 \times 10^{-2} \text{ ft}$$

$$u_z = 21.7 \text{ ft/sec}$$

$$\therefore \quad u_* = 21.7/5.75 \log (7.5\times10^{-2}/2.75\times10^{-4})$$

$$u_* = \underline{\underline{1.55 \text{ ft/sec}}}$$

c) **Calculation of N**

$$\underline{N = \sqrt{A}/(2.72\times10^{4})\, \nu_e \Delta C} \qquad (26)$$

$$\nu_e = \nu/\sigma = \nu/0.6 \qquad (27)$$

$$\nu = \eta/\rho \qquad (28)$$

At an air temperature of 17.7°C,

$$\eta = 1.21 \times 10^{-5} \text{ lb/sec - ft}$$

$$\rho = 7.60 \times 10^{-2} \text{ lb/ft}^3$$

$$\therefore \quad \nu = 1.592 \times 10^{-4} \text{ ft}^2\text{/sec}$$

$$\text{and} \quad \nu_e = 2.65 \times 10^{-4} \text{ ft}^2\text{/sec}$$

$$\underline{\Delta C = C_s - C_a} \qquad (29)$$

C_s (at water temp. = 13.8°C) = 7.4×10^{-4} lb/ft^3

C_a (at air temp. = 17.7°C and relative humidity = 69.5 %),

$C_a = (0.695)(9.3 \times 10^{-4}\ lb/ft^3) = 6.46 \times 10^{-4}\ lb/ft^3$

$\therefore\ \Delta C = 0.94 \times 10^{-4}\ lb/ft^3$

$\therefore\ N = (0.429)\sqrt{2}/(2.72 \times 10^4)(2.65 \times 10^{-4})(0.94 \times 10^{-4})$

$N = \underline{\underline{895}}$

d) Calculation of R_*

$$\underline{R_* = u_* \sqrt{A}/\nu_e} \qquad (24)$$

$R_* = (1.55)\sqrt{2}/(2.65 \times 10^{-4})$

$R_* = \underline{\underline{8270}}$

4. Computations Using Existing Equations

a) Norris (Figure 8)

$$\underline{E = (2.72 \times 10^4) k_o^2\ \rho\, u_z (q_s - q_z)/\ell n(z/z_o)(\ell n(z/z_o) - 0.88)} \qquad (31)$$

u_z (at z = 0.075 ft) = 21.7 ft/sec

$\underline{q_s = (C_s/\rho)}$ water temp = 13.8 °C

$q_s = 7.4 \times 10^{-4}/7.71 \times 10^{-2} = 9.6 \times 10^{-3}$

$\underline{q_z = (C/\rho)}$ air temp. = 17.6 °C,
relative humidity = 71%

$q_z = (0.71)(9.25 \times 10^{-4})/7.6 \times 10^{-2} = 8.64 \times 10^{-3}$

$\therefore\ (q_s - q_z) = 0.96 \times 10^{-3}$

$\ell n(z/z_o) = \ell n(7.5 \times 10^{-2}/2.75 \times 10^{-4})$

$$\ell n(z/z_o) = \ell n\ 273 = 5.61$$

$$\therefore\ E = (2.72 \times 10^4)(7.60 \times 10^{-2})(0.4)^2(21.7)(0.96 \times 10^{-3})/(5.61)(5.61-0.88)$$

$$E = \underline{\underline{0.260\ \text{gm/ft}^2 - \text{min}}}$$

b) Thornthwaite and Holzman (Figure 9)

$$\underline{E = (5.54 \times 10^3)\rho\,(e_1 - e_2)(\bar{u}_2 - \bar{u}_1)/\,P\left(\ell n\frac{z_2}{z_1}\right)^2} \qquad (32)$$

For $z_1 = 0.025$ ft, $\bar{u}_1 = 17.6$ ft/sec

Air temp = 17.4°C, relative humidity = 73%

$$e_1 = (0.73)(14.90\ \text{mm Hg}) = 10.89\ \text{mm Hg}$$

For $z_2 = 0.100$ ft, $\bar{u}_2 = 22.8$ ft/sec

Air temp = 17.6 °C, relative humidity = 71%

$$\therefore\ e_2 = (0.71)(15.09\ \text{mm Hg}) = 10.70\ \text{mm Hg}$$

$$(\ell n\ z_2/z_1)^2 = 1.92, \quad P = 30.03\ \text{in Hg} = 763\ \text{mm Hg}$$

$$\therefore\ E = \frac{(5.54 \times 10^3)(7.60 \times 10^{-2})(10.89 - 10.70)(22.8 - 17.6)}{(763)(1.92)}$$

$$E = \underline{\underline{0.284\ \text{gm/ft}^2 - \text{min}}}$$

c) Sutton (Figure 10)

$$\underline{a = (0.1276)(\nu + u_* z_o)^{0.25}} \qquad (34)$$

$$\nu = (1.592 \times 10^{-4})(9.29 \times 10^2) = 0.148\ \text{cm}^2/\text{sec}$$

$$u_* = (1.55)(30.5) = 47.2 \text{ cm/sec}$$

$$z_o = (2.75 \times 10^{-4})(30.5) = 8.4 \times 10^{-3} \text{cm}$$

$$a = (0.1276)(0.148 + (47.2)(8.4 \times 10^{-3}))^{0.25}$$

$$a = 0.1083$$

$$\underline{G = (0.1585)(\psi_o - \psi_i) a^{0.888}} \qquad (35)$$

$$\psi_o - \psi_i = \Delta C \, (1.602 \times 10^{-2})$$

$$\psi_o - \psi_i = (0.94 \times 10^{-4})(1.602 \times 10^{-2})$$

$$\psi_o - \psi_i = 1.507 \times 10^{-6} \text{ gm/cm}^3$$

$$\therefore G = (0.1585)(1.507 \times 10^{-6})(0.1083)^{0.888}$$

$$G = 3.32 \times 10^{-8}$$

$$\underline{E = (5.71 \times 10^4) \, G \bar{u}^{0.778}} \qquad (36)$$

$$u_1 = (\text{at } 7.5 \times 10^{-2} \text{ ft}) = 21.7 \text{ ft/sec}$$

$$u_1 = (21.7)(30.5) = 662 \text{ cm/sec}$$

$$\therefore E = (5.71 \times 10^4)(3.32 \times 10^{-8})(662)^{0.778}$$

$$E = \underline{\underline{0.300 \text{ gm/ft}^2 \text{ - min}}}$$

d) Delay and Seaders (Figure 11)

$$\underline{E = \frac{Mu(e_o - e_a)}{0.262 \, L}} \qquad (38)$$

$$M = 0.57$$

$$u = 24.0 \text{ ft/sec}$$

L (at water temp = 13.8°C) = 588.5 cal/gm

e_o (at water temp = 13.8°C) = 11.83 mm Hg

e_a (at air temp = 17.7°C, relative humidity = 69.5%)

$$e_a = (0.695)(15.18) = 10.53 \text{ mm Hg}$$

$$\therefore E = (0.57(24.0)(11.83 - 10.53)/(0.262)(588.5)$$

$$E = \underline{\underline{0.115 \text{ gm/ft}^2 - \text{min}}}$$

e) Cermak and Koloseus (Figure 12)

$$\underline{N = 0.256 R_*^{0.87}} \qquad (39)$$

$$R_* = 8270$$

$$\therefore N = (0.256)(8270)^{0.87} = 655$$

$$\underline{E = (2.72 \times 10^4)\nu_e \Delta C N/\sqrt{A}} \qquad (26)$$

$$E = (2.72 \times 10^4)(2.65 \times 10^{-4})(0.94 \times 10^{-4})(655)/\sqrt{2}$$

$$E = \underline{\underline{0.314 \text{ gm/ft}^2 - \text{min}}}$$

5. Computations Using Experimentally Developed Equations

See Table 5 for the empirical coefficients developed for surface configuration C.

a) Equation 4 (Figure 13)

$$\underline{E = (A + Bu)(e_s - e_a)} \qquad (4)$$

$$A = 0.0264$$

$$B = 0.01063$$

$$u = 24.0 \text{ ft/sec}$$

$$(e_s - e_a) = 1.30 \text{ mm Hg}$$

$$\therefore E = (0.0264 + (0.01063)(24.0))(1.30)$$

$$E = \underline{\underline{0.366 \text{ gm/ft}^2 - \text{min}}}$$

b) Equation 21 (Figure 14)

$$\underline{E = B'u(e_s - e_a)} \qquad (21)$$

$$B' = 12.01 \times 10^{-3}$$

$$\therefore E = (12.01 \times 10^{-3})(24.0)(1.30)$$

$$E = \underline{\underline{0.375 \text{ gm/ft}^2 - \text{min}}}$$

c) Equation 5 (Figure 15)

$$\underline{E = a(u)^b(e_s - e_a)} \qquad (5)$$

$$a = 0.01952$$

$$b = 0.834$$

$$\therefore E = (0.834)(24.0)^{0.01952}(1.30)$$

$$E = \underline{\underline{0.360 \text{ gm/ft}^2 - \text{min}}}$$

d) Equation 22 (Figure 16)

$$\underline{N = \alpha R_*^{\beta}} \qquad (22)$$

$$\alpha = 0.097$$

$$\beta = 0.992$$

$$\therefore N = (0.097)(8270)^{0.992}$$

$$N = 747$$

$$\therefore E = (2.72 \times 10^{4})(2.65 \times 10^{-4})(0.94 \times 10^{-4})(747)/\sqrt{2}$$

$$E = \underline{\underline{0.358 \text{ gm/ft}^2 \text{ - min}}}$$

C. Data Summary

The following tables contain pertinent data, including the information necessary for the plotting of Figures 8 - 16. All evaporation rates are in gm/ft^2 - min, z_o is in feet, and all u values are in ft/sec.

Model Series	Test Date	Model Section	Measured Evap.	z_o	u_*	$u_{0.075}$	u	N	R_*
A	8-17-65	2, 3	0.464	1.68×10^{-4}	0.492	7.5	8.4	208	3480
A	8-18-65	2, 3	0.294	1.74×10^{-4}	0.433	6.6	7.3	227	3180
A	8-19-65	2	0.313	1.77×10^{-4}	0.850	12.4	14.6	285	4360
A	8-20-65	2	0.461	4.20×10^{-4}	1.262	15.6	19.4	376	6290
A	8-21-65	3	0.380	3.4×10^{-5}	0.857	16.5	18.7	---	4350
A	8-22-65	2	0.595	1.40×10^{-4}	1.223	19.2	21.6	386	6100
A	8-22-65	3	0.403	1.9×10^{-5}	0.945	19.6	21.6	335	4760
A	8-23-65	2, 3	0.599	7.1×10^{-5}	1.298	21.8	24.6	553	9440
B	9-22-65	2	0.506	1.20×10^{-3}	0.601	6.2	7.1	250	3100
B	9-21-65	3	0.250	4.7×10^{-4}	0.537	6.5	7.1	232	2840
B	9-23-65	2	0.950	6.0×10^{-4}	1.03	12.4	14.1	343	5260
B	9-24-65	3	0.968	8.4×10^{-4}	1.08	12.2	14.0	321	5460
B	9-28-65	2	0.617	2.4×10^{-4}	1.14	16.4	18.5	545	6130
B	9-27-65	3	0.410	4.2×10^{-4}	1.17	15.1	17.4	430	6290
B	9-29-65	2	0.664	1.46×10^{-4}	1.284	20.0	22.0	681	6880
B	9-30-65	3	0.534	1.85×10^{-4}	1.227	18.4	20.9	585	6570
B	10-4-65	2	0.350	4.5×10^{-4}	1.72	22.0	24.3	1082	9100
B	10-1-65	3	0.666	2.47×10^{-4}	1.53	21.8	24.6	746	8100
C	10-20-65	2	0.234	2.10×10^{-3}	0.655	5.8	6.8	291	3480
C	10-21-65	3	0.238	5.9×10^{-4}	0.496	6.0	6.8	278	2680
C	10-25-65	2	0.265	8.6×10^{-4}	1.06	11.8	13.5	443	5690
C	10-24-65	3	0.212	7.5×10^{-4}	1.01	11.6	13.3	477	5440
C	10-26-65	2	0.356	6.4×10^{-4}	1.34	16.0	18.4	666	7240
C	10-27-65	3	0.234	8.8×10^{-4}	1.41	15.6	18.0	667	7610
C	10-29-65	2	0.429	4.7×10^{-4}	1.62	20.5	22.6	824	8750

Model Series	Test Date	Model Section	Measured Evap.	z_o	u_*	$u_{0.075}$	u	N	R_*
C	10-28-65	3	0.435	2.25×10^{-4}	1.34	19.5	22.0	582	7270
C	11-1-65	2	0.429	2.75×10^{-4}	1.55	21.7	24.0	895	8270
C	11-2-65	3	0.341	2.52×10^{-4}	1.46	20.8	24.3	705	7780
D	11-12-65	2	0.108	7.4×10^{-4}	0.437	5.1	5.8	367	2340
D	11-11-65	3	0.138	1.25×10^{-3}	0.504	5.1	6.2	298	2720
D	11-14-65	2	0.308	9.9×10^{-4}	1.08	11.7	13.5	603	5750
D	11-15-65	3	0.292	1.07×10^{-3}	1.06	11.3	13.3	466	5650
D	11-19-65	2	0.438	4.7×10^{-4}	1.10	14.0	16.0	614	5870
D	11-17-65	3	0.312	5.3×10^{-4}	1.12	13.8	15.9	636	5910
D	11-20-65	2	0.500	6.2×10^{-4}	1.42	17.0	19.4	740	7500
D	11-21-65	3	0.445	8.0×10^{-4}	1.40	15.9	19.3	645	7420
D	11-24-65	2	0.766	2.8×10^{-4}	1.42	19.8	21.9	616	7500
D	11-23-65	3	0.620	2.0×10^{-4}	1.28	18.9	21.0	578	6650
E	12-1-65	2	0.183	9.7×10^{-5}	0.337	5.6	5.9	276	1814
E	12-3-65	3	0.130	2.8×10^{-4}	0.363	5.1	5.7	241	1940
E	12-5-65	2	0.286	1.8×10^{-4}	0.764	11.5	12.4	441	4070
E	12-4-65	3	0.292	1.9×10^{-4}	0.744	11.1	12.2	425	3940
E	12-6-65	2	0.413	3.2×10^{-4}	1.13	15.4	16.9	521	5960
E	12-7-65	3	0.552	1.5×10^{-4}	0.941	14.6	16.0	484	5020
E	12-10-65	2	0.572	3.3×10^{-5}	0.948	18.3	19.9	591	5660
E	12-8-65	3	0.729	8.0×10^{-5}	1.06	18.1	20.2	519	4970

Table of Computed Evaporation Rates

Model Series	Test Date	Existing Equations					Experimentally Developed Equations			
		Norris	Thornthwaite and Holzman	Sutton	Delay and Seaders	Cermak and Koleseus	$E=(A+Bu)(e_s-e_a)$	$E=B'u(e_s-e_a)$	$E=a(u)^b(e_s-e_a)$	$N=\alpha R_*^{\beta}$
A	8-17-65	0.491	0.532	0.589	0.177	0.692	0.545	0.449	0.521	0.525
A	8-18-65	0.265	0.383	0.340	0.092	0.368	0.298	0.234	0.279	0.279
A	8-19-65	0.296	0.189	0.328	0.108	0.418	0.291	0.275	0.290	0.312
A	8-20-65	0.565	0.203	0.432	0.155	0.626	0.395	0.394	0.397	0.476
A	8-21-65	0.197	0.095	0.360	0.106	0.372	-----	-----	-----	-----
A	8-22-65	0.482	0.359	0.620	0.253	0.776	0.633	0.643	0.635	0.592
A	8-22-65	0.232	0.420	0.497	0.162	0.490	0.406	0.411	0.407	0.370
A	8-23-65	0.561	0.481	0.730	0.262	0.832	0.645	0.667	0.650	0.631
B	9-22-65	0.705	0.278	0.510	0.163	0.565	0.381	0.407	0.440	0.451
B	9-21-65	0.286	0.219	0.244	0.086	0.279	0.206	0.220	0.237	0.216
B	9-23-65	1.360	0.366	0.943	0.434	1.220	1.070	1.090	1.080	1.190
B	9-24-65	1.710	0.575	1.300	0.471	1.370	1.160	1.180	1.180	1.350
B	9-28-65	0.490	0.224	0.537	0.280	0.578	0.703	0.703	0.681	0.588
B	9-27-65	0.564	0.231	0.469	0.187	0.489	0.468	0.469	0.459	0.510
B	9-29-65	0.381	0.235	0.516	0.236	0.540	0.626	0.592	0.563	0.580
B	9-30-65	0.414	0.302	0.465	0.209	0.491	0.535	0.524	0.501	0.515
B	10-4-65	0.204	0.167	0.229	0.069	0.231	-----	-----	-----	0.273
B	10-1-65	0.546	0.268	0.543	0.234	0.515	0.594	0.588	0.557	0.650

Evaporation Rates Continued

		Existing Equations					Experimentally Developed Equations			
Model Series	Test Date	Norris	Thornthwaite and Holzman	Sutton	Delay and Seaders	Cermak and Koleseus	$E=(A+Bu)(e_s-e_a)$	$E=B'u(e_s-e_a)$	$E=a(u)^b(e_s-e_a)$	$N=\alpha R_*^{\beta}$
C	10-20-65	0.420	0.174	0.224	0.060	0.246	0.236	0.195	0.230	0.253
C	10-21-65	0.202	0.083	0.197	0.063	0.212	0.246	0.205	0.242	0.211
C	10-25-65	0.267	0.272	0.268	0.112	0.284	0.279	0.256	0.284	0.313
C	10-24-65	0.182	0.159	0.191	0.059	0.199	0.202	0.193	0.203	0.218
C	10-26-65	0.436	0.221	0.303	0.100	0.311	0.312	0.325	0.324	0.352
C	10-27-65	0.212	0.077	0.210	0.067	0.215	0.220	0.218	0.220	0.242
C	10-29-65	0.430	0.148	0.363	0.131	0.327	0.421	0.429	0.414	0.406
C	10-28-65	0.357	0.249	0.416	0.171	0.437	0.573	0.555	0.539	0.494
C	11-1-65	0.260	0.284	0.300	0.115	0.314	0.366	0.375	0.360	0.358
C	11-2-65	0.290	0.394	0.274	0.120	0.299	0.382	0.390	0.374	0.341
D	11-12-65	0.059	0.055	0.058	0.018	0.065	0.109	0.061	0.099	0.093
D	11-11-65	0.148	0.099	0.104	0.031	0.115	0.177	0.102	0.162	0.160
D	11-14-65	0.295	0.086	0.234	0.071	0.246	0.261	0.234	0.264	0.297
D	11-15-65	0.365	0.363	0.281	0.084	0.296	0.311	0.279	0.313	0.347
D	11-19-65	0.332	0.213	0.329	0.124	0.346	0.424	0.413	0.426	0.388
D	11-17-65	0.240	0.197	0.222	0.078	0.238	0.268	0.260	0.269	0.278
D	11-20-65	0.446	0.206	0.396	0.137	0.407	0.431	0.453	0.431	0.459
D	11-21-65	0.454	0.387	0.413	0.135	0.410	0.429	0.450	0.429	0.452

Evaporation Rates Continued

Model Series	Test Date	Existing Equations					Experimentally Developed Equations			
		Norris	Thornthwaite and Holzman	Sutton	Delay and Seaders	Cermak and Koleseus	$E=(A+Bu)(e_s-e_a)$	$E=B'u(e_s-e_a)$	$E=a(u)^b(e_s-e_a)$	$N=\alpha R_*^{\beta}$
D	11-24-65	0.728	0.474	0.719	0.300	0.723	0.907	0.998	0.899	0.829
D	11-23-65	0.476	0.151	0.544	0.237	0.588	0.728	0.786	0.720	0.657
E	12-1-65	0.067	0.043	0.114	0.041	0.118	0.191	0.118	0.187	0.169
E	12-3-65	0.072	0.050	0.092	0.031	0.100	0.147	0.089	0.137	0.144
E	12-5-65	0.373	0.115	0.212	0.083	0.230	0.261	0.237	0.274	0.285
E	12-4-65	0.137	0.077	0.220	0.083	0.235	0.261	0.235	0.274	0.294
E	12-6-65	0.366	0.142	0.398	0.149	0.390	0.413	0.424	0.429	0.454
E	12-7-65	0.395	0.193	0.451	0.202	0.486	0.574	0.578	0.599	0.574
E	12-10-65	0.286	0.234	0.436	0.213	0.455	0.551	0.599	0.565	0.533
E	12-8-65	0.388	0.310	0.584	0.286	0.585	0.797	0.870	0.816	0.700

D. Evaporation Equations Not Given in the Text

1. General Equations

a) Meyer's Formula (28, p. 168)

$$E = c(e_s - e_a)(1 + \frac{\overline{V}w}{10})$$

where,

E = monthly evaporation, inches;

e_s = saturation vapor pressure corresponding to the monthly mean air temperature, inches of mercury;

e_a = average monthly vapor pressure, inches of mercury;

$\overline{V}w$ = mean monthly wind speed, miles per hour;

c = empirical constant having a value ranging from 11 to 15.

b) Horton's Equation (28, p. 168)

$$E = c[(2 - e^{-2Vw})e_w - e_a]$$

where,

E = daily evaporation, inches;

e_w = saturation vapor pressure at the temperature of the water, inches of mercury;

e_a = vapor pressure of the ambient air, inches of mercury;

Vw = wind velocity, miles per hour;

c = empirical constant, 0.36 for a pan 12 inches square.

c) Rohwer's Equation (41, p. 21)

$$E = (0.44 + 0.118\ W)(e_s - e_d)$$

where,

E = evaporation rate, inches per day;

W = mean velocity of water-surface wind, miles per hour;

e_s = mean vapor pressure of saturated vapor at the temperature of the water surface, inches of mercury;

e_d = mean vapor pressure of saturated air at the temperature of the dew point, inches of mercury.

2. Discontinuous Mixing Equations

a) Sverdrup's Equation (7, p. 23)
(For both smooth and rough surfaces)

$$F = \frac{0.623 \rho k_o u_* (e_\delta - e_z)}{\ell n \frac{z + z_o}{\delta + z_o}}$$

where,

F = evaporation rate, gm/cm^2 - sec;

ρ = air density, gm/cm^3;

k_o = von Karman's constant = 0.4;

u_* = friction velocity, cm/sec;

e_δ and e_z = vapor pressures at heights δ and z_o, respectively, gm/cm - sec^2;

z = height above water surface within the turbulent boundary region, cm;

z_o = roughness parameter, cm;

δ = thickness of the laminar layer, cm.

b) Montgomery's Equation (32, p. 2)
(For smooth surfaces)

$$E = \frac{\rho k_o u_* (q_s - q)}{\frac{\lambda \nu k_o}{D} + \ln \frac{k_o u_* z}{D}}$$

where,

E = evaporation rate,

ρ = air density,

k_o = von Karman's constant,

u_* = friction velocity,

q_s = saturated specific humidity at the water surface temperature,

q = specific humidity at height z,

λ = non-dimensional constant with reported values from 7.8 to 11.6,

ν = kinematic viscosity of air,

D = kinematic coefficient of water vapor through air.

c) Pasquill's Equation (35, p. 294)
(For rough surfaces)

$$E = \frac{\rho k_o^2 (u_2 - u_1)(q_1 - q_2)}{\left[\ell n \dfrac{z_2 - d}{z_1 - d} \right]^2}$$

where,

E = evaporation rate,

ρ = air density,

k_o = von Karman's constant,

u_1 and u_2 = wind speed at heights z_1 and z_2, respectively,

q_1 and q_2 = specific humidity at heights z_1 and z_2, respectively,

z_1 and z_2 = heights within the turbulent boundary region,

d = "zero point displacement," a type of roughness parameter.

E. Instrument Specifications

1. DISA Constant Temperature Hot-wire Anemometer-Type 55A01

a) Frequency Response

0 - 60 kilocycles/sec.

b) Probe Resistance Range

1 - 50 ohms.

c) Maximum Available Probe Current

250 milliamps, continuous or peak.

d) Amplifier Transconductance

AC, approximately 8 milliamps/millivolt

DC, approximately 300 milliamps/millivolt

at 125 milliamps output current.

e) Equivalent Input DC Drift

± 25 microvolts at 125 milliamps output current.

f) Cold Resistance Measurement

Accuracy = 0.5%. Steps of 0.01 ohms below 10 ohms and steps of 0.05 ohms from 10 to 50 ohms.

g) Operating Resistance

Set with a three-stage system. Resistance change of less than 1% with probe current of 200 milliamps.

h) DC Voltmeter

Ranges: 20, 10, 5, 2 volts full scale.

Zero-shift voltages: 1, 2, 5, 10 volts.

Accuracy: 1%.

i) RMS Indicator

Reading independent of wave form.

Ranges: 5, 10, 20, 50, 100, 200, 500, 1000 millivolts RMS full-scale.

Accuracy: 2%.

j) Low Pass Filter

RC filter with seven calibrated positions, 100, 50, 20, 10, 5, 2, 1 kilocycles/sec (-3db).

k) High Pass Filter

RC filter with seven calibrated positions, 5, 20, 50, 100, 200, 500, 1000 cycles/sec (-3db).

l) Square Wave Generator

Approximately 2.5 kilocycles/sec generator for performance checking.

m) Recording and Observation

Coaxial connector for recording instrument and oscilloscope.

n) Output Impedance

Approximately 1000 ohms.

o) Noise Level

Under normal operating conditions with a standard probe, the RMS noise level at 1 kilocycle/sec bandwidth is less than 0.45 millivolts RMS (corresponding to approximately 0.03% turbulence) and at 5 kilocycles/sec bandwidth less than 0.9 millivolts RMS (corresponding to approximately 0.06% turbulence).

p) Power Supply

110/220 volts ± 10%.

50 to 60 cycles/sec.

Power consumption = 180 watts.

q) Probe Temperature Change Data

Output voltage increment per change of 1°C in ambient air temperature:

15 millivolts	at	1 meter/sec
20 millivolts	at	10 meters/sec
25 millivolts	at	100 meters/sec.

2. Bourns Linear Motion Potentiometer - Model 108

a) Mechanical Travel

4 inches.

b) Total Resistance

9920 ohms.

c) Insulation Resistance

20,000 megohms at 500 DC volts.

d) Linearity

± 0.21%.

e) Operating Temperature Range

-55 to 175°C (-67 to 347°F).

f) Life at Normal Operating Conditions

1,000,000 cycles.

F. Photographs of Four Sine Wave Surfaces
(Series B, C, D, E)

Figure 1 shows the flat model surface (Series A) The installations of the four sine wave surfaces are shown in the following photographs.

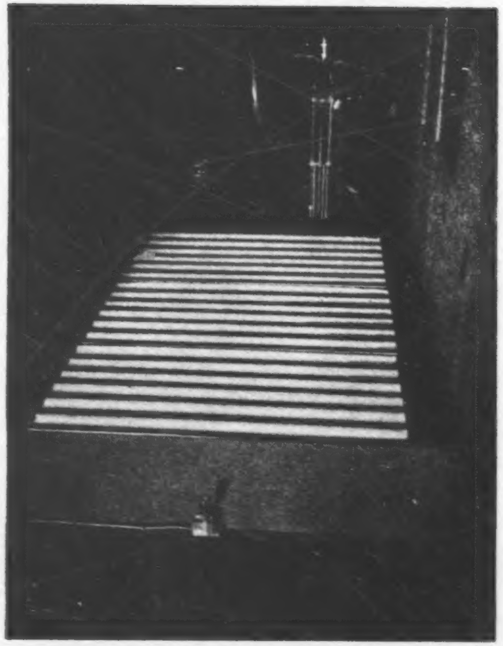

Surface Configuration B
(H = 1/4", L = 2")

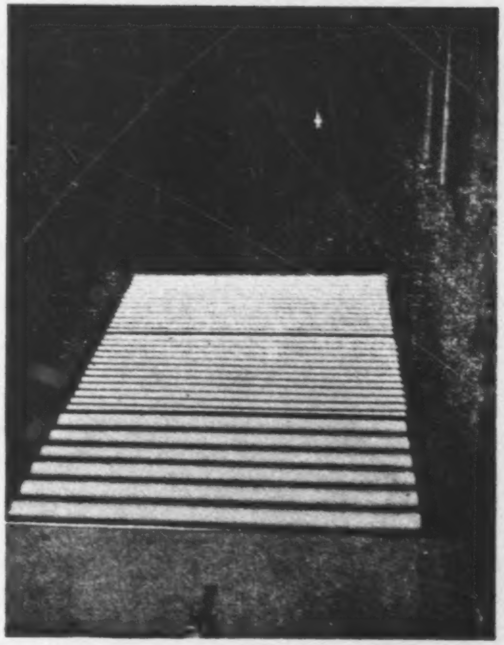

Surface Configuration C
(H = 1/4", L = 1")

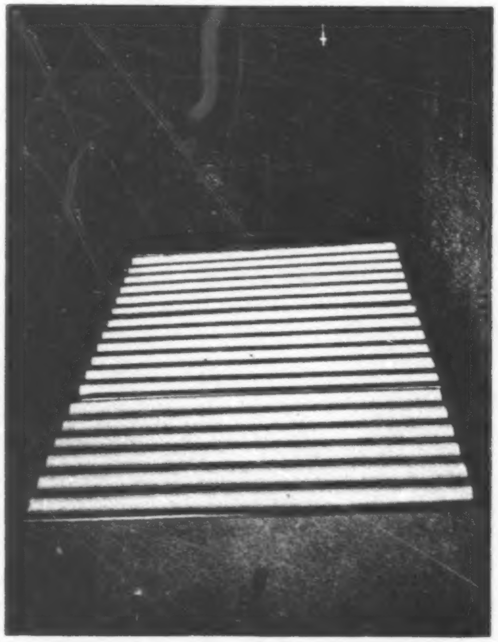

Surface Configuration D

(H = 1/2", L = 2")

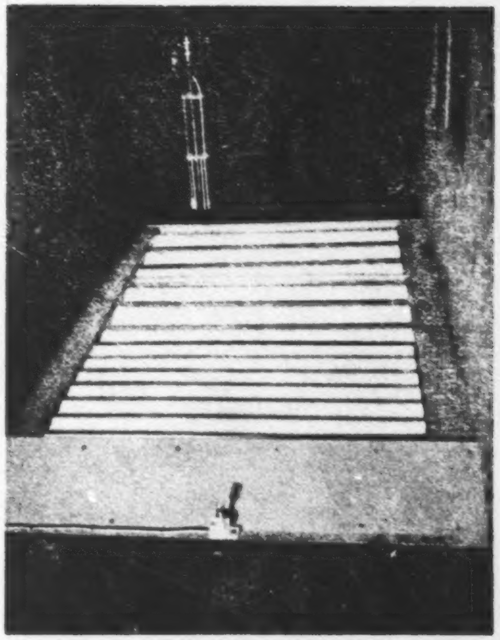

Surface Configuration E

(H = 1/2", L = 4")